Cravens, D. and D. Letts. *Practical Techniques In CF Research - Triggering Methods*. in *Tenth International Conference on Cold Fusion*. 2003. Cambridge, MA: LENR-CANR.org. This paper was presented at the 10th International Conference on Cold Fusion. It may be different from the version published by World Scientific, Inc (2003) in the official Proceedings of the conference.

Practical Techniques In CF Research – Triggering Methods

D. J. Cravens
Cloudcroft, NM 88317, USA
E-mail: dennis@Tularosa.net

D. G. Letts
Austin TX 78727, USA
E-mail: lettslab@austin.rr.com

A collection of useful techniques for triggering CF events is presented which are gleaned from 14 years of CF research and thousands of experiments by the authors. Special attention is give to those techniques that trigger excess heat by dynamic conditions that are imposed upon CF systems. These triggering techniques include changes in cell temperature, pulsing the current to electrolytic systems, acoustical stimulation of gas systems, chemical triggering of electrolytic system, pressure changes, radio frequency excitation, magnetic field variations and laser stimulation. Laser stimulation is found to be a potentially fruitful technique to trigger heat events, to probe the cathode surface by scanning for active locations and to compare products from at active and inactive regions.

1 Background

1.1 Static Equilibrium Often Produces Sporadic Results

The study of nuclear events at low temperatures often has resulted in frustrating investigations. The field of cold fusion has often been marked with sporadic and non-reproducible work. Critics have often pointed to the sporadic nature of the heat generation in electrolytic systems as indication of poor experimental procedure. However, it now seems that the sporadic nature of the results is a characteristic of an electrolytic system, which is initially near equilibrium, and slowly loaded to a transition point which is best described by the mathematical term as a chaotic transition. For example: slowly loading palladium can be driven between beta and gamma states and cause internal fluxes of deuterium.

Electrolytic cells using bulk palladium often require loading times of 10 to 20 times longer than would be expected by diffusion times of deuterium within the metal before they be expected to produce excess heat.[1] This was likely the cause of failure of early researchers who rushed to replicate Fleischmann's and Pons' early work.[2] In the first few years after the announcement, it was easier for a researcher to rush to print and claim negative results than to patiently wait until the system was fully loaded and driven into internal transitions that drive the reactions. As a result, early work more often than not failed to see excess heat.

This work will illustrate methods that will help drive CF systems off equilibrium and trigger internal events that lead to production of excess heat. The viewpoint taken here is that a system must be allowed to depart from static equilibrium before the required reactions can take place.

1.2 Theoretical Limitations

Most simple theoretical models fail to predict that nuclear reactions within a deuterated metal lattice can take place at significant rates. Such models rely on reaction rates that are based on equilibrium placement of deuterium within a metal lattice or on wave functions based on such placements. In particle models, the global average of the deuterium density within the metal is on the order of an Angstrom or more even for extreme loading ratios of D/Pd. It is clear that deuterium at such remote nuclear separations would not be expected to lead to nuclear events.

The imposition of dynamic conditions can cause the local separations of deuterium to be significantly different from the value predicted by the global density alone. It also seems that dynamic conditions provide ways for coupling of energy to drive the reactions and impurities within the lattice can allow for spin exchanges required for spin selection rules. It is a surety that the energy required to drive any nuclear events and energy released from such events are much larger than any external energy available to the deuterium based on a per atom division of energy.[3] This means that any external energy driving the possible nuclear events must act in a coherent way to channel energy from a large region of many atoms to the active sites.[4,5,6] This coherent channeling must involve over 10^8 atoms and likely many more. The experimental conditions then must make use of non-equilibrium events acting on a system that has some group coherent nature. The methods described here are simple and practical methods that can be used to produce such dynamic conditions, which may lead to the desired nuclear events. The assumption here is that the reactive nuclear species must be driven to a dynamic active state before the desire events can produce excess energy within the system.

2 Practical Triggering Methods Background

2.1 Variation in temperature

Good calorimetry often requires that the system under study be held at constant temperatures for long times. These are often run near room temperature to help control the environment around the systems. However, this is not beneficial in observing excess heat from CF cells. The electrolytic CF systems generate more heat at higher temperatures and maintaining them at or near boiling often yields greater excess power levels.[7] One simple method that is often useful in triggering excess power is the employment of a calibration resistor within the cell.[8] After the metal has been loaded slowly for times at least 10 times the calculated diffusion rates, power is supplied to a calibration resistor within the cell, raising the temperature of the cathode. Afterwards the baseline temperature of the cell may be seen to rise. (Figure 1) In other words, the heat pulse to the cell has triggered events within the cathode, which cause it to run hotter after the pulse for the same input power. The baseline temperature of the system is higher after the pulse than before. Some researchers have been known to reset their baseline after such events mistaking it for calorimeter drift- in effect throwing out the very signal that they seek.[9] This effect can also be seen occasionally in flowing electrolyte systems when the flow is pulsed instead of using a continual flow. The pulsing of the fluid flow allows the system to have temporary temperature rises. Many early experimenters falsely assumed that a continual flow through a bead bed system was better than the prescribed pulsed flow. Future researchers need to be aware of the heat trigger effect, plan for it and design for it.

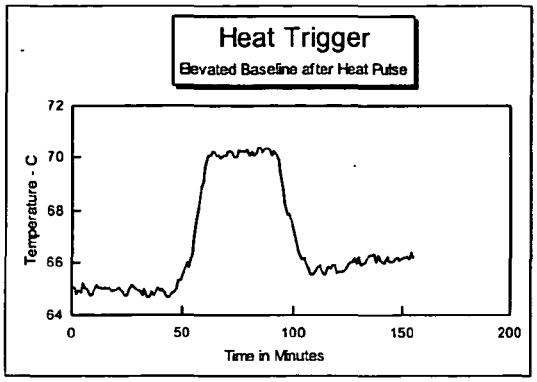

Figure 1. Baseline is elevated after a pulse to the calibration resister illustrating that more heat is now released from the cell with the same input power. Pd on Ag screen with Co, Re, and Th in LiOD using a 0.5 W pulse on 10W of electrolytic power.

Operating the cells at elevated temperatures is also beneficial in seeing excess heat effects.[7] The temptation is to use temperatures near room temperature for setting up CF systems. The elevation of the author's laboratory limits the temperature of liquid electrolytes due to its altitude of 2650 meters. This means that water based systems are limited to about 92 C in this lab due to the boiling point of the natural water control cells. One way around this is to run the cells at boiling. Fitting them with a reflux column so that they can run continually at their boiling points can help. As seen in Figure 2, there is an increase in the power output of the cells as their operating temperatures are elevated. Flow calorimetry can be done on such systems when connected to the water flow used in the condenser coils.

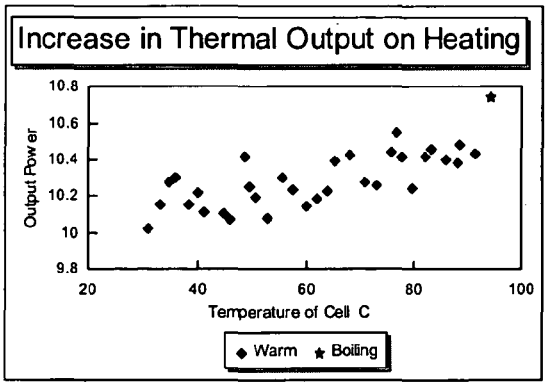

Figure 2. The cell's thermal output is seen to increase with increase in its operating temperature. This cell was a codepostion of Pd on to Ag with additives of Rh, Th, and Sm. The system is a flow system where water flows in both the condensing tube above the cell and about the cell. Changing the inlet temperature of the recovery water system controlled the temperature reached by the electrolyte.

2.2 Pressure

Pulsing the deuterium pressure to CF systems can occasionally trigger gas systems. This can be done by either gas supply systems or by acoustical excitation. The goal is to cause a flux of deuterium in an out of the system and across a gradient of chemical potential. For example, palladium black was prepared from solution by hydrazine reduction in which Ni was also included. This caused the palladium black to have an outer surface containing more Ni than the interior due to their relative chemical reactivities. The material was placed within an epoxy encased glass tube and deuterium gas was supplied to the material. The

temperature of the palladium black was found to rise upon the cycling of deuterium gas between 500 and 15,000 torr. In a separate experiment was conducted using a standing acoustical signal of 5,000 Hz by exciting a similarly filled tube. Temperature variations were found between the node and anti-node regions.

2.3 Current

Pulsing the current to palladium metal that has been loaded with deuterium can also trigger the release of excess heat. One author, Letts, has successfully triggered excess heat by superimposing RF signal on top of the electrolytic supply to electrolytic system.[10] This work was done at near 82 MHz. In a separate system a frequency near 25 MHz was used. First getting RF spectra of an active cell and then supplying the frequency that was being emitted by the active cell chose this.

Supplying pulsed current from end to end of a palladium wire used in an electrolytic system can also generate excess power. This results in electro migration of deuterium down the length of the wire.[11,12,13] Placing defects along the length of wire can enhance this effect. This can be achieved by ion implantation into the wire. The idea is to cause a "choke point" for the deuterium that is forced to migrate down the length of the wire. The deuterium flux undergoes both spatial and temporal changes as the wire is pulsed down its length.

The triode system also allows for a flux of deuterium with the host metal lattice. Two anodes are used in that design with different currents and voltages. The voltages are switched from side to side so that the deuterium within the cathode is not at equilibrium. A simpler design is to have the anode on only one side of the cathode and push the deuterium through the metal. In this configuration, it is best for the deuterium to transverse a chemical potential difference. For example, palladium can be coated thinly with another metal such Ni, Au, or other material in which the deuterium is at a higher chemical potential than the bulk palladium or other material used as the cathode. A simple and easy way to have a gradient is to temporarily reverse the current in the early stages of the electrolysis so that a resultant black or tan coating is applied to the cathode. However, the codeposition of palladium with additives such as Th and Co is usually beneficial to help the production of excess heat. The pulsing of the deuterium flux through the chemical potential seems to trigger the release of excess power (Figure 3). Some theoreticians have surmised that phonons are generated as deuterium falls from one chemical potential to another and those phonons coherently allow for the activation energy required for the assumed nuclear processes.

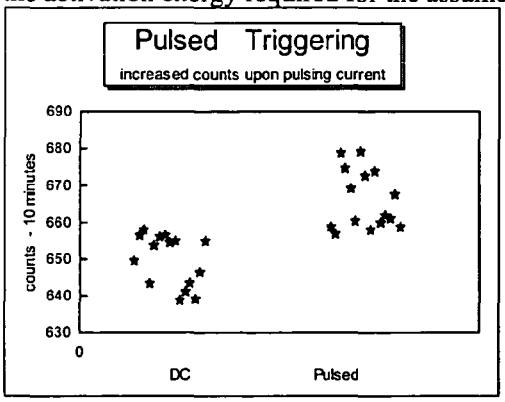

Figure 3. Both the excess power and radiation counts increase upon pulsing the current to an active cell. A cell using LiOD electrolyte and a cathode produced by codeposition of Pd black on Ag was used. Additions of Ni, Re and Th were used. The current was pulsed at 400 Hz with a 20% duty cycle. The average input power was 10W as read by a Clark Hess. The average 10-minute counts were elevated from 651 to 668 or about a 0.6 sigma signal. The excess heat of the cell also changed from 120 mW to and average of 287 mW.

2.4 .Chemical Triggering

Often cells are run in pristine conditions with highly refined LiOD, Pt and Pd. The cathode is normally seen to remain in a clean shiny condition and no excess is seen. The addition of Pd salts with additives into such a system often will help trigger the production of excess power.[14,15,16,17] The rational is that there needs to be a gradient in the deuterium's chemical potential for the production of excess power. It seems that the effect requires the deuterium flux to transverse between energy levels before the onset of the excess heat phenomena. Additives that have strong magnetic properties or elements with quadrapole moments seem to be beneficial in triggering the excess power events. A systematic search was taken to see what materials might increase any excess power production. The search was conducted by adding a range of metal salts to the Pd salts and codeposit them onto Ag. Chemical limitations due to chloride precipitation limited the uniformity of the method between elements but a general trend is seen in Figure 4, which is based on a range of chemical methods on the same mechanical system. Only a few of the cathodes have been analyzed to check what materials where actually plated out of solutions (Figure 5) and results in Figure 5 are based on pre-deposition compositions.

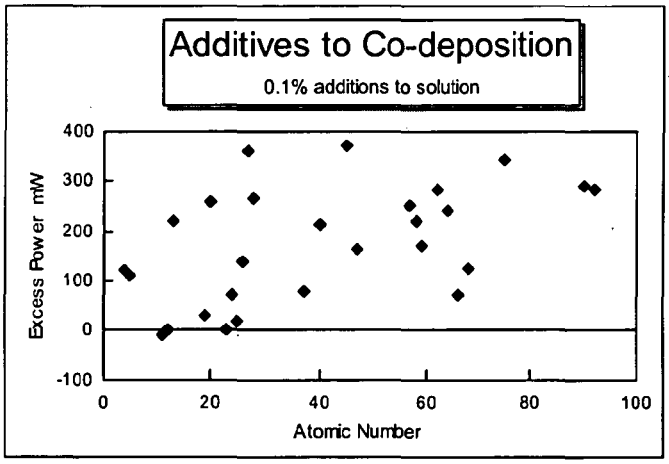

Figure 4. Relative effects of adding metals to during co-deposition of Pd on to Pt cathode. Excess power normalized for mW per cm^2 using 10 Watts of electrolytic power. Materials deposited from chloride salts where metal chlorides possible. Some elements required changes in plating chemistry. The elements of Rh, Re, Co, Th and U seem to be especially good for doping co-deposition systems.

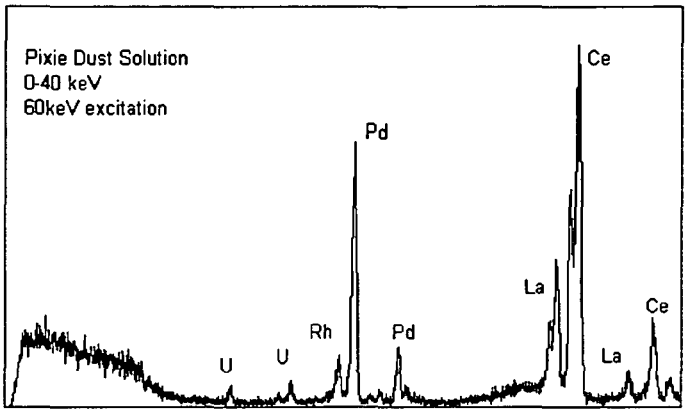

Figure 5. XRF analysis of cathode after codeposition of Pd with additives of U, Rh ,La and Ce. The U was added for increased D occupation at near lattice sites and the Rh to increase the absorption of D within the Pd black. The La and Ce where added to allow for spin exchanges to aid spin conservation terms for wave functions in the D + D> He nuclear channel.

Some theorists have proposed that the inclusion of He within the lattice structure is required for the D+ D > He reaction to proceed. Many of the chemical and laser triggering tests replaced air and any evolved gases with He before the triggering agent was employed. This assured that the triggering would not be of any chemical events with trapped oxygen and evolved hydrogen or similar events. Also some trials were made with He added during the codeposition process to see if He could be trapped within the deposition and affect any rates. No effects were seen by such He additions. This seems to rule out the possibility that the triggering was of some chemical reactions from the gas phase. Helium was also used in a similar manner to rule out hydrogen recombination effects here and in other systems presented here. However, it was not possible to test samples totally void of all He due to the ubiquitous He within all atmospheric and metal samples. Thus we could not see if the He was a necessary condition for excess heat production.

2.5 Magnetic Triggering

Changing the magnet field in the region of the cathode seems to often trigger the release of excess power. It is unclear at this time if this is truly a magnetic effect or if the changed magnetic field alters the flow of ions during electrolysis due to the Lorentz forces on the ions in solution and thus change the heat flow within the cell. However the effect is also seen in flow systems that are less subject to the location of heat production. The effect is most often seen when the cell is loaded with the magnetic field in one direction and then it is either reversed or placed 90 degrees from its original orientation when the cell is run at higher current densities. The effect was not seen when the magnetic field at the cathode drops below 200 gauss or when the magnetic field is uniform across the entire cell. The presence of small additions of Co and similar magnetic materials within codeposited systems seem to enhance the effect.

The important feature of the apparent magnetic effect is that the magnetic field be changed. However it is very difficult to run a well-controlled system when magnets are employed. This is because their orientation and placements close to the cell changes the "heat fin" effects when permanent magnets are used. The ion flows within the cell severely limits the certainty of isoperabolic systems unless stirring is employed and magnetic stirring

cannot be used in these systems. In short, the effect is not clearly shown and quantified at this time. It is illustrated here just to show other possibilities for study of the triggering of CF events. The effect deserves to be carefully studied by a specialized calorimeter that can be used despite the complications that the magnets bring to the problem.

2.6 Laser Triggering

Laser triggering of cold fusion events holds great promise as both a heat production method and as an investigative probing method. The cathode is first slowly loaded by electrolysis or by co deposition. It is then given a very thin overcoat of Au. At this time the current to the cathode is normally maintained at around 0.5 A/cm^2. Once in equilibrium, it is irradiated with a laser of specific frequency. The irradiation often produces a shift from equilibrium and the triggering of excess power. It should be noted that the system often responds at higher gains when the cathode is loaded for longer times (for example weeks) and that even a temporary stops in the electrolytic currents of 10 seconds is enough to de-load the cathode and prevent observation of the effect. Investigators are encouraged to maintain the cathode at 0.05A/cm^2 or better at all times once they are deposited with black and over-plated with Au. The use of uninterrupted power supplies is recommended to avoid the loss of a good cathode once identified.

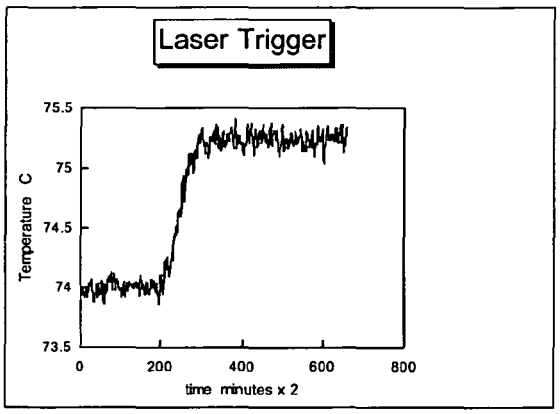

Figure 6. A laser of 670 nm is irradiated on a codeposition of Pd black containing additives of Co, Rh, and U placed on Ag. The temperature of the cell increases by 1.24C while the input power remains constant at 10 W. The laser power is 20 mW over an approximately 2mm spot diameter.

The cathode is first slowly loaded from a 1M LiOD solution over 3 to 5 days. It is then covered with a codeposited layer of Pd by adding Pd salts and any additives to the solution. It is quickly transferred to a new container for calorimetric studies after it acquires the Pd black surface. It is then loaded for at least a day to assure that it is fully loaded. A thin layer of Au is plated over the Pd black surface. A base line is obtained for the system and then the laser is applied to a spot on the cathode's surface. This normally results in about 200 to 300 mW of apparent excess power from the 30 mW of laser power. The excess power sometime reaches 500 to 800 mW of excess. It should be noted that some systems have run long enough to rule out all possible chemical reactions and recombinations as the source of the effect. Some excess power normally remains for a few hours even after the laser is removed. The addition of multiple lasers applied to the same spot on the cathode does not seem to increase the excess power signal above that expected from the addition of the laser power alone. This

would seem to indicate that the excess power is not proportional to the incident laser power but that it triggers the excess power events.

Our investigations are still underway at this time. However, there seems to be some indications that the polarization of the laser beam with respect to the external magnetic field may play a role in the level of excess power. At the present it seems that the excess power has a term that goes as E x B. The magnetic field is held fixed and the laser beam rotated by rotating the laser housing or by the insertion of quarter wave and half wave plates in the beam. The effect is not large but it is hard to think of a conventional explanation of why the polarization of the beam should affect the cell's temperature. Seeing the excess heat change by rotating the laser housing outside the calorimeter seems to rule out trivial conjectures as to the internal heat source. However the Poynting vector from such radiation would be directed in and out of the cathode's surface and could affect the deuterium flux in near surface areas. The optimum configuration at this time seems to be when the B field is parallel to the cathode's surface and more than 200 gauss as measured in the region of the cathode within the cell, and the laser beam is linearly polarized perpendicular to the B field and directed toward one of the corners where there is maximum loading gradients. There also seems to be a frequency reliance on the effect as addressed the authors' companion article in the proceedings. These effects deserve greater study.

3 Conclusion

We have omitted the details of the individual experiments due to space limitation but have seen that dynamic conditions are beneficial to observing the excess heat effect in CF system. The temptation is to design CF systems that have little or no variation in input conditions and temperatures. This is because of the restraints placed on experiments by good calorimetry. However, it is possible to do reasonable calorimetry and at the same time produce the required dynamic conditions that trigger the production of anomalous heat. It is important that future researchers realize that non- equilibrium events are often required for the effect to by initiated. Variations of input currents, operating temperatures, light intensity; magnetic fields, gas pressures, and chemical potentials all play a role in triggering the CF events.

Laser stimulation of CF cathodes is a promising approach that allows for surface probing and comparisons between surface conditions on the same cathode. The stimulation of the excess heat effect seems to be more a triggering of events than absolute requirements. Once triggered by the laser the excess heat can last for several hours.

References

1. McKubre, M.C.H., et al. *Excess Power Observations in Electrochemical Studies of the D/Pd System; The Influence of Loading.* in *Third International Conference on Cold Fusion, "Frontiers of Cold Fusion".* Nagoya Japan: Universal Academy Press, Inc., Tokyo, Japan (1992).
2. Fleischmann, M., S. Pons, and M. Hawkins, *Electrochemically induced nuclear fusion of deuterium.* J. Electroanal. Chem. **261**: p. 301 and errata in Vol. 263 (1989).
3. Schwinger, J., *Nuclear energy in an atomic lattice.* Prog. Theor. Phys., **85**: p. 711 (1991).

4. Chubb, S.R. and T.A. Chubb. *Theoretical Framework for Anomalous Heat and 4He in Transition Metal Systems.* in *8th International Conference on Cold Fusion*, Lerici (La Spezia), Italy: Italian Physical Society, Bologna, Italy(2000).
5. Chubb, T.A. and S.R. Chubb. *Radiationless Cold Fusion: Why Small "Crystals" Are Better, N(cell) Requirement, and Energy Transfer to Lattice.* in *Sixth International Conference on Cold Fusion, Progress in New Hydrogen Energy.* Lake Toya, Hokkaido, Japan: Industrial Technology Development Organization, Tokyo Institute of Technology, Tokyo, Japan. (1996).
6. Hagelstein, P.L., *Coherent fusion theory.* J. Fusion Energy, **9**: p. 451(1990).
7. Cravens, D. *Factors Affecting Success Rate of Heat Generation in CF Cells.* in *Fourth International Conference on Cold Fusion.* Lahaina, Maui: Electric Power Research Institute 3412 Hillview Ave., Palo Alto, CA 94304(1993).
8. Fleischmann, M. *The Experimenters' Regress.* in *5th International Conference on Cold Fusion.* Monte-Carlo, Monaco: IMRA Europe, Sophia Antipolis Cedex, France (1995).
9. Mallove, E., *MIT Special Report.* Infinite Energy, **4**(24): p. 64 (1999).
10. Bockis, J., Sundaresan, R., Letts, D., Minevski, Z., Triggering of Heat and Sub-Surface Change in Pd-D Systems, *Fourth International Conference on Cold Fusion.* Lahaina, Maui: Electric Power Research Institute 3412 Hillview Ave., Palo Alto, CA 94304 (1993).
11. Celani, F., et al. *Measurement of Excess Heat and Tritium During Self-Biased Pulsed Electrolysis of Pd-D2O.* in *Third International Conference on Cold Fusion, "Frontiers of Cold Fusion".* Nagoya Japan: Universal Academy Press, Inc., Tokyo, Japan (1992).
12. Celani, F., et al. *High Power μs Pulsed Electrolysis for Large Deuterium Loading on Pd Plates.* in *Fourth International Conference on Cold Fusion.* Lahaina, Maui: Electric Power Research Institute 3412 Hillview Ave., Palo Alto, CA 94304(1993).
13. Celani, F., et al., *Deuterium overloading of palladium wires by means of high power microsecond pulsed electrolysis and electromigration: suggestions of a "phase transition" and related excess heat.* Phys. Lett. A, **214**: p. 1(1996).
14. Miles, M., K.B. Johnson, and M.A. Imam. *Electrochemical loading of hydrogen and deuterium into palladium and palladium-boron alloys.* in *Sixth International Conference on Cold Fusion, Progress in New Hydrogen Energy.* Lake Toya, Hokkaido, Japan: New Energy and Industrial Technology Development Organization, Tokyo Institute of Technology, Tokyo, Japan (1996).
15. Miles, M. *Calorimetric Studies of Palladium Alloy Cathodes Using Fleischmann-Pons Dewar Type Cells.* in *8th International Conference on Cold Fusion.* 2000. Lerici (La Spezia), Italy: Italian Physical Society, Bologna, Italy.
16. Szpak, S., et al., *Electrochemical charging of Pd rods.* J. Electroanal. Chem., **309**: p. 273 (1991).
17. Szpak, S., P.A. Mosier-Boss, and J.J. Smith, *On the behavior of Pd deposited in the presence of evolving deuterium.* J. Electroanal. Chem., **302**: p. 255(1991).

(Paper presented at the American Physical Society Centennial Conference March 26th, 1999)

Production of ^{4}He from deuterium during contact with nano-particle palladium on carbon at 200° C and 3 atmosphere deuterium pressure

Russ George* (Palo Alto, CA)
(* Communicating author - rgeorge@d2fusion.com)

(Participating scientists from SRI declined to be listed as co-authors of this paper and later presented similar paper(s) on these experiments along with results from additional replications)

Abstract: When a suitable material (nano-particles of palladium on a carbon support) is saturated with deuterium gas (D_2) at a pressure of 3 atmospheres and 200° C an isotopic temperature effect (D_2 is hotter) is accompanied by an increasing concentration of ^{4}He. The helium concentration as measured by on-line mass spectroscopy is observed to increase over several weeks ultimately reaching a concentration well in excess of the concentration of ^{4}He measured in the surrounding air. Control phases of experiments with both H_2 and D_2 (in an apparently inactive experiment) show neither excess heat nor increasing ^{4}He.

Recently, April 1998, Les Case (New Hampshire, USA) reported at the ICCF-7 scientific conference *[1]* his work with palladium on carbon materials where saturation with deuterium (D_2) gas and hydrogen (H_2) gas at elevated temperatures revealed an isotope dependent heating effect. This effect was reported to be observable as a higher steady state temperature in D_2 , more than 5° C and roughly equivalent to a few watts in his reaction vessel, when compared with H_2. Further Case reported on observations of ^{4}He found at a concentrations above 10 ppm measured via giant sector mass spectroscopy at Oakridge National Laboratory. Recognizing Case's work bore similarities of nano-particle palladium, deuterium loading conditions, and helium findings George was familiar with from his own work he contacted Case with the purpose of proposing to replicate the nano-particle palladium on carbon experiments. Cooperating with Case by phone George designed new experiments to be operated within a laboratory provided by SRI International with the active participation of SRI scientists Fran Tanzella and Mike McKubre. We have now replicated and improved upon the measurement of ^{4}He from experiments with the identical materials reported by Case.

The experiments are operated while affixed to an Extrel quadrapole mass spectrometer belonging to the Electric Power Research Institute of Palo Alto, CA. and located at SRI International in near-by Menlo Park, CA. The material (~0.4% by weight Pd on carbon – G75/d) was provided by United Catalyst of Louisville, KY., the same palladium on carbon material used by Case. A variation to Case's experiment was made to conduct the reaction in 50cc stainless steel (SS) Nupro sample flasks (25mm x 135mm) considerably smaller than Case's standard 1.7 liter SS reaction vessels. The experiments are semi-permanently fixed via all metal SS Swagelok and Cajon fittings to an Extrel C-50 Quadrapole Mass Spectrometer. The mass spec is carefully configured and calibrated to provide baseline peak resolution of ^{4}He and D_2 in small gas samples at concentrations of helium down to a few hundred parts per billion (see figure 1). To minimize the deuterium background a liquid nitrogen carbon cold trap was employed on the inlet to the mass spec *[2]*.

The experiment is run by initially loading the 50cc vessel with 10 grams of Pd

carbon material (0.5gm/cc) and high purity hydrogen (~ 0.1 ppm ^{4}He) to ~3.4 atm (50 psig). The vessel is repeatedly flushed to a LN_2 cold trapped vacuum (10^{-4} torr) and re-filled with H_2 to reduce any contaminants on the material. During the gas loading procedure a wrapped Joule heater on the outside of each vessel at about 10 watts establishes a steady state temperature of about 200° C as measured by an internal thermocouple. One vessel was then switched to D_2 via several flushes of high purity deuterium (~ 0.1 ppm ^{4}He) interspersed with evacuation to vacuum performed to remove the residual H_2. The vessels are located within a pair 2 liter dewars filled with vermiculite to help support and insulate them. A computer based data acquisition system collects power and temperature readings in the vessels on five-minute intervals.

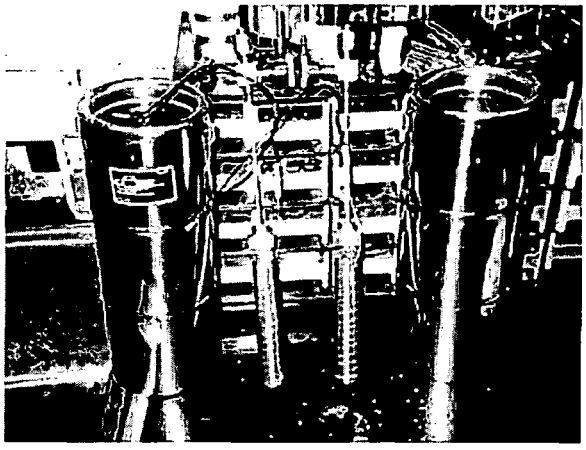

Experiment Vessels and Dewars Prior to Start of the Experiment

The protocol for helium analysis is to run three gas samples (two calibration control and one experiment sample) through the mass spectrometer, operated by Tanzella and George, one after another over the course of approximately half an hour. Prior to each sample a calibration background sample from the MS instrument and cold trap is analyzed to establish instrument background. The first and third samples are of lab air at ~20 torr, that is taken to be approximately 5.22 ppm ^{4}He based on earlier work and confirmed by the use of calibrated gas standards. These samples are allowed to fill the few ml volume manifold and then passed through the active carbon liquid nitrogen cold trap and into the mass spec. Between the samples the mass spec is evacuated to vacuum. The experiment vessel sample analyses are made in the same fashion. As the experiment is always exposed to this laboratory air it is important to carefully calibrate the mass spec and to insure that any helium found in the experiment vessel cannot be sourced from the helium available as contamination from the lab air. Based on a concentration of 5.22 ppm ^{4}He in the lab air and the pressure of ~3.4 atm in the experiment vessels the maximum helium concentration that could arise in the vessel from a diffusion leak into the vessel would be ~ 1.2 ppm ^{4}He.

At the start of the experiments the helium content of the D_2 and H_2 used to fill the vessels was measured and found to be 0.1 – 0.3 ppm ^{4}He or less. This appears to be the limit of sensitivity of the mass spec instrument. Once the vessels were filled with D_2 and H_2 (as initial control) the gases were allowed to remain in the vessels for several days at ~ 200° C and then measured for ^{4}He. The ^{4}He was found to still be at the 0.1- 0.3 ppm level in both vessels essentially at the limit of sensitivity of the mass spec instrument.

After loading the now-modified vessel with D_2 and raising the temperature to about 200° C using about 9.3 watts of heating, helium was measured at 0.2ppm (the same level found in the D_2 source cylinder). The Joule heating for the control vessel was ~ 9.7 watts. Our thermometry / calorimetry at this point in time is insufficient to make any declaration as to an excess heat effect. After about 4 days the helium content of the D_2 vessel began to increase on a steady basis. (see data figure 2) while the other "control" vessel showed ^4He remaining at the instrument background level of 0.1-0.3 ppm. After several days observing that the background levels of helium had not grown in the control vessel while it appeared to be growing steadily in the D_2 vessel it was decided to flush the H_2 from the control vessel and add D_2. A series of several flushes to vacuum and fills with D_2 was undertaken finally leaving the vessel filled with ~3.4 atm D_2. Over the course of 27 subsequent days analysis samples were taken on a frequent but not quite daily basis (see data figure 1) while the paired vessels were held at ~ 200° - 210° C.

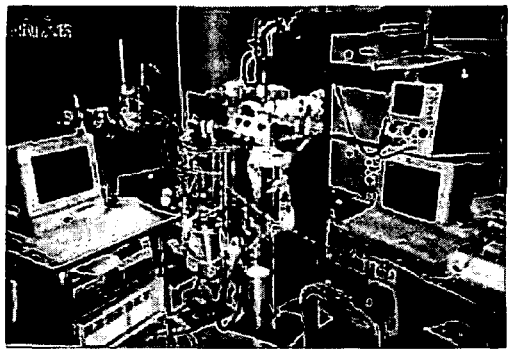

Experimental Set-Up in SRI's Laboratory where the helium findings reported here were obtained. Experiments are in the center bounded by the Extrel Quadrapole Mass Spec on the right and control electronics to the left

Helium steadily increased in the one vessel exceeding the potential "diffusion leak" concentration of 1.2 ppm on approximately day eight. By day 27 the helium content of the vessel had reached 11.0 ppm ($5x10^{16}$ atoms 4He) well above the ambient air concentration of 5.22 ppm. The rate of ^4He production conforms to approximately 90-100 milliwatts of power. This power output conforms very favorably to the expected power of ~100 milliwatts predicted from Case's originally reported power measurements when adjustment is made for the substantially smaller vessel used in these experiments. The "control" experiment tells us the helium we observe is coming from neither the walls of the experimental vessel nor from helium somehow entrained in the starting material and now being cooked out. It is believed this "control" cell is not producing helium because of inadequate flushing of the hydrogen with deuterium during the deuterium filling process. However it is noted that in the extensive experience of Case many palladium on carbon catalyst samples both from United Catalysts and other suppliers do not produce the observed isotopic heating effect.

To further confirm that helium was not trapped in the material before the start of this experiment a sample(~10mg UC G75-d catalyst) was analyzed in the laboratory of Prof. Y. Arata in Osaka Japan. Heating the sample to a temperature in excess of 1300° C in Prof. Arata's high vacuum QMS that is sensitive to approximately $1x10^6$ atoms of ^4He revealed no significant helium was released from the Pd carbon material [3].

Lending some support to this work is the published work of Y. Arata of Osaka Japan reported in the Japan Academy in 1997 [4] on anomalous heat and production of ^3He and ^4He in ratios highly skewed from natural abundance ratios when deuterium under high pressure is contacted with nano-particle palladium. George whose work in the field has recently focused on nano-domains as the location for these reactions collaborated with Arata in his laboratory in the summer and fall of 1997. That effort contributed to an assumption that the work reported by Case had commonalties to many experiments in this general field.

One feature of the apparent nuclear fusion reactions that this evidence suggests but is unexpected is the absence of energetic penetrating radiation (especially 14Mev neutrons and 23 Mev gammas) which are expected from D+D fusion under plasma or ion beam collision conditions. Further absent are lower energy neutrons that would result from energetic alpha particles (greater than 2 Mev) producing neutrons from spallation reactions on a variety of trace element nuclei. Case had reported that he had looked diligently for the signature of neutrons, tritium, and other energetic nuclear radiations. In spite of enlisting the support in this search of outside labs with suitable equipment to observe these kinds of products none have been observed.

A theoretical mechanism to explain the experimental results is desirable and this data may help us make progress in this direction. Two theoretical aspects of fusion must be attended to in any explanation. First one must somehow get past the Coulomb barrier and fuse the two deuterons. If this occurs then the resulting compound nucleus is expected to decay into a ^4He nucleus in a time frame on the order of $1x10^{-22}$ seconds with the emission of a 23.8 Mev gamma. Since in the present reactions we do not see this energetic and penetrating gamma the second requirement is that this large amount of energy must be coupled to the lattice over a long time frame so that in small packets, phonons perhaps, the 23.8 Mev is conveyed away as heat.

Thus the reaction might be written D+D ® alpha + phonons (23.8Mev)

Conditions needed for such reaction are found within the condensed matter environment of deuterium saturated palladium. The rates of nuclear reactions can differ drastically from those expected in vacuum, due to strong inter-nuclear many-body correlation effects and/or the statistical-mechanical effects inherent in condensed matter systems [5].

Additional experiments are now underway which will contribute to the understanding of these reactions. These include expanded mass spectroscopy studies quantify ^3He and its ratio with ^4He. Studies of the helium production rates of various similar materials are also scheduled to cross correlate with Case's report that some similar materials do not produce the observed deuterium heating effect. Materials and micro-chemical studies of the active and similar though inactive Pd carbon materials have also been initiated by the George with help from colleagues in allied organizations.

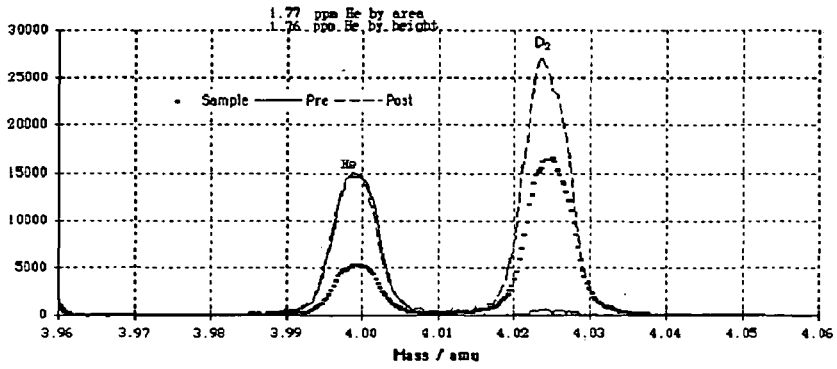

Figure 1 - Typical output from the Extrel Quadrapole mass spectrometer showing full baseline resolution of ^4He and D_2. During part of the time of these experiments this excellent mass resolution was somewhat less but did not diminish to less than full peak separation.

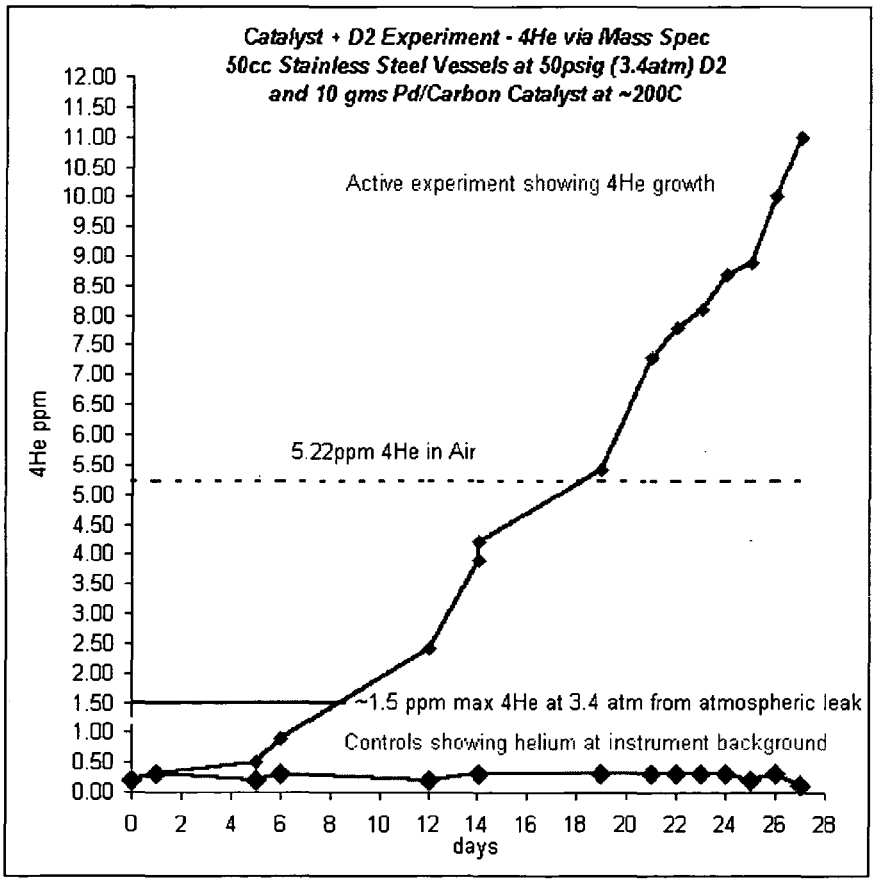

Figure 2- Chart of data showing increasing helium in "hot" experiment vs. no increase in control experiment. The control experiment started out with H_2 and was changed to D_2 after several days.

The author(s) acknowledge the assistance provided by Mike McKubre and Fran Tanzella (SRI International), Doug Perkins (United Catalysts of the Sud Chemie companies), Roger Ray

and Len Marshall (mass spectroscopy Oakridge National Laboratory), Prof. John Dash (Physics Portland State University), Andrey Chuvilin (Boreskov Inst. Of Catalysis, Russia), and Tom Passell (EPRI Nuclear Power Division).

---

[1] Case, ICCF-7 Conference Presentation, Vancouver, B.C., Canada, April 1998 (soon to be published in conf. Proceedings)

[2] H. Farrar and B. Oliver, A Mass Spectrometer to Determine very low Levels of Helium in small Solid and Liquid Samples, J. Va. Sci. Technology, A4, 1740, 1968

[3] Personal communication Dr. Fran Tanzella present in Arata Laboratory for analysis

[4] Arata and Zhang, Presence of Helium (^{4}He, ^{3}He) Confirmed in Deuterated Pd-black by the "V_i Effect" in a "closed QMS" Environment, Japan Academy Series B Physical Sciences, April 1997

[5] Nuclear Fusion in Dense Plasmas, Setsuo Ichimaru, Reviews of Modern Physics Vol. 65, No.2, April 1993

Contact the author via e-mail at rgeorge@d2fusion.com

Details from this work have appeared in popular media including WIRED Magazine Oct. 98 and in various other news reports. Work by the author continues via d2fusion Technologies in cooperation with organizations and National Laboratories in the United States and abroad.

Back to top of page

Back to d2fusion Home Page

1.C

Nuclear Physics A175 (1971) 225—271; © *North-Holland Publishing Co., Amsterdam*

NEUTRON STAR MATTER

GORDON BAYM †, HANS A. BETHE †† and CHRISTOPHER J. PETHICK †††

Nordita, Copenhagen, Denmark

Received 4 May 1971

Abstract: The matter in neutron stars is essentially in its ground state and ranges in density up to and beyond 3×10^{14} g/cm^3, the density of nuclear matter. Here we determine the constitution of the ground state of matter and its equation of state in the regime from 4.3×10^{11} g/cm^3 where free neutrons begin to "drip" out of the nuclei, up to densities $\approx 5 \times 10^{14}$ g/cm^3, where standard nuclear-matter theory is still reliable. We describe the energy of nuclei in the free neutron regime by a compressible liquid-drop model designed to take into account three important features: (i) as the density increases, the bulk nuclear matter inside the nuclei, and the pure neutron gas outside the nuclei become more and more alike; (ii) the presence of the neutron gas reduces the nuclear surface energy; and (iii) the Coulomb interaction between nuclei, which keeps the nuclei in a lattice, becomes significant as the spacing between nuclei becomes comparable to the nuclear radius. We find that nuclei survive in the matter up to a density $\backsim 2.4 \times 10^{14}$ g/cm^3; below this point we find no tendency for the protons to leave the nuclei. The transition between the phase with nuclei and the liquid phase at higher densities occurs as follows. The nuclei grow in size until they begin to touch; the remaining density inhomogeneity smooths out with increasing density until it disappears at about 3×10^{14} g/cm^3 in a first-order transition. It is shown that the uniform liquid is unstable against density fluctuations below this density; the wavelength of the most unstable density fluctuation is close to the limiting lattice constant in the nuclear phase.

1. Introduction

The identification of pulsars as rotating neutron stars [1]) has renewed interest in the properties of matter at very high densities. The density of matter in a neutron star increases with depth from low values near the surface to central densities on the order of the density of matter in nuclei (≈ 0.2 nucleons/fm^3 or 3×10^{14} g/cm^3) or greater. Except in the outermost layer of a neutron star, the matter is relatively very cold in the sense that characteristic energies required for microscopic excitations are very much greater than the characteristic thermal energy, $k_B T$. If the matter has had sufficient time in the earlier hot stages of the star to reach nuclear equilibrium, one may consider it to be in its absolute ground state. This requires that nuclear equilibration rates be fast compared with cooling rates.

Up to a mass density $\rho \sim 10^7$ g/cm^3, the ground state of matter consists of ^{56}Fe nuclei arranged in a lattice, most likely body-centered cubic (bcc), together with a

† Permanent address: Department of Physics, University of Illinois, Urbana, Illinois, 61801.
†† Permanent address: Laboratory of Nuclear Studies, Cornell University, Ithaca, New York 14850.
††† Fellow of Magdalen College, Oxford, England. Permanent address now University of Illinois, Urbana, Illinois 61801.

sea of electrons [2,3,4]). Beyond $\rho \sim 10^3$ g/cm^3 the electrons are fully ionized, and above $\sim 10^6$ g/cm^3 they are relativistic and virtually free. As the density of matter rises, with increasing depth in the star, the equilibrium nucleus present becomes more and more neutron rich, as a result of electron capture. The binding energy of the last neutron in the equilibrium nucleus becomes smaller, and eventually, at a density [4]) $\rho_d = 4.3 \times 10^{11}$ g/cm^3, it becomes favorable for neutrons to begin to "drip" out of the nuclei. At densities between ρ_d and $\rho \sim 2.4 \times 10^{14}$ g/cm^3, the matter is still solid, and consists of a lattice of nuclei immersed in a pure neutron gas, in addition to the electron gas; we shall refer to this regime as the *free neutron regime*. The nuclei dissolve at about nuclear matter density and at higher densities the matter consists of a uniform liquid of neutrons with a small fraction of protons and electrons. As we shall see, muons also appear at about this point. Finally, at densities a few times higher, various hyperons, Σ^-, Λ°, etc., make their appearance.

In this paper we shall be concerned with determining the nuclei present in the free neutron regime, as well as the properties of the liquid phase, the nature of the transition between these two phases, and the equation of state of the matter in these phases. The calculations given here are for densities below $\approx 5 \times 10^{14}$ g/cm^3, beyond which the usual techniques of nuclear matter theory require modification.

In two recent papers [5,6]) on the properties of the free neutron regime, the semi-empirical mass formula [7]) was used to describe the nuclear energies. The dissolving of the nuclei was found in both these papers to take place at $\rho \approx 5 \times 10^{13}$ g/cm^3. We have found on closer examination that this result is very sensitive to the particular description used for the neutron gas surrounding the nuclei; in ref. [5]), the Nemeth-Sprung "1a" description [8]), and in ref. [6]), a description based on a Levinger-Simmons potential were used. In particular when more accurate calculations of the properties of neutron matter are used, one finds the curious result that it is impossible to construct a thermodynamically consistent picture of the dissolving of the nuclei. Both μ_n, the neutron chemical potential (equal to minus the separation energy) and the pressure P must be continuous through the transition. The inconsistency arises from the fact that according to the semi-empirical mass formula, μ_n must always be less than ≈ 8.3 MeV for the nuclei present. This number is a sum of ≈ -16 MeV volume energy and ≈ 24 MeV symmetry energy; surface and Coulomb terms contribute $\sim 5\,\%$ of the total. However, the pressure in the nuclear phase is always *higher* than that for the liquid phase at the same μ_n. The nuclear phase remains thermodynamically preferable; there is no way to have both μ_n and P continuous across the transition. This limitation on μ_n is clearly unphysical, and is due to the use of the semi-empirical mass formula in the region of very neutron-rich nuclei, for which it is not designed.

One important physical feature not taken into account in the semi-empirical mass formula is that the matter inside very neutron-rich nuclei is quite similar to both the pure neutron gas outside the nuclei, as well as to the neutron matter in the uniform liquid state. However, the bulk terms in the usual semi-empirical mass formula

describe this matter very differently from the calculations one uses for the neutron matter. In the present work we shall remove this inconsistency by using a single expression for the energy of bulk nuclear matter, as a function of density and proton concentration, to describe both the nuclear matter in nuclei, the neutron gas outside, and the uniform liquid state. As a result we shall find that it is possible to have coexistence of bulk nuclear matter with a pure neutron gas up to $\mu_n \sim 30$ MeV (compared with the ≈ 8.3 MeV result earlier); this allows us to develop a consistent picture of the transition.

A second important physical effect not taken into account in the earlier work is the attractive Coulomb interaction between nuclei – the ordinary solid-state lattice binding energy. The optimal nuclear size in neutron star matter is determined by a delicate balance between nuclear Coulomb and surface energies; the surface energy favors nuclei with a large number of nucleons, A, while the nuclear Coulomb self-energy, that of protons within a nucleus, favors small nuclei. The lattice energy, of similar structure to the Coulomb self-energy, but of opposite sign, favors large nuclei. When the lattice energy begins to become comparable in magnitude with the nuclear Coulomb self-energy, that is, when the nuclear radius becomes comparable with the spacing between nuclei, the effect on the equilibrium value of A becomes considerable. For example, when neutron drip first sets in, inclusion of the lattice energy raises A by $\sim 15\,\%$. At much higher densities the effect is dominant and can no longer be treated as a perturbation. Indeed, were the nuclei to fill all of space, the total Coulomb energy would vanish, since the uniform electron distribution would exactly compensate the uniform proton distribution. It is vital then to include the lattice Coulomb energy in order to have a consistent description of the matter at densities approaching that of nuclear matter. In addition, the lattice energy, by favoring the existence of nuclei, tends to raise the maximum density at which nuclei can exist.

The third physical feature that requires a more careful treatment in the free neutron regime is the nuclear surface energy. One expects the presence of the outside neutron gas to reduce the surface energy, since as the density of the system increases the inside and outside matter become more and more alike; were they the same there would of course be no surface energy. The semi-empirical mass formula takes no account of this reduction of the surface energy. In ref. [5]) it was estimated that this reduction would be only $\sim 15\,\%$, but this was because the transition was thought to be at a much lower density than we find here. At higher mass densities the effect is very large; the reduction of the surface energy lowers the energy of the nuclear phase and thus in turn also raises the maximum density at which nuclei can be present.

Furthermore, the pressure of the neutron gas to which the nuclei are exposed is now sufficiently high that its effect on the nuclei cannot be treated as a perturbation, as was done in ref. [5]). To remedy these various difficulties with the semi-empirical mass formula we describe the nuclei by a *compressible liquid-drop model*† which has

† Generalizations in this spirit of the semi-empirical mass formula for ordinary nuclei with no external neutron gas have been given by Myers and Swiatecki [9]) and Weiss and Cameron [10]).

the following features:

(i) The nucleus is pictured as a drop of compressible nuclear matter with a well-defined surface; unlike in the semi-empirical mass formula the density of the matter inside the nucleus is treated as a variable, determined by equating the pressure of the nucleus to the outside neutron gas pressure.

(ii) The energy of the nucleus we take to be a sum of a volume energy, given by the same energy function used to describe the neutron matter; a Coulomb energy, including the lattice energy; and a surface energy appropriately modified by the presence of the outside neutron gas.

(iii) The parameters of the model are chosen to give reasonable fits to masses of observed nuclei. These energies depend on the density of the interior matter, on A, the total nucleon number, and Z, the total proton number, and, in the case of the surface energy, on the outside neutron gas density as well.

We shall treat A and Z as continuous variables and neglect shell effects and possible deformations of the nuclei. We shall also neglect pairing effects both in the nuclei and the neutron matter.

The most important conclusion of our work is that nuclei are present in neutron star matter up to mass densities on the order of symmetric nuclear matter density (3×10^{14} gm/cm^3), some 4–5 times higher than predicted by the earlier calculations [refs. [5, 6])]. This rather large difference comes about since the effects we have taken into account here encourage the formation of nuclei, and they all become increasingly important as the density is increased. An important consequence of this for the structure of neutron stars is that the crust can be much thicker than previously thought and in fact, there can exist completely solid stable neutron stars [4]). The crust is also capable of storing substantially more elastic energy than previously believed [11]).

We find that as the matter density increases, Z, the number of protons per nucleus, increases rather slowly from about 40 at neutron drip to about 100 at $\rho \sim 10^{14}$ g/cm^3, and then increases rapidly to several hundred by the transition. On the other hand the nucleon number A increases steadily with increasing mass density, starting at ~ 120 at neutron drip, increasing to ~ 700 at $\rho \sim 10^{14}$ g/cm^3; near the transition where the nuclei dissolve the proton concentration in nuclei is about 5 %, only slightly above that in the uniform liquid.

The structure of this paper is the following. In sect. 2 we derive the general equilibrium conditions that determine the type and density of nuclei present in the free neutron regime. To evaluate these conditions we need an expression for the energy of nuclei immersed in a free neutron sea, as well as the energy of bulk neutron matter. The nuclear energy formula is developed in sects. 3, 4 and 5. In sect. 3 we construct an expression for the energy of bulk nuclear matter as a function of density and proton concentration; for zero proton concentration this expression gives the energy of pure neutron matter. We also discuss here the coexistence between bulk nuclear matter and a pure neutron gas. Sect. 4 is devoted to the nuclear surface energy while in sect. 5 we discuss the Coulomb energy.

With the resulting nuclear mass formula we carry out, in sect. 6, an explicit evaluation of the properties of the free neutron regime. In sect. 7 we consider the possibility of protons also dripping from the nuclei, and conclude that this is unlikely to occur. In sect. 8 we determine the properties of the uniform liquid, and in sect. 9 we discuss the instability of this liquid against proton clustering, and the nature of the transition between the phase with nuclei and the uniform liquid. Finally, sect. 10 contains a discussion of the equation of state of the matter in neutron stars.

2. Equilibrium conditions

In the free neutron regime (4.3×10^{11} g/cm^3 $\leqq \rho \lessapprox 2.5 \times 10^{14}$ g/cm^3) the matter consists of a lattice of nuclei immersed in neutron and electron seas. Free protons do not appear, except possibly just before the nuclei dissolve. In this section we construct an expression for the total energy of the system, and derive the conditions that determine, at any given matter density in complete nuclear equilibrium at zero temperature, the type of nucleus present and the relative numbers of nuclei and free neutrons.

We picture the nucleus as having a well-defined surface; nucleons within this surface we associate with the nucleus. We let Z be the total number of protons within the surface and A the total number of nucleons within the surface. The energy † $W_N(A, Z, V_N, n_n)$ of a given nucleus in the matter depends on A and Z, as well as on the number density n_n of the neutron gas *outside* the nucleus and the volume V_N of the nucleus. W_N is taken to include the rest mass of the nucleons. The outside neutrons affect the energy of the nuclei both by modifying the nuclear surface energy and by exerting a pressure on the nuclei; the pressure tends to decrease the nuclear volume, while the modification of the surface energy has the opposite effect. (Nuclei in ordinary matter have zero pressure on their surfaces.) For this reason the nuclear volume must be considered a variable.

We assume the neutron gas outside the nuclei to be uniform and of density

$$n_n = \frac{N_n}{V - N_N V_N}, \tag{2.1}$$

where N_n is the total number of neutrons outside nuclei, in a volume V, and N_N is the total number of nuclei in that volume; $V - N_N V_N$ is thus the total volume outside the nuclei. We denote by $E_n(n_n)$ the energy (including rest masses) of the neutron gas per unit volume occupied. Because electron screening lengths are relatively large, the electrons completely penetrate the nuclei and have a uniform density n_e throughout. Charge neutrality implies that

$$n_e = \frac{ZN_N}{V} \equiv Zn_N \tag{2.2}$$

† We shall use the subscript N to refer to nuclei and n to neutrons; the letter W shall denote energies, while the letter E shall denote energies per unit volume.

as long as all the protons are in nuclei, and no muons are present. The energy density $E_e(n_e)$ of the electrons is, to within terms of order $Z^{\frac{2}{3}}e^2/\hbar c$, just the energy of a free electron gas.

Finally, we must take into account Coulomb interactions between nuclei immersed in a uniform background of electrons. This "lattice" energy, denoted by W_L per nucleus, is negative and for a body-centered cubic (bcc) lattice, for example, is given by [12])

$$W_L = -\frac{1.82Z^2e^2}{a}, \tag{2.3}$$

where $a = (2/n_N)^{\frac{1}{3}}$ is the lattice constant; thus when a is $\sim r_N$, the nuclear radius, this energy is of the same order as the Coulomb energy, $\approx \frac{3}{5}(Z^2e^2/r_N)$, of an individual nucleus. In particular, if one imagines the nuclei filling all of space, then both the protons and electrons are uniformly distributed, and the *total* Coulomb energy, nuclear plus lattice, must vanish. The lattice energy thus plays a crucial role in determining the type of nuclei present. At higher densities, $\gtrsim 10^{14}$ g/cm^3, the corrections to (2.3) due to the finite size of the nucleus become important; these will be considered in sect. 5. It should be emphasized that the lattice energy is not an effect peculiar to the solid state; it is only a few percent smaller in magnitude for a liquid [13]).

The total energy per unit volume of the system, including all rest masses, is then

$$E_{tot}(A, Z, n_N, V_N, n_n) = n_N(W_N + W_L) + (1 - V_N n_N)E_N(n_n) + E_e(n_e). \tag{2.4}$$

The factor $1 - V_N n_N$ is the fraction of the total volume occupied by the neutron gas.

The equilibrium conditions for determining A, Z, n_N, V_N and n_n at a given mean density n_b of baryons,

$$n_b = An_N + (1 - V_N n_N)n_n, \tag{2.5}$$

are derived by minimizing E_{tot} with respect to its arguments, keeping n_b fixed. This leads to four independent conditions, which we now discuss. Consider first the determination of the optimal number of nucleons in a nucleus. Let us ask the question: given, in a unit volume, a certain number $n_N Z$ of protons and $n_N(A - Z)$ of neutrons in nuclei, a fixed total fraction $n_N V_N$ of the volume occupied by nuclei, and a fixed number of neutrons outside the nuclei, what is the optimal A? This is determined by minimizing E_{tot} with respect to A at fixed $n_N A$, $n_N Z$, n_n and $n_N V_N$. In this variation n_e, and the free neutron energy are unaltered, and the resulting condition is simply

$$\frac{\partial}{\partial A}\left(\frac{W_N + W_L}{A}\right)_{x, n_N A, n_N V_N, n_n} = 0, \tag{2.6}$$

where

$$x = \frac{Z}{A} \tag{2.7}$$

is the fractional concentration of protons in nuclei. Eq. (2.6) simply states that the energy per nucleon in nuclei is a minimum.

Secondly, the nuclei must be stable against β-decay. This is the statement that changing a proton (and electron) into a neutron must raise the energy, or in other words, that E_{tot} is minimized with respect to variations in Z at fixed A, n_N, V_N and n_n. Carrying out this minimization, using (2.2), yields the condition

$$\mu_e = -\frac{\partial}{\partial Z}(W_N + W_L)_{A, n_N, V_N, n_n} = -\frac{\partial}{\partial x}\left(\frac{W_N + W_L}{A}\right)_{A, n_N, V_N, n_n}, \tag{2.8}$$

where

$$\mu_e = \frac{\partial E_e}{\partial n_e} \tag{2.9}$$

is the electron chemical potential (including the rest mass).

The minimum energy (measured with respect to the neutron rest mass m_n) required to add a neutron to a nucleus, i.e., the chemical potential of the neutrons in nuclei, is given by

$$\mu_n^{(N)} = \left.\frac{\partial(W_N + W_L)}{\partial A}\right|_{Z, n_N, V_N, n_n} - m_n c^2. \tag{2.10}$$

Similarly, the chemical potential of protons in nuclei (measured with respect to the proton rest mass m_p) is given by the minimum energy required to add a proton to a nucleus at fixed neutron number $A-Z$:

$$\mu_p^{(N)} = \frac{\partial}{\partial Z}(W_N + W_L)_{A-Z, n_N, V_N, n_n} - m_p c^2. \tag{2.11}$$

In terms of the proton and neutron chemical potentials, the β-stability condition (2.8) reads

$$\mu_e - (m_n - m_p)c^2 = \mu_n^{(N)} - \mu_p^{(N)}. \tag{2.12}$$

This equation determines the electron chemical potential in terms of the nuclear parameters.

If $\mu_n^{(N)}$ is negative, then there is no neutron gas outside the nuclei; $\mu_n^{(N)}$ increases with increasing baryon density, and when it reaches zero †, neutrons begin to "drip" out of the nuclei. In order for the neutrons in the gas to be in equilibrium with those in nuclei, the neutron chemical potential, $\mu_n^{(G)}$, in the gas must equal that in the nuclei. This condition is derived by minimizing E_{tot} with respect to A, now at fixed V_N, n_N, Z and n_b, a variation corresponding to transferring a neutron from the gas to the nucleus, a process that should cost zero energy in equilibrium. At fixed n_b, we have

$$\frac{\partial n_n}{\partial A} = -\frac{n_N}{1 - V_N n_N}, \tag{2.13}$$

† Strictly speaking, the lowest energy of a free neutron state outside the nuclei differs slightly from zero due to the interaction of the neutron with the nuclei; this effect is very small however, since at the threshold for free neutrons, the nuclei occupy only about 10^{-3} of the total volume of space.

so that

$$\left.\frac{\partial E_{\rm tot}}{\partial A}\right|_{V_{\rm N}, n_{\rm N}, Z, n_{\rm b}} = 0$$

$$= n_{\rm N}\left[\frac{\partial}{\partial A}(W_{\rm N}+W_{\rm L})_{V_{\rm N}, n_{\rm N}, Z, n_{\rm b}} - \frac{\partial E_{\rm n}}{\partial n_{\rm n}}\right]. \tag{2.14}$$

Using (2.10) and (2.13) we then find

$$\mu_{\rm n}^{\rm (G)} \equiv \left(\frac{\partial E_{\rm n}}{\partial n_{\rm n}} - m_{\rm n}c^2\right) + \frac{n_{\rm N}}{1-V_{\rm N}n_{\rm N}}\left.\frac{\partial W_{\rm N}}{\partial n_{\rm n}}\right|_{A, Z, V_{\rm N}, n_{\rm N}} = \mu_{\rm n}^{\rm (N)}. \tag{2.15}$$

We have used the fact that $W_{\rm L}$ is independent of $n_{\rm n}$. The right side of (2.15) is the neutron chemical potential in the gas. The first term is the neutron chemical potential of the bulk neutron gas while the second term is the change in the nuclear surface energy caused by adding a neutron to the gas. In this term $n_{\rm N}W_{\rm N}/(1-V_{\rm N}n_{\rm N})$ is the energy of nuclei per unit volume occupied by the outside neutron gas.

Lastly we write down the condition that equates the pressure of the outside neutron gas to that of the nucleus. This corresponds to minimizing $E_{\rm tot}$ with respect to $V_{\rm N}$ at fixed A, Z, $n_{\rm N}$ and $n_{\rm n}(1-V_{\rm N}n_{\rm N})$, which is the total number of outside neutrons in a unit volume. We find then

$$P^{\rm (N)} = P^{\rm (G)}, \tag{2.16}$$

where

$$P^{\rm (N)} = -\frac{\partial}{\partial V_{\rm N}}(W_{\rm N}+W_{\rm L})|_{Z, A, n_{\rm n}, n_{\rm N}} \tag{2.17}$$

is the pressure on a nucleus, and

$$P^{\rm (G)} = n_{\rm n}\mu_{\rm n}^{\rm (G)} - (E_{\rm n} - n_{\rm n}m_{\rm n}c^2) \tag{2.18}$$

is the outside neutron gas pressure. It may be verified that the total pressure

$$P = n_{\rm b}^2\frac{\partial}{\partial n_{\rm b}}\left(\frac{E_{\rm tot}}{n_{\rm b}}\right) \tag{2.19}$$

is given by

$$P = P^{\rm (G)} + P_{\rm c}. \tag{2.20}$$

The charged particle contribution to the pressure is

$$P_{\rm c} = P_{\rm e} + P_{\rm L}, \tag{2.21}$$

where

$$P_{\rm e} = n_{\rm e}^2\frac{\partial}{\partial n_{\rm e}}\left(\frac{E_{\rm e}}{n_{\rm e}}\right) \tag{2.22}$$

is the electron pressure and

$$P_L = n_N^2 \left(\frac{\partial W_L}{\partial n_N}\right)_{Z, A, V_N, n_n} \tag{2.23}$$

is the (negative) lattice pressure.

To summarize, the equilibrium conditions are given by (2.6), (2.8), (2.15) and (2.16). In order to make use of these conditions we must specify W_N, W_L, E_n and E_e explicitly. We turn now to this task.

3. Nuclear matter energy

The description of the nuclei that we shall study is that of compressible drops of of nuclear matter. We write the energy W_N of a nucleus as a sum of a bulk energy, a surface energy and a Coulomb energy, in the spirit of the semi-empirical mass formula:

$$W_N(A, Z, V_N, n_n) = [(1-x)m_n c^2 + x m_p c^2 + W(k, x)]A + W_{Coul}(A, Z, V_N, n_n) + W_{surf}(A, Z, V_N, n_n). \tag{3.1}$$

Here $W(k, x)$ is the energy per particle of bulk nuclear matter of density

$$n = \frac{k^3}{1.5\pi^2} \tag{3.2}$$

nucleons per unit volume, and x is the fractional concentration of protons. We consider now the determination of $W(k, x)$, and discuss in sects. 4 and 5 the surface and Coulomb energies.

In order to describe the matter within the nuclei and the outside neutron gas in a consistent manner, we use the same function $W(k, x)$, for $x = 0$, to describe the neutron gas, i.e.

$$\frac{E_n(n_n)}{n_n} = W(k_n, 0) + m_n c^2, \tag{3.3}$$

where

$$n_n = \frac{k_n^3}{1.5\pi^2} \tag{3.4}$$

(note that the neutron Fermi wave number equals $2^{\frac{1}{3}} k_n$). In addition, the uniform neutron-proton fluid present at densities above that at which the nuclei dissolve is also described by the same function $W(k, x)$.

The standard methods of nuclear matter theory can be used to calculate W. In this theory one describes the nucleon-nucleon interaction by a two-body potential. The particular potential used in calculations described below was the Reid soft-core potential [14]), which fits nucleon-nucleon scattering data below 300 MeV, as well as the properties of the deuteron, essentially within experimental error. Other potentials [15])

do the same, but only a few of these also give good fits to nuclear matter, and those which do, do not differ greatly from the Reid soft-core potential.

One first calculates the correlation (wave function) of two interacting nucleons. For symmetric nuclear matter ($x = \frac{1}{2}$) at nuclear densities this "pair approximation" gives a binding energy [16]) of 11 MeV per nucleon, compared with the empirical value $\sim$ 16 MeV. The remaining 5 MeV come from various corrections, the most important of which are the correlations between three [17]) and four [18]) interacting nucleons, and the three-nucleon *forces* arising from meson exchange [19]). The methods of nuclear matter theory also give excellent results for the density distribution and energy levels of finite nuclei [20]).

The energy of symmetric nuclear matter is of the form

$$W(k, \tfrac{1}{2}) = -w_0 + \tfrac{1}{2}K\left(1 - \frac{k}{k_0}\right)^2 \tag{3.5}$$

in the neighborhood of nuclear densities; w_0 is $\approx$ 16 MeV, while $k_0^3/1.5\pi^2$ is the saturation density, $\approx$ 0.2 nucleons per fm^3, or $k_0 \approx 1.4$ fm^{-1}. The conventional compressibility parameter K has been calculated in the pair approximation [16]) to be $\sim$ 135 MeV.

For slightly unsymmetric ($x \approx \frac{1}{2}$) nuclear matter one has

$$W(k, x) \approx W(k, \tfrac{1}{2}) + S(k)(1-2x)^2 \tag{3.6}$$

where the symmetry energy coefficient has been found by Siemens [16]) to have the approximate form

$$S(k) \approx 31\left(\frac{k}{k_0}\right)^2 \text{MeV} \tag{3.7}$$

(compared with the value of 28 MeV occurring in the Myers and Swiatecki semi-empirical mass formula). The approximate k^2 dependence of the symmetry energy is due in part to the variation of the kinetic energy [see (3.15)], which near $x = \frac{1}{2}$ behaves as $(\hbar^2k^2/6m_n)(1-2x)^2 \approx 14(k/k_0)^2(1-2x)^2$ MeV.

Nuclear matter theory has also been applied in calculating the properties of pure neutron matter [8, 21-23]), $x = 0$. Here one expects the pair approximation alone to be quite good. The reason is that corrections to the nuclear matter energy coming from three- or more-body correlations, and especially the three-nucleon forces depend chiefly on tensor forces, which are important in triplet even states, ^{3}S and ^{3}D. However, triplet even states are forbidden for two neutrons (only $T = 1$ states are possible) and hence these corrections are not important in pure neutron matter †.

† Ref. [5]) adopted the Németh and Sprung calculation "1a" of neutron matter, in which both isospin $T = 0$ and $T = 1$ interactions were increased by 22 % to simulate the effects of three-body correlations and three-body forces. This correction makes their pair-approximation calculations for symmetric nuclear matter give 16 MeV binding energy. However, we now believe Németh and Sprung's calculation "1b", in which interactions in $T = 1$ states were left unchanged while interactions in $T = 0$ states were increased by 54 %, to be the more reliable.

The most refined calculations for pure neutron matter are those of Siemens [23]); his results for the energy per particle can be fitted by the monotonically increasing function

$$W(k, 0) \approx 19.74k^2 - k^3 \frac{(40.4 - 1.088k^3)}{(1 + 2.545k)}, \tag{3.8}$$

(in MeV, and k in fm^{-1}) for $k \lesssim 1.5$ fm^{-1}. The first term in (3.8) is the kinetic energy, $3\hbar^2(2^{\frac{1}{3}}k)^2/10m_n$, of a free neutron gas, and is the dominant term at low densities.

Siemens' calculations do not include pairing correlations in the ground state. The effect of pairing on the energy has been estimated by Yang and Clark [24]), who find that while at very low neutron gas densities, $k \sim 0.3$, where the neutrons have little effect on the nuclei, the condensation energy can be as great as 25 % of the normal state energy, it is down to 10 % by $k \sim 0.7$, and falls rapidly with further increase in density. We shall not include these effects in $W(k, x)$.

The modification of $W(k, x)$ for very small x involves the properties of a single proton in a pure neutron gas. Since the proton can be in relative $T = 0$ states, three-body corrections are expected to play a role; these can be taken into account by the Németh-Sprung prescription † of increasing the $T = 0$ interaction to get agreement in the pair approximation with the symmetric nuclear matter binding energy. The increase required in the Siemens pair-approximation calculation is ~ 30 %; this is less than that required by Németh and Sprung since their pair-approximation calculation yields a lower binding energy than Siemens'. Increasing the $T = 0$ interaction increases the effective attraction of protons to neutrons, which favors a larger percentage of protons in neutron matter of given density.

Siemens finds that the energy required to add a proton to a pure neutron gas, i.e., the proton chemical potential $\mu_p^{(0)}$, is fitted (for $k \lesssim 1.5$ fm^{-1}) by

$$\mu_p^{(0)} = -k^3 \frac{218 + 277k}{1 + 8.57k^2} \tag{3.9}$$

(in MeV and k in fm^{-1}); $k^3/1.5\pi^2$ is the density of the neutron gas.

For small x, then, W has the form

$$W(k, x) = W(k, 0) + x(\mu_p^{(0)} - \mu_n^{(0)}), \tag{3.10}$$

where $\mu_n^{(0)}$, the chemical potential of pure neutron matter, is given by

$$\mu_n^{(0)}(k) = \frac{\partial E_n(n_n)}{\partial n_n} = W(k, 0) + \tfrac{1}{3}k \frac{\partial W(k, 0)}{\partial k}. \tag{3.11}$$

The next correction in powers of x comes from the proton kinetic energy and is given by

$$\frac{3\hbar^2[(2x)^{\frac{1}{3}}k]^2}{10m_p^*} x = 19.74k^2x^{5/3} \frac{m_n}{m_p^*} \text{(MeV)}; \tag{3.12}$$

† See preceding footnote.

$m_p^*(k)$ is the effective mass of a single proton in pure neutron matter. Not having calculations of $m_p^*(k)$ we take it to be equal to m_n. One expects however that because of the strong proton-neutron attraction a single proton in a pure neutron gas will carry a considerable dressing cloud of neutrons with it, which will lead to a significant enhancement of the proton effective mass. This should be contrasted with symmetric nuclear matter where empirically m_p^*/m_n on the Fermi surface is close to unity (see e.g., ref. [25])], and where the average effective mass entering the calculation of the energy is $m_p^*/m_n \approx 0.65$.

In the absence of detailed calculations of $W(k, x)$ for intermediate values of x between almost zero and nearly symmetric nuclear matter, we have, for use in calculations, interpolated W smoothly to fill in the gaps in our knowledge. In constructing the interpolation we have the following information about W:

(a) For symmetric nuclear matter in the neighborhood of saturation density W has the form:

$$W(k, \tfrac{1}{2}) = -w_0 + \frac{K}{2k_0^2}(k-k_0)^2. \tag{3.13}$$

(b) For small x, one has from eqs. (3.8)–(3.12):

$$W(k, x) = W(k, 0) + x(\mu_p^{(0)} - \mu_n^{(0)}) + \frac{3(2^{\frac{1}{3}}\hbar k)^2}{10m_n} x^{5/3}. \tag{3.14}$$

(c) At low k, the energy becomes just the free particle kinetic energy (ignoring free deuteron formation, which is not relevant here):

$$W_{\text{kin}}(k, x) = \frac{3(2^{\frac{1}{3}}\hbar k)^2}{10m_n}(x^{5/3} + (1-x)^{5/3}). \tag{3.15}$$

(d) The symmetry energy, that is, the correction to W as one moves away from $x = \frac{1}{2}$, is given for small

$$\alpha \equiv 1 - 2x \tag{3.16}$$

by

$$W_{\text{symm}} = W(k, x) - W(k, \tfrac{1}{2}) \approx \frac{sk^2}{k_0^2}\alpha^2. \tag{3.17}$$

We shall assume this k^2 dependence to be valid in the range of k of interest.

First we do a polynomial interpolation, for $x = \frac{1}{2}$, between the $k \approx k_0$ form (3.13) and the $k \to 0$ form (3.15); written in a somewhat lengthy but transparent form we have:

$$W(k, \tfrac{1}{2}) = \frac{3\hbar^2 k^2}{10m_n}\left(1 - \frac{k}{k_0}\right)^3 - w_0\left(\frac{k}{k_0}\right)^3\left[1 + \left(1 - \frac{k}{k_0}\right)\left(9 - 6\frac{k}{k_0}\right)\right] + \tfrac{1}{2}K\left(1 - \frac{k}{k_0}\right)^2\left(\frac{k}{k_0}\right)^3. \tag{3.18}$$

To interpolate between $x = 0$ and $x = \frac{1}{2}$ we first subtract kinetic energy contributions from (3.14), (3.18) and the symmetry energy (3.17), and then construct the fit to the interaction energy as a polynomial in even powers of α up to order α^6. The resulting interpolation formula for $W(k, x)$ is then:

$$W(k,x) = \left[W(k,\tfrac{1}{2}) - \frac{3\hbar^2k^2}{10m_n}\right](1-3\alpha^4+2\alpha^6) + \left[s\left(\frac{k}{k_0}\right)^2 - \frac{\hbar^2k^2}{6m_n}\right]\alpha^2(1-\alpha^2)^2$$
$$+ \left[W(k,0) - \frac{3\cdot 2^{\frac{2}{3}}}{10}\frac{\hbar^2k^2}{m_n}\right](3\alpha^4-2\alpha^6) + \left(\mu_p^{(0)} - \mu_n^{(0)} + 2^{\frac{2}{3}}\frac{\hbar^2k^2}{2m_n}\right)\tfrac{1}{4}(\alpha^4-\alpha^6)$$
$$+ W_{\text{kin}}(k,x). \tag{3.19}$$

As $x \to \frac{1}{2}$, (3.19) agrees with (3.17) and (3.18), while as $x \to 0$, it agrees with (3.14). As $k \to 0$, (3.19) approaches

$$W_{\text{kin}} + \left[2\left(\frac{k}{k_0}\right)^2 - \frac{\hbar^2k^2}{6m_n}\right]\alpha^2(1-\alpha^2)^2; \tag{3.20}$$

the failure of the interaction part of the symmetry energy to drop out in this limit is due to the assumed k^2 dependence being incorrect as $k \to 0$. At worst however, this

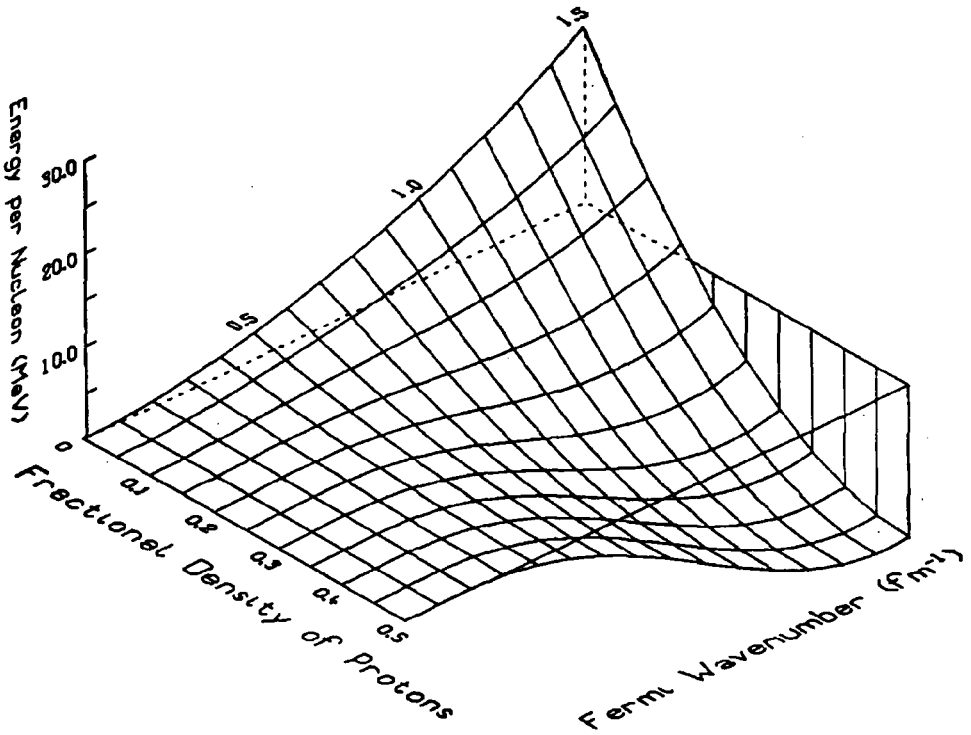

Fig. 1. Energy, W, per nucleon in bulk nuclear matter, as calculated from eq. (3.19), and plotted as a function of x, the fractional concentration of protons, and k, the mean Fermi wave number, related to the density of nucleons by $n = k^3/1.5\pi^2$. At $x = 0$ and $k = 1.5$ fm^{-1}, $W = 18.7$ MeV.

makes an $\sim 15\%$ error in W in this limit. In any event, this is irrelevant, since we are never interested in $W(k, x)$ at very low densities for finite x. Note that $W(k, x)$ is symmetric about $x = \frac{1}{2}$.

The complete $W(k, x)$ is shown in fig. 1. The parameters of nearly symmetric nuclear matter, w_0, k_0, K and s used here are:

$$w_0 = 16.5 \text{ MeV}, \quad k_0 = 1.43 \text{ fm}^{-1}, \quad K = 143 \text{ MeV}, \quad s = 33.0 \text{ MeV}. \tag{3.21}$$

These were chosen empirically by fitting our compressible liquid-drop nucleus model to the binding energies and radii of real stable nuclei [26]); the parameters (3.21) are in fact quite close to the values calculated by nuclear matter theory [16-19]). The fact that w_0 and s differ somewhat from the values $w_0 = 15.7$ MeV and $s = 1.79\, w_0 = 28.1$ MeV of Myers and Swiatecki's mass formula [7]) is primarily due to our fixing the Coulomb energy from measured nuclear sizes, rather than treating it as an empirical quantity to be determined from binding energies. The effective value of our symmetry energy coefficient is $(k/k_0)^2 s$, which for $k \approx 1.35 \text{ fm}^{-1}$ equals 29.3 MeV, a value close to that of Myers and Swiatecki.

The possibility of having nuclei immersed in a neutron fluid may be viewed as the coexistence of nuclear matter at two separate densities and proton concentrations. While the finer details of the coexistence densities and proton concentration depend on finite-size effects, namely Coulomb and surface energies, these effects, as we shall see, become small as the density of the outside neutron gas approaches the density of matter inside the nuclei. The major features of the coexistence between nuclear matter and a pure neutron gas are determined primarily by the properties of bulk matter, as described by $W(k, x)$, neglecting Coulomb forces.

In order for a pure neutron gas to be in equilibrium with nuclear matter, the pressures, as well as the neutron chemical potentials in the two phases, must be equal. In fig. 2 we have plotted the neutron and proton chemical potentials of the bulk matter, given by

$$\begin{aligned} \mu_n &= W + \frac{k}{3}\frac{\partial W}{\partial k} - x\frac{\partial W}{\partial x}, \\ \mu_p &= \mu_n + \frac{\partial W}{\partial x}, \end{aligned} \tag{3.22}$$

as a function of x, the fractional concentration of protons, for a number of *fixed* pressures:

$$P = \frac{k^3}{1.5\pi^2}\left(\tfrac{1}{3}k\frac{\partial W}{\partial k}\right). \tag{3.23}$$

The upper curves are the neutron chemical potentials while the lower are the proton chemical potentials. The μ_p and μ_n curves meet, for each pressure, at $x = \frac{1}{2}$.

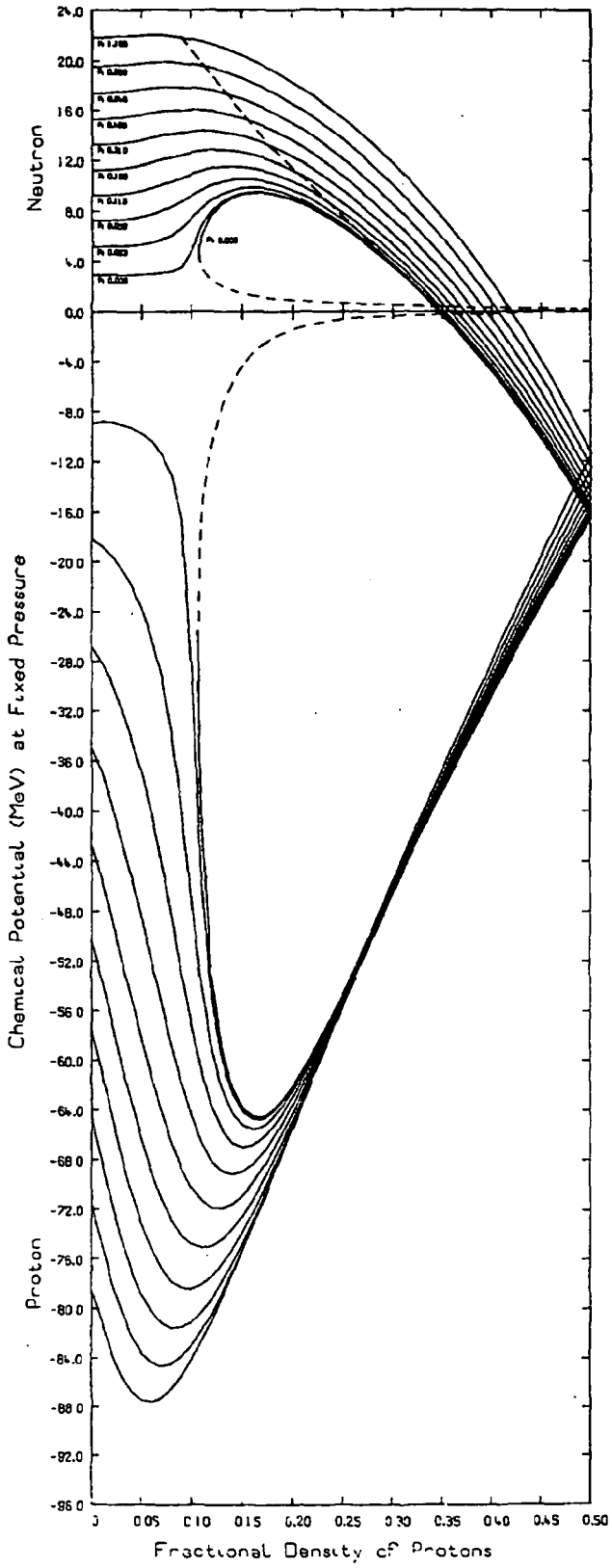

Fig. 2. The neutron and proton chemical potentials for bulk nuclear matter, plotted for given pressures P as a function of x, the fractional density of protons. The pressures, constant along each curve, are measured in MeV/fm^3. The neutron chemical potential (μ_n) curves begin for $x = 0$, at positive values, while the proton chemical potentials (μ_p) begin at negative values at $x = 0$. Note that $\mu_p(P, x = 0)$ decreases with increasing pressure. The dashed line intersecting the μ_n curves is the coexistence curve; for a given value of μ_n, this curve tells the proton concentration of bulk matter that has the same pressure as, and hence can coexist with, a pure neutron gas at the given μ_n. The $P = 0$ curve, starting at saturated symmetric nuclear matter, $x = \frac{1}{2}$, $\mu_p = \mu_n = -16.5$ MeV, never reaches concentrations lower than $x \approx 0.11$, but instead it doubles back; matter corresponding to the dashed region of the $P = 0$ curve has negative compressibility and hence is unstable. It can be seen that for any point on the coexistence curve, the value of $\mu_p(P, x)$ is always greater than $\mu_p(P, 0)$, indicating that proton drip does not occur for bulk matter. Also it can be seen that it is impossible to have coexistence, that is, equal μ_n and P between two phases each with finite proton concentration.

To construct the coexistence curve we first pick a pressure for the pure neutron gas. This fixes the value of μ_n and hence the density of the pure neutron gas. The nuclear matter that can coexist with the neutron gas obeys $\mu_n(x, P) = \mu_n(0, P)$; its value of $x(P)$ can be read from the graph. The dashed line is the coexistence curve.

The concentration of protons in the coexisting nuclear matter falls steadily with increasing μ_n, while it may be shown that the density, or k, falls slightly as μ_n increases, goes through a minimum, and then rises slightly. There appears to be no equilibrium possible in bulk for $\mu_n \gtrsim 30$ MeV, which corresponds to a limiting density $\sim 4 \times 10^{14}$ g/cm^3, a little greater than symmetric nuclear matter density. One can also see that along the coexistence curve the proton chemical potential in the nuclear matter is always less than that in the pure neutron gas, i.e., $\mu_p(x, P) < \mu_p(0, P)$ when $\mu_n(x, P) = \mu_n(0, P)$. Thus there is no tendency in bulk matter for "proton drip".

4. Nuclear surface energy

The energy density in the interior of nuclei can be described by the calculations for uniform nuclear matter discussed in sect. 3. This volume energy, $W(k, x)$ per nucleon, includes through its x-dependence the symmetry energy, and through its density dependence, the effect of a finite neutron gas pressure outside the nuclei. The Coulomb energy of the nuclei, including the important Coulomb interaction between nuclei, is straightforward to evaluate, and will be considered in the next section. We look now at the nuclear surface energy.

As the density of the matter, and hence the density of neutrons outside the nuclei grows, the nuclear surface energy decreases. This is because the matter inside the nuclei becomes more and more neutron rich, and at the same time the density difference between the matter inside and outside the nuclei becomes small. Were the matter inside and outside the nuclei the same there would, of course, be no surface energy. We shall attempt now to construct an approximate formula for the nuclear surface energy (as a function of the matter densities n_i and n_o inside and outside the nuclei, and the Z and A of the nuclei) that accounts for this lowering of the surface energy.

We begin in the spirit of the Thomas-Fermi theory of finite nuclei, developed by one of us [27]), by studying the variation in the bulk energy across the nuclear surface. We assume that the surface thickness is small compared to the nuclear radius, and consider first a plane surface perpendicular to the z-axis separating two semi-infinite regions. We assume that $n(r)$, the density of nucleons, approaches n_i, the bulk density inside the nucleus, as $z \to -\infty$, and approaches n_o, the density of the outside neutron gas, as $z \to +\infty$. The energy of the system, neglecting terms $\sim (\nabla n)^2$ for the moment, is, in a local density approximation,

$$\int d^3r\, W(n(r))n(r), \tag{4.1}$$

where we denote the bulk energy $W(k, x)$ simply by $W(n)$. To construct the surface energy we imagine a reference system with a sharp surface at $z = a$, at which the density falls discontinuously from n_i to n_o. The location of the reference surface is defined by the condition that the reference system have the same number of nucleons as the original system, that is †

$$\int_{z=-\infty}^{a} d^3r[n(r)-n_i]+\int_{a}^{\infty} d^3r[n(r)-n_o] = 0. \tag{4.2}$$

Then the surface part E_σ of the energy (4.1) is found by subtracting from (4.1) the energy

$$\int_{z<a} d^3r\, W_i n_i+\int_{z>a} d^3r\, W_o n_o \tag{4.3}$$

of the reference system, where $W_o = W(n_o)$ and $W_i = W(n_i)$. Per unit area we have

$$E_\sigma = \int_{-\infty}^{a} dz[W(n(z))n(z)-W_i n_i]+\int_{a}^{\infty} dz[W(n(z))n(z)-W_o n_o]. \tag{4.4}$$

For any given surface profile, $n(z)$ and $x(z)$, one could calculate (4.4) directly, using W as given in sect. 3. Note that if $W(n(z))n(z)$ varies linearly with n across the surface, i.e.,

$$W(n(z))n(z) = W_o n_o+\frac{n(z)-n_o}{n_i-n_o}(W_i n_i-W_o n_o), \tag{4.5}$$

then (4.4) vanishes identically.

Here we shall estimate (4.4) by writing the density and energy profiles in the form

$$n(z) = n_o+(n_i-n_o)f\left(\frac{z}{b}\right) \tag{4.6}$$

and

$$W(z) = W_o+(W_i-W_o)g\left(\frac{z}{b}\right), \tag{4.7}$$

where f and g are dimensionless functions obeying

$$f(-\infty) = g(-\infty) = 1, \qquad f(\infty) = g(\infty) = 0. \tag{4.8}$$

The length b is proportional to the surface thickness. From (4.4) we then find

$$E_\sigma = b(W_o-W_i)\left[(n_i-n_o)\int d\zeta f(\zeta)(1-g(\zeta))+n_o\int d\zeta(f(\zeta)-g(\zeta))\right]. \tag{4.9}$$

If we assume $f = g$, that is, that the energy per particle is a linear function of the

† For the spherically symmetric case the reference surface defines the nuclear volume, $\frac{4}{3}\pi r_N^3$. In general, eq. (4.2) applied to the neutron and proton distributions separately yields slightly different reference surfaces. We shall, for simplicity, assume these two surfaces to be the same.

density, as one crosses the surface, then

$$E_\sigma = \lambda b(W_o - W_i)(n_i - n_o), \tag{4.10}$$

where

$$\lambda = \int_{-\infty}^{\infty} d\zeta f(\zeta)(1-f(\zeta)). \tag{4.11}$$

For example, if $f(z/b)$ falls from 1 to 0 linearly between 0 and b then b is the surface thickness and $\lambda = \frac{1}{6}$; for a Fermi-function surface profile

$$f\left(\frac{z}{b}\right) = \frac{1}{e^{z/b}+1}, \tag{4.12}$$

$\lambda = 1$, and b is $\sim \frac{1}{4}$–$\frac{1}{6}$ of the surface thickness. We shall, for simplicity, assume that $f(z/b)$ depends only on the single scale parameter b, i.e., that $f(\zeta)$ is the same for all nuclei, and also take $g = f$; then λ is simply a constant of order unity.

Eq. (4.10) for the surface energy has the correct gross dependence on the properties of the matter inside and outside, and in particular it has the desired feature of vanishing as $n_o \to n_i$, provided that the surface thickness, $\sim b$, is well behaved. The main problem at hand is to determine the surface thickness. We consider first how this is done in the Thomas-Fermi theory.

A further contribution to the surface energy comes from corrections to the local density approximation (4.4). In the *differential* Thomas-Fermi theory [27]) of ordinary nuclei composed of symmetric nuclear matter the energy is given by

$$\int W(n) n \, d^3r + \frac{B}{n_{NM}} \int (\nabla n)^2 d^3r, \tag{4.13}$$

where $B \approx 24$ MeV · fm^2 is a constant related to the strength and range of the nuclear forces, and n_{NM} is the saturation density. For unequal numbers of neutrons and protons, we must generalize the B-term in (4.13) to

$$\frac{1}{n_{NM}} \int d^3r (B_{nn}(\nabla n_n)^2 + B_{pp}(\nabla n_p)^2 + 2B_{np}(\nabla n_n) \cdot (\nabla n_p)), \tag{4.14}$$

where n_n and n_p are the neutron and proton densities respectively. The coefficients B_{nn} and B_{pp} are nearly equal, since they depend on the long-range part of the nuclear forces, which is not strongly affected by many-body correlations. On the other hand this part of the force between unlike nucleons is probably about twice that between like ones so that $B_{np} \sim 2B_{nn}$. Thus (4.14) can be written approximately as

$$\frac{1}{n_{NM}} \int [B(\nabla n)^2 - B'(\nabla n_n - \nabla n_p)^2], \tag{4.15}$$

where $B' \sim \frac{1}{3}B$.

The B' term in (4.15) has the interesting effect of favoring spatial fluctuations of the density difference $n_n - n_p$. We do not believe, however, that such fluctuations can

be important in the still rather thin surface of a nucleus imbedded in neutron matter. If one assumes that the *gradients* of n_n and n_p are proportional to each other everywhere, that is,

$$nx = \frac{n_i x_i}{n_i - n_o}(n - n_o), \tag{4.16}$$

then (4.15) reduces to

$$\frac{B_1}{n_{NM}} \int (\nabla n)^2 d^3r, \tag{4.17}$$

where $B_1 \sim B$. For the plane surface density profile (4.6), the energy (4.17) becomes

$$\nu \frac{B_1}{n_{NM}} \frac{(n_i - n_o)^2}{b}, \tag{4.18}$$

where

$$\nu = \int_{-\infty}^{\infty} d\zeta \left(\frac{\partial f}{\partial \zeta}\right)^2; \tag{4.19}$$

for the Fermi-function surface (4.12), $\nu = \frac{1}{6}$.

In the Thomas-Fermi theory the surface thickness b is chosen to minimize the total surface energy, (4.10) plus (4.18). Thus

$$b = \left(\frac{B_1 \nu}{\lambda n_{NM}} \frac{n_i - n_o}{W_o - W_i}\right)^{\frac{1}{2}}, \tag{4.20}$$

and the total surface energy per unit area is

$$E_{surf,\,TF} = 2\left(\frac{\nu \lambda B_1}{n_{NM}}\right)^{\frac{1}{2}} (W_o - W_i)^{\frac{1}{2}} (n_i - n_o)^{\frac{1}{2}}. \tag{4.21}$$

The surface energy of a nucleus of A nucleons is then (4.21) times $4\pi r_N^2$, where r_N is the nuclear radius. Since

$$A = n_i V_N = \frac{k^3}{1.5\pi^2} \frac{4\pi r_N^3}{3}, \tag{4.22}$$

we have

$$r_N = \left(\frac{9\pi}{8}\right)^{\frac{1}{2}} \frac{A^{\frac{1}{2}}}{k}; \tag{4.23}$$

the total surface energy is

$$W_{surf,\,TF} = \frac{\sigma (W_o - W_i)^{\frac{1}{2}}}{w_o^{\frac{1}{2}}} \frac{(n_i - n_o)^{\frac{1}{2}}}{n_{NM}^{\frac{1}{2}}} \frac{k_0^2}{k^2} A^{\frac{1}{2}}, \tag{4.24}$$

where

$$\sigma = 4\left(\frac{3}{\pi}\right)^{\frac{1}{2}} k_0 (\nu \lambda B_1 w_0)^{\frac{1}{2}} \tag{4.25}$$

is a coefficient of order 20 MeV.

The result (4.22) appears to have somewhat strange consequences for ordinary nuclei, for which $n_o = 0$, $W_o = 0$; since $n_i \sim k^3$, (4.24) becomes

$$W_{surf} = \sigma \left(- \frac{W_i}{w_0} \right)^{\frac{1}{2}} \left(\frac{k}{k_0} \right)^{\frac{4}{3}} A^{\frac{2}{3}}. \tag{4.26}$$

The $\sim k^{\frac{4}{3}}$ dependence appears to say that the surface energy increases rapidly with internal density, and hence is decreased by making *larger* nuclei. If this dependence were believed away from the equilibrium value of k, for given Z and A, then one would find nuclei with extremely low equilibrium density, a feature not found in detailed Thomas-Fermi theory calculations [see e.g., refs. [28,29])]. The basic reason for this paradoxical behavior is that the variational nature of the Thomas-Fermi theory implies certain stationary conditions on the surface energy; these take the form of implicit constraints on the variation of the surface energy away from equilibrium. (This paradox could be avoided by inserting in the denominator of (4.18) a factor n_i^m; then (4.26) would be changed to $W_{surf} \sim k^{(5-3m)/2}$. However, such a modification would be quite arbitrary.)

Due to the subtle nature of the variations of the surface energy away from equilibrium, we shall not use the result (4.24) here, but adopt instead a simpler approach, which we believe to give a fairly similar description of the nuclei in neutron stars. We shall assume that the *total* surface energy has the form (4.10) with the constant λ being appropriately adjusted to account for corrections to the local density approximation (4.4).

To estimate the surface thickness, we consider first the case of no outside neutrons, and imagine the nucleus as composed of free particles in a square-well potential. The thickness of the surface, that is, the range over which the density varies, scales generally as the Fermi wavelength inside the well. When the well is filled to overflowing, corresponding to neutron drip, the scale of the surface thickness is determined by the inverse of the momentum k_c of the nucleons just at the top of the well, i.e., with zero kinetic energy outside. The momentum k_c is given by

$$\frac{k_c^3}{1.5\pi^2} = n_i - n_o. \tag{4.27}$$

In the case that $n_o = 0$, k_c reduces to the Fermi momentum inside the well. The surface thickness, b, in general cannot be smaller than $\sim \pi k_c^{-1}$. The finite range of the forces also tends to increase b, but this effect becomes less important as n_o approaches n_i. We shall then for a first approximation assume that the surface thickness is directly proportional to k_c^{-1}:

$$b = \frac{\eta \pi}{k_c} \tag{4.28}$$

where $\eta \approx 1$.

Putting this in (4.10), we find as an approximation to the surface energy

$$E_{\text{surf}} = \left(\frac{2}{3}\pi\right)^{\frac{1}{3}} \eta\lambda(W_o - W_i)(n_i - n_o)^{\frac{2}{3}}, \tag{4.29}$$

and multiplying by the area of the nucleus we find a total surface energy

$$W_{\text{surf}} = \frac{\sigma(W_o - W_i)}{w_0}\left(1 - \frac{n_o}{n_i}\right)^{\frac{2}{3}} A^{\frac{2}{3}} \equiv w_{\text{surf}} A^{\frac{2}{3}}, \tag{4.30}$$

where

$$\sigma = 2(3\pi^2)^{\frac{1}{3}}\lambda\eta w_0. \tag{4.31}$$

We shall treat σ as an adjustable parameter to be determined by fitting the model nuclear masses and radii to experiment.

It is interesting to note that for ordinary nuclei, where $n_o = 0$, (4.30) reduces to

$$W_{\text{surf}} = -W_i \frac{\sigma}{w_0} A^{\frac{2}{3}}, \tag{4.32}$$

which says that the total surface energy is proportional to the bulk energy per particle. Since W_i includes the bulk symmetry energy, the surface energy (4.32) includes the "surface symmetry energy"; exactly as in Myers and Swiatecki's [7]) semi-empirical mass formula, the ratio W_{surf}/AW of the surface energy to the volume energy (including symmetry energy) is independent of x.

The surface energy (4.30), while only a first estimate, has the property of approaching zero as $n_o \to n_i$; furthermore, when applied to ordinary nuclei (4.30) yields reasonable nuclear sizes. Better than using the local density approximation would be to calculate the density distributions and energies of the nuclei by a Hartree-Fock model, which gives very good results for ordinary nuclei [20]). Preliminary Hartree-Fock calculations, using Skyrme's form for the effective nucleon-nucleon interaction, have been carried out by Negele and Vautherin, and give results in reasonable agreement with our simplified model [38]). Differential Thomas-Fermi calculations of an isolated nucleus in a neutron gas have recently been given by Buchler and Barkat [30]).

5. Coulomb energy

The total Coulomb energy of the system is a sum of the usual nuclear Coulomb energy, the energy of interaction between the nuclei, the nucleus-electron interaction energy and the electron-electron interaction energy. The *nuclear Coulomb energy*, in a first approximation, is simply that of a uniformly charged sphere of radius r_N, (4.23) and total charge Ze:

$$w_{c,0} Z^2 A^{-\frac{1}{3}} = \frac{3}{5}\frac{Z^2 e^2}{r_N}. \tag{5.1}$$

If we take into account effects of finite surface thickness b, this energy is reduced by terms of relative order b^2/r_N^2; for the particular case of a Fermi-function charge distribution

$$n_p(r) = \frac{Z}{(\frac{4}{3}\pi r_N^3)} \frac{1}{e^{(r-r'_N)/d}+1}, \tag{5.2}$$

where the surface thickness b is $\approx 2d \ln 9$ and $r'_N = r_N(1-\pi^2 d^2/3r_N^2 + O(d^4/r_N^4))$, the surface thickness correction to the Coulomb energy is

$$W_{thick}(k, x)A = -\frac{\pi^2}{2}\frac{d^2Z^2e^2}{r_N^3} = -\tfrac{4}{9}\pi Ze^2d^2k^3x. \tag{5.3}$$

A further correction to (5.1) is the proton exchange energy [31],

$$W_{exch}A \approx -\frac{3}{4\pi} Ze^2(2x)^{\frac{1}{3}}k. \tag{5.4}$$

The exchange energy per nucleon, dependent only on k and x, is a small correction to the bulk energy W, and may be neglected. While the thickness energy is also generally a small correction to W, it does depend on the geometry of the surface, and for thick surfaces it could be important; we choose for this reason to include it in our calculations.

The electrostatic energy in the system, beyond the Coulomb self-energy of the nuclei, is the lattice energy, that is, the energy of a regular lattice of positively charged nuclei in an essentially uniform background of electrons. The lattice Coulomb energy is most simply calculated by the Wigner-Seitz method. One divides the lattice up into unit cells with one nucleus at the center of each cell. Since each cell is electrically neutral, the Coulomb interaction between different cells comes only from quadrupole and higher moments; these interactions may, to a first approximation, be neglected. To estimate the Coulomb energy of a cell, one replaces the cell by a sphere of the same volume. The radius r_c of the sphere is given by

$$\tfrac{4}{3}\pi r_c^3 n_N = 1. \tag{5.5}$$

If we assume the Z electrons in the sphere to be uniformly distributed, the total electrostatic energy of the cell is simply that of the nuclei, (5.1), (5.3) and (5.4), plus the lattice energy

$$W_L = -\frac{9}{10}\frac{Z^2e^2}{r_c}\left(1-\frac{5}{9}\frac{\langle r^2\rangle}{r_c^2}\right), \tag{5.6}$$

where $\langle r^2\rangle$ is the mean square radius of the nuclear charge distribution. For point nuclei, $W_L = -\frac{9}{10}Z^2e^2/r_c$, which is a reasonably good approximation to the exact result for a bcc lattice; in terms of r_c, the exact results for bcc, fcc (face-centered cubic),

and simple cubic point lattices are [12])

$$W_L = -\frac{Z^2e^2}{r_c} \times \begin{cases} 0.89593; & \text{bcc} \\ 0.89588; & \text{fcc} \\ 0.88006; & \text{sc}. \end{cases} \tag{5.7}$$

The $\frac{1}{2}Z^2e^2\langle r^2\rangle/r_c^3$ term is the change in the lattice energy due to the finite size of the nucleus. In fact this term, for a uniform electron sea, is the exact finite-size correction to the total lattice Coulomb energy and does not depend on the Wigner-Seitz approximation.

For a uniform proton charge distribution in the nucleus, one has

$$\langle r^2\rangle = \tfrac{3}{5}r_N^2. \tag{5.8}$$

The total Coulomb energy per nucleus, without exchange or surface thickness terms, thus reduces to

$$w_c\frac{Z^2}{A^{\frac{1}{3}}} = \frac{3}{5}\frac{Z^2e^2}{r_N}\left(1-\frac{3}{2}\frac{r_N}{r_c}+\frac{1}{2}\frac{r_N^3}{r_c^3}\right) = \frac{3}{5}\frac{Z^2e^2}{r_N}\left(1-\frac{r_N}{r_c}\right)^2\left(1+\frac{r_N}{2r_c}\right). \tag{5.9}$$

We see explicitly that this form for the total Coulomb energy is always positive (which it would not be were the finite-size term neglected), and furthermore it goes to zero as $(r_c-r_N)^2$, as r_N goes to r_c, i.e., as the nuclei grow to fill all of space.

The first correction to the lattice energy due to the modification of the electron wave functions in the Coulomb field, that is, electron screening, has been calculated by Salpeter [2]) using the Wigner-Seitz method, and exactly by Dyson [32]), who finds for a bcc lattice (per nucleus)

$$W_{\text{screening}} = 0.12k_{FT}^2r_c^2W_L < 0, \tag{5.10}$$

where W_L is the lattice energy for a point lattice and k_{FT}^{-1} is the electron screening length, given, for relativistic electrons, by

$$k_{FT} = \left(\frac{4}{\pi}\frac{e^2}{\hbar c}\right)^{\frac{1}{2}}k_e; \tag{5.11}$$

here k_e is the electron Fermi wave number. Thus

$$W_{\text{screening}} = 0.004Z^{\frac{7}{3}}W_L; \tag{5.12}$$

this correction shall be neglected.

All electron Coulomb energy, except electron exchange energy, has already been included in W_L, (5.6). The electron exchange energy is $\sim e^2k_e$ per electron, where k_e is the electron Fermi wave number; for relativistic electrons, this energy is $\sim e^2/\hbar c$ times the mean electron kinetic energy and may be neglected. The total electron energy

E_e is then just the free electron kinetic energy, given by

$$E_e = \tfrac{3}{4}\hbar c k_e n_e \tag{5.13}$$

for completely relativistic electrons.

We have chosen to include all electrostatic electron energies in W_L and take for E_e the free electron result. The electron chemical potential, defined by (2.8) and (5.13) is thus measured with respect to the electrostatic energy, $-e\phi_0$, required to add an electron at the bottom of the electron conduction band. The quantity

$$\phi_0 = \frac{3}{10}\frac{Ze}{r_c}\left(1-\frac{r_N^2}{r_c^2}\right) \tag{5.14}$$

is the average electrostatic potential in the system. The proton chemical potential, defined by (2.11) is measured with respect to $+e\phi_0$, and the sum $\mu_p^{(N)}+\mu_e$, which is the physically significant combination, is independent of the choice of the zero of electrostatic energy.

6. Evaluation of equilibrium conditions

In sects. 3, 4 and 5 we have constructed the various contributions to the energy of the system. We now summarize these results and write out the detailed form of the equilibrium conditions for the present nuclear model.

The total energy of a single nucleus specified by A, Z and mean wave number k is

$$W_N(A, Z, k, k_n) = [(1-x)m_n + xm_p]c^2A + [W + W_{thick} + W_{exch}]A + w_{surf}A^{\frac{2}{3}} + w_{c,0}Z^2A^{-\frac{1}{3}}. \tag{6.1}$$

For fixed x the entire A-dependence is explicit. The volume energy W is given by (3.19), the surface energy by (4.30), the Coulomb energy contributions by (5.1) and (5.3), and the exchange energy by (5.4); $k_n = (1.5\pi^2 n_n)^{\frac{1}{3}}$. To include W_L, the lattice energy, one simply replaces $w_{c,0}$ by w_c. The length d in W_{thick} is chosen to be $0.74/k_c$, to give agreement with surface thicknesses determined from electron scattering experiments. Eq. (6.1) is the analog of the semi-empirical mass formula for nuclear energies, and it contains five parameters, w_0, k_0, K and s in the volume energy and σ in the surface energy.

We have evaluated these parameters by fitting (6.1) to ordinary nuclei. For this case the surface energy is given by (4.32), and the equilibrium value of k for a given A and Z is determined by the condition

$$\frac{\partial W_N(A, Z, k)}{\partial k} = 0; \tag{6.2}$$

this is the condition that ordinary nuclei are under zero pressure. The values of the five parameters that give good fits to nuclear masses and radii over a wide range of

A- and Z-values ($A \geqq 40$) are given in (3.21), together with $\sigma = 21.0$ MeV. Details of this fitting of parameters will be given elsewhere [26]).

The general equilibrium condition (2.6) becomes, on using (6.1), (5.6) and (5.8):

$$w_{\text{surf}} A^{\frac{1}{3}} = 2(w_{c,0} x^2 A^{5/3} + W_L) = 2w_c Z^2 A^{-\frac{1}{3}}. \tag{6.3}$$

Here we have used the fact that at fixed x, n_n, $n_N A$ and $n_N V_N$, both the neutron density n_n (denoted by n_0 in sect. 4) and k remain fixed, r_c scales as $A^{\frac{1}{3}}$, while r_N/r_c remains fixed. Eq. (6.3) is the remarkably simple statement that for the correct Z and A *the surface energy per nucleus is just twice the total Coulomb energy* (5.9) *per nucleus including the lattice energy*. Solving (6.3) for A as a function of x and r_N/r_c we have

$$A = \frac{w_{\text{surf}}}{2w_c x^2} = \frac{w_{\text{surf}}}{x^2 \left(\frac{4}{5}\left(\frac{3}{\pi}\right)^{\frac{1}{3}} e^2 k\right)\left(1 - \frac{3}{2}\frac{r_N}{r_c} + \frac{1}{2}\left(\frac{r_N}{r_c}\right)^3\right)}. \tag{6.4}$$

This equation is the generalization of eq. (15) of ref. [5]). The decrease of w_{surf}, as the density of outside neutrons increases, tends to lower A. We note on the other hand, that the inclusion of the lattice energy, the r_N/r_c terms, tends, for given k and x, to produce larger nuclei; for example when the nuclei occupy only one one-thousandth of the volume of space, $\rho \sim 10^{-3}\rho_{NM}$, A is increased by 18 %. For ρ close to nuclear matter densities the effect on A is a few hundred percent. This modification of A due to lattice interactions strikingly illustrates the subtle interplay between nuclear and solid-state physics that takes place in neutron stars.

Eq. (6.4) relates A to k, k_n, x and k_e the electron Fermi wave number. This is because

$$u \equiv \left(\frac{r_N}{r_c}\right)^3 = V_N n_N = \frac{A}{n}\frac{n_e}{Z} = \frac{1}{2x}\left(\frac{k_e}{k}\right)^3. \tag{6.5}$$

Here and in the following, n denotes the density inside nuclei. We can in turn write a relation for k_e in terms of A, k, k_n and x by using the β-stability condition (2.8):

$$\mu_e = \hbar c k_e = (m_n - m_p)c^2 - \left(\frac{\partial W'}{\partial x} + 2w_c x A^{\frac{1}{3}} + \frac{\partial w_{\text{surf}}}{\partial x} A^{-\frac{1}{3}}\right), \tag{6.6}$$

where

$$W' = W + W_{\text{exch}} + W_{\text{thick}} \tag{6.7}$$

is the effective volume energy per nucleon. Making use of (6.3) we write (6.6) as

$$\hbar c k_e = (m_n - m_p)c^2 - \frac{\partial W'}{\partial x} - \frac{1}{x}\frac{\partial}{\partial x}(x w_{\text{surf}}) A^{-\frac{1}{3}}. \tag{6.8}$$

The A-dependence of the right side is explicit; we can therefore combine (6.8), (6.5) and (6.4) to arrive at a simple cubic equation for $A^{\frac{1}{3}}$ in terms of x, k and k_n:

$$(2 - 3\lambda + \lambda^3)A + 3\nu(1 - \lambda^2)A^{\frac{2}{3}} + 3\nu^2 \lambda A^{\frac{1}{3}} - \nu^3 - \xi = 0, \tag{6.9}$$

where

$$\lambda = \frac{(m_n - m_p)c^2 - \partial W'/\partial x}{\hbar c k (2x)^{\frac{1}{3}}}, \tag{6.10}$$

$$\nu = \frac{\partial(x w_{\rm surf})/\partial x}{\hbar c k 2^{\frac{1}{3}} x^{4/3}}, \tag{6.11}$$

$$\xi = \frac{5}{2}\left(\frac{\pi}{3}\right)^{\frac{1}{3}} \frac{w_{\rm surf}}{x^2 e^2 k}. \tag{6.12}$$

Eq. (6.9) can be solved explicitly by the standard formula for cubic equations; it has one real root whose cube we denote as $A(x, k, k_n)$ but do not write out explicitly. Thus in terms of x, k and k_n we know A and, from (6.8), k_e or μ_e; furthermore eq. (6.5) tells us u, the fraction of space occupied by nuclei.

It remains then to determine k and k_n as functions of x, which is a monotonically decreasing function of the mass density. The two equations that do this are the conditions for equality of neutron chemical potentials (2.15) and pressures (2.16) inside and outside the nuclei. Below neutron drip, of course, $k_n = 0$ and the only condition we need is $P^{(N)} = 0$. The point of neutron drip is where (2.15) and (2.16) can first have a common solution; this is basically where $\mu_n^{(N)}$ passes through zero. We straightforwardly find that in the neutron gas

$$\mu_N^{(G)} = \frac{\partial}{\partial n_n}(n_n W(k_n, 0)) + \frac{nu}{1-u}\left(\frac{\partial W_{\rm thick}}{\partial n_n} + A^{-\frac{1}{3}}\frac{\partial w_{\rm surf}}{\partial n_n}\right) \tag{6.13}$$

and

$$P^{(G)} = n_n(\mu_n^{(G)} - W(k_n, 0)). \tag{6.14}$$

To calculate the neutron chemical potential in nuclei we write $(\partial/\partial A)_Z$ in eq. (2.10) as $(\partial/\partial A)_x - (x/A)(\partial/\partial x)_A$; together with eq. (2.8) this gives

$$\mu_n^{(N)} = \frac{\partial}{\partial A}(W_N + W_L)_{x, n_N, V_N, n_n} - m_n c^2 + x\mu_e. \tag{6.15}$$

Next we use eqs. (6.1), (5.9) and (5.1) for $W_N + W_L$. The Coulomb energy at fixed nuclear volume and density of nuclei scales as $Z^2 = x^2 A^2$; thus in (6.5), $\partial(w_c Z^2 A^{-\frac{1}{3}})/\partial A = 2w_c Z^2 A^{-\frac{1}{3}} = w_{\rm surf} A^{-\frac{1}{3}}$. To evaluate the bulk and surface contributions to $\mu_n^{(N)}$ we note that since $nV_N = A$ we may write $(\partial/\partial A)_{V_N}$ as $(\partial/\partial A)_n + (n/A)(\partial/\partial n)_A$. Thus we find

$$\mu_n^{(N)} = \frac{\partial}{\partial n}(nW') + \left(\tfrac{5}{3}w_{\rm surf} + n\frac{\partial w_{\rm surf}}{\partial n}\right)A^{-\frac{1}{3}} + x(\mu_e - m_n c^2 + m_p c^2). \tag{6.16}$$

The pressure on a nucleus is given by (2.17), which may be written as

$$P^{(N)} = n^2 \frac{\partial}{\partial n}\left(\frac{W_N + W_L}{A}\right)_{Z, A, n_n, n_N}. \tag{6.17}$$

Writing the Coulomb contribution to (6.17) as $-\frac{1}{3}nr_N(\partial/\partial r_N)(w_c Z^2 A^{-\frac{1}{3}})$, we find that

$$P^{(N)} = n^2 \frac{\partial}{\partial n} W' + n^2 \left(\frac{\partial}{\partial n} w_{surf}\right) A^{-\frac{1}{3}} + \tfrac{1}{3} n w_{c,0} x^2 A^{\frac{1}{3}}(1-u). \tag{6.18}$$

The conditions $\mu_n^{(N)} = \mu_n^{(G)}$ and $P^{(N)} = P^{(G)}$ completely determine k and k_n as functions of x. The explicit solution of these two simultaneous non-linear algebraic equations must be done numerically.

In carrying out this numerical evaluation we have omitted the term $\propto \partial W(k_n, 0)/\partial n_n$ that occurs in $\partial w_{surf}/\partial n_n$ in eq. (6.13). The reason for this is that while eq. (4.10) has the correct gross dependence on $W(k, x)$ and $W(k_n, 0)$, its n_n derivative has a spurious $n_n^{-\frac{1}{3}}$ singularity for small n_n. Omitting this derivative avoids this singularity at small n_n, and makes negligible difference above $\rho \sim 10^{13}$ g/cm^3.

TABLE 1

Properties of the free neutron regime

ρ (g/cm^3)	A	Z	x	k (fm^{-1})	k_n (fm^{-1})	μ_n (MeV)	$\mu_p^{(N)}$ (MeV)	μ_e (MeV)	P (MeV/fm^3)	$n_N \times 10^6$ (fm^{-3})
4.66×10^{11}	127	40	0.313	1.32	0.07	0.14	−24.89	26.31	5.00×10^{-4}	2.02
6.61×10^{11}	130	40	0.310	1.32	0.12	0.37	−25.33	26.98	5.68×10^{-4}	2.13
8.79×10^{11}	134	41	0.307	1.32	0.15	0.55	−25.67	27.51	6.42×10^{-4}	2.23
1.20×10^{12}	137	42	0.304	1.32	0.18	0.75	−26.08	28.13	7.60×10^{-4}	2.34
1.47×10^{12}	140	42	0.302	1.32	0.20	0.91	−26.38	28.58	8.73×10^{-4}	2.43
2.00×10^{12}	144	43	0.299	1.31	0.23	1.15	−26.88	29.33	1.11×10^{-3}	2.58
2.67×10^{12}	149	44	0.295	1.31	0.26	1.42	−27.44	30.15	1.47×10^{-3}	2.74
3.51×10^{12}	154	45	0.291	1.31	0.29	1.71	−28.05	31.05	1.98×10^{-3}	2.93
4.54×10^{12}	161	46	0.286	1.30	0.32	2.01	−28.72	32.02	2.69×10^{-3}	3.14
6.25×10^{12}	170	48	0.280	1.30	0.36	2.45	−29.69	33.43	4.04×10^{-3}	3.45
8.38×10^{12}	181	49	0.273	1.29	0.40	2.91	−30.78	34.98	6.02×10^{-3}	3.82
1.10×10^{13}	193	51	0.266	1.28	0.44	3.41	−31.98	36.68	8.81×10^{-3}	4.23
1.50×10^{13}	211	54	0.256	1.27	0.49	4.07	−33.64	39.00	1.38×10^{-2}	4.84
1.99×10^{13}	232	57	0.246	1.26	0.54	4.77	−35.50	41.56	2.09×10^{-2}	5.54
2.58×10^{13}	257	60	0.234	1.25	0.59	5.51	−37.57	44.37	3.09×10^{-2}	6.36
3.44×10^{13}	296	65	0.220	1.24	0.65	6.47	−40.34	48.10	4.77×10^{-2}	7.52
4.68×10^{13}	354	72	0.202	1.22	0.72	7.67	−43.99	52.95	7.62×10^{-2}	9.12
5.96×10^{13}	421	78	0.186	1.21	0.78	8.77	−47.49	57.56	0.111	10.7
8.01×10^{13}	548	89	0.163	1.20	0.86	10.36	−52.66	64.32	0.176	13.1
9.83×10^{13}	683	100	0.146	1.20	0.92	11.66	−56.86	69.81	0.243	15.0
1.30×10^{14}	990	120	0.121	1.21	1.01	13.77	−63.52	78.58	0.384	17.8
1.72×10^{14}	1640	157	0.096	1.24	1.11	16.39	−71.16	88.84	0.616	19.6
2.00×10^{14}	2500	210	0.081	1.27	1.17	18.11	−75.79	95.19	0.803	18.8
2.26×10^{14}	4330	290	0.067	1.29	1.22	19.59	−79.69	100.57	0.988	15.4
2.39×10^{14}	7840	445	0.057	1.30	1.25	20.37	−81.92	103.57	1.09	11.0

ρ is the total mass density; $x = Z/A$. The density of nucleons inside the nuclei $= k^3/1.5\pi^2$; the density of the free neutron gas $= k_n^3/1.5\pi^2$; μ_n is the neutron chemical potential, $\mu_p^{(N)}$ the proton chemical potential inside nuclei, μ_e the electron chemical potential; P is the pressure and n_N the number density of nuclei.

TABLE 2

Densities and pressures in the free neutron regime

ρ (g/cm^3)	ρ_c (g/cm^3)	P (MeV/fm^3)	P_c (MeV/fm^3)	n_b (fm^{-3})	a (fm)	u	ζ_N
4.66×10^{11}	4.27×10^{11}	5.00×10^{-4}	4.99×10^{-4}	2.79×10^{-4}	98	1.6×10^{-3}	2.2
8.79×10^{11}	4.98×10^{11}	6.42×10^{-4}	5.96×10^{-4}	5.25×10^{-4}	96	1.9×10^{-3}	2.2
1.47×10^{12}	5.68×10^{11}	8.73×10^{-4}	6.94×10^{-4}	8.79×10^{-4}	94	2.2×10^{-3}	2.3
2.67×10^{12}	6.84×10^{11}	1.47×10^{-3}	8.58×10^{-4}	1.59×10^{-3}	90	2.7×10^{-3}	2.4
6.25×10^{12}	9.83×10^{11}	4.04×10^{-3}	1.29×10^{-3}	3.73×10^{-3}	83	4.0×10^{-3}	2.5
1.50×10^{13}	1.71×10^{12}	1.38×10^{-2}	2.38×10^{-3}	8.91×10^{-3}	75	7.3×10^{-3}	2.7
3.44×10^{13}	3.74×10^{12}	4.77×10^{-2}	5.48×10^{-3}	2.04×10^{-2}	64	1.7×10^{-2}	2.9
8.01×10^{13}	1.21×10^{13}	0.176	1.74×10^{-2}	4.75×10^{-2}	53	6.2×10^{-2}	2.9
1.30×10^{14}	2.97×10^{13}	0.384	3.86×10^{-2}	7.89×10^{-2}	48	0.15	2.4
2.00×10^{14}	7.97×10^{13}	0.803	8.31×10^{-2}	0.118	47	0.34	1.6
2.39×10^{14}	1.46×10^{14}	1.09	0.116	0.141	57	0.58	0.9

ρ_c is the mass density of the nuclei plus electrons, P_c is the sum of the electron gas pressure plus the negative lattice pressure [eq. (2.21)]; n_b is the density of baryons; a is the bcc lattice constant, u is the fraction of space occupied by nuclei, and $\zeta_N = (A-Z-n_n V_N)/Z$ is the number of excess neutrons per proton in nuclei.

TABLE 3

Effective nuclear energies

ρ (g/cm^3)	A	Z	W' (MeV)	w_{surf} (MeV)	w_c (MeV)	r
4.66×10^{11}	127	40	−12.1	15.4	0.62	1.5×10^{-4}
8.79×10^{11}	134	41	−11.8	15.4	0.61	1.5×10^{-3}
1.47×10^{12}	140	42	−11.5	15.3	0.60	3.5×10^{-3}
2.67×10^{12}	149	44	−11.2	15.2	0.59	7.8×10^{-3}
6.25×10^{12}	170	48	−10.4	14.9	0.56	2.1×10^{-2}
1.50×10^{13}	211	54	− 9.00	14.2	0.51	5.7×10^{-2}
3.44×10^{13}	296	65	− 6.71	12.5	0.44	0.14
8.01×10^{13}	548	89	− 2.60	8.67	0.30	0.37
1.30×10^{14}	990	120	0.88	5.61	0.19	0.58
2.00×10^{14}	2500	201	5.17	2.85	0.088	0.79
2.39×10^{14}	7840	445	7.98	1.42	0.028	0.89

The total energy per nucleus, W_N+W_L, can be written in the form $W_N+W_L = W'A+w_{surf}A^{\frac{2}{3}}+w_c Z^2/A^{\frac{1}{3}}$, plus rest masses, where W' is the effective bulk energy coefficient, w_{surf} the surface energy coefficient, and w_c the net Coulomb energy coefficient, evaluated for the equilibrium nuclei. $r = (k_n/k)^3$ is the density of outside neutrons divided by the density inside the nuclei.

Tables 1, 2 and 3 summarize the results of our calculations in the free neutron regime. The mass density is given by the total energy density (2.4), divided by c^2, and P by eq. (2.20). We note from table 1 that x decreases monotonically with density while k goes through a minimum for $\rho \sim 9\times10^{13}$ g/cm^3; these features agree with our findings (fig. 2) for coexistence between bulk nuclear matter and a pure neutron gas.

Comparing the equation of state in this regime with that of a pure neutron gas (see table 7) at the same total mass density, we see that at $\rho \sim 2\times10^{12}$ g/cm^3 the pressure is about a factor of two higher than in a pure neutron gas, while at $\rho \sim 2\times10^{14}$ g/cm^3, the pure neutron gas pressure is $\sim 30\,\%$ higher.

The fraction of space, u, occupied by nuclei is seen in table 2 to increase monotonically until the nuclei begin to touch. For a bcc lattice the value $u = \sqrt{3}\pi/8 = 0.68$ corresponds to the nuclei just touching. The picture of nuclei as spherical drops is certainly not valid beyond this point. The nuclear parameters A, Z and n_N, given for $\rho = 2.26\times10^{14}$ and 2.39×10^{14} g/cm^3 should be regarded as highly tentative since they are particularly sensitive to the precise way in which the surface energy tends to zero as $n_n/n \to 1$. Furthermore, our model has neglected deformations of the nuclei, which become important here. In fact, it might be more favorable, beyond $u = 0.5$, for the nuclei to "turn inside out", that is, for the neutron gas to exist as a lattice of droplets in a sea of nuclear matter.

Although the number of nuclei beyond 1.8×10^{14} g/cm^3 appears to decrease, the fraction of nucleons in nuclei continues to increase. It is very interesting to note, in table 2, the rough constancy of the parameter

$$\zeta_N = \frac{A-Z-n_n V_N}{Z} = \frac{1-x-r}{x} \tag{6.19}$$

which is the number of excess neutrons (measured with respect to the outside neutron gas) per proton in nuclei. Neutron drip occurs when $\zeta_N \approx 2.3$; at high neutron gas densities, the nuclei can be regarded as proton clusters in the neutron gas, and the number of neutrons that must be added to the pure neutron gas when one proton is added, to keep μ_n constant, is $\sim$ 2–4 (see ζ in table 7).

Table 3 gives the effective nuclear energies in the free neutron regime. As in the semi-empirical mass formula we may write the nuclear energy as

$$W_N + W_L = [(1-x)m_n + xm_p]c^2A + W'A + w_{surf}A^{\frac{2}{3}} + w_c Z^2 A^{-\frac{1}{3}}, \tag{6.20}$$

where W' is given by (6.7). We see in table 3 that as r, the ratio of outside neutron density to the density of nucleons in the nucleus, grows, the effective surface energy drops by a factor of 10, the Coulomb energy by a factor of 20, and the effective bulk energy becomes positive. Even though the nuclei are unbound, they are held together by the outside neutron gas pressure.

In order to study the sensitivity of our results to the particular form of the nuclear surface energy, we have repeated the calculations using two other expressions for the surface thickness: (case a) $d = \eta\pi/k$, a surface thinner by a factor k_c/k than our preferred expression (case b), $d = \eta\pi/k_c$; and (case c), $d = \eta\pi/k(1-r)$, a surface that becomes quite diffuse as $r \to 1$. As is seen in table 4, the pressure for a given mass density increases negligibly with increasing surface thickness; the resulting equation of state in the free neutron regime is essentially independent of the details of the

TABLE 4

Comparison of results in the free neutron regime for three different surface energies

	ρ (g/cm^3)	P (MeV/fm^3)	A	Z	u	r
a)	1.47×10^{12}	8.72×10^{-4}	139	42	2.2×10^{-3}	3.5×10^{-3}
b)	1.47×10^{12}	8.73×10^{-4}	140	42	2.2×10^{-3}	3.5×10^{-3}
c)	1.47×10^{12}	8.74×10^{-4}	140	42	2.2×10^{-3}	3.5×10^{-3}
a)	1.10×10^{13}	8.80×10^{-3}	190	51	5.8×10^{-3}	4.1×10^{-2}
b)	1.10×10^{13}	8.81×10^{-3}	193	51	5.7×10^{-3}	4.0×10^{-2}
c)	1.10×10^{13}	8.82×10^{-3}	197	52	5.6×10^{-3}	4.0×10^{-2}
a)	1.05×10^{14}	0.270	588	84	0.101	0.49
b)	1.05×10^{14}	0.270	738	103	0.099	0.48
c)	1.05×10^{14}	0.271	1120	151	0.093	0.47
a)	2.38×10^{14}	1.09	2120	151	0.44	0.83
b)	2.39×10^{14}	1.09	7840	445	0.58	0.89

Surface term b), with the thickness $\eta\pi/k_e$ is the one we have used in all the calculations, as given in tables 1, 2, 3, 5 and 9. In a) we take the surface thickness to be $\eta\pi/k$, and therefore thinner than in b), while in c) we take a relatively thick surface, $\eta\pi n/k(n-n_n)$. The notation is the same as in tables 1 and 2.

nuclear surface thickness. But, as one expects from eqs. (4.10) and (6.4), w_{surf} and hence the nuclear size grows with increasing surface thickness.

We have calculated here the properties of the ground state of matter in the free neutron regime, assuming complete nuclear equilibrium. This is a very good assumption in this regime, because the presence of the free neutron and electron gases readily allows processes that change both A and Z. There is, however, the possibility that the wrong lattice structure was frozen in at higher temperatures; then the system at zero temperature would have complete nuclear equilibrium for the metastable lattice. The type of nucleus present in the ground state is insensitive though to the particular lattice structure.

The lattice, however, does play a role in determining the thermal fluctuations from complete equilibrium that are likely to be present in a neutron star at non-zero temperature, since a local fluctuation of Z will distort the lattice and modify the local lattice energy. This effect will tend to inhibit thermal fluctuations of Z.

7. Proton drip

We have so far assumed that the protons remain confined in the nuclei, that is, that there is no proton drip. In order for this to be so the chemical potential $\mu_p^{(N)}$ of the protons in the nuclei must be smaller than $\mu_p^{(G)}$, the energy required to add a proton to the neutron gas. When a proton is added to the neutron gas, electrostatic effects will tend to keep it far away from the nuclei: the electrostatic potential outside the

nuclei has a minimum, for a bcc lattice, half way along the cube edges, and equivalently, in the face centers of the cube. Were it not for zero-point oscillations, this would be the position of a proton in the neutron gas.

Its energy there would be a sum of the nuclear energy $\mu_p^{(0)}(k_n)$, eq. (3.9), required to add the proton to the neutron gas, plus the electrostatic potential at the minimum point. In the Wigner-Seitz approximation, the electrostatic potential outside a nucleus is

$$\phi(r) = \frac{Ze}{r} - \frac{Ze}{2r_c}\left(3 - \left(\frac{r}{r_c}\right)^2\right) \tag{7.1}$$

and the minimum point corresponds to the surface of the cell, $r = r_c$, where $\phi(r) = 0$. Recalling that we are measuring all proton energies with respect to $e\phi_0$, eq. (5.14), we find that the total energy required to add a proton outside the nucleus, neglecting zero-point energy, is

$$\mu_p^{(G)} = \mu_p^{(0)}(k_n) + \mu_{p,es}^{(G)}, \tag{7.2}$$

where

$$\mu_{p,es}^{(G)} = \frac{-Ze^2}{r_c}\left(\frac{3}{10} - \frac{3r_N^2}{10r_c^2}\right). \tag{7.3}$$

In a more exact calculation for the face centers of a bcc lattice the first $\frac{3}{10}$ in (7.2) is replaced by† 0.33, while the term $\frac{3}{10}r_n^2$ becomes half the nuclear $\langle r^2\rangle$.

The zero-point motion of the proton about the minimum points can also be estimated, in the Wigner-Seitz approximation, by expanding $\phi(r)$ about r_c to second order; this yields an effective one-dimensional harmonic oscillator potential

$$e\phi(r) = \frac{3Ze^2}{2r_c^3}(r - r_c)^2 + \ldots. \tag{7.4}$$

The proton is confined in this well radially, but is free to move over the surface of the cell, $r = r_c$. In a bcc lattice this corresponds to a proton at a face center being rather free to have large excursions from equilibrium within the face, but experiencing large restoring forces if it moves towards the nuclei at the nearest body centers.

The frequency of oscillations in the well (7.4) is

$$\omega = \left(\frac{3Ze^2}{m_p r_c^3}\right)^{\frac{1}{2}}; \tag{7.5}$$

adding the zero-point energy

$$\mu_{p,zp}^{(G)} = \tfrac{1}{2}\hbar\omega = \left(\frac{e^2/\hbar c}{3\pi m_p c^2}\right)^{\frac{1}{2}}\mu_e^{\frac{1}{2}} \tag{7.6}$$

to (7.2), we have, as a final result

$$\mu_p^{(G)} = \mu_p^{(0)}(k_n) - \frac{Ze^2}{r_c}\left[\frac{3}{10} - \frac{3}{10}\frac{r_n^2}{r_c^2} - \left(\frac{3}{16\pi}\right)^{1/6}\frac{1}{Z^{\frac{1}{2}}}\left(\frac{\mu_e}{m_p c^2}\frac{\hbar c}{e^2}\right)^{\frac{1}{2}}\right]. \tag{7.7}$$

† This result is $1/3Z$ times the coefficient of x in eq. (1.6) of ref. [32]).

The zero-point energy, equal to $0.908(\mu_e/100)^{\frac{3}{4}}$ in MeV, is generally on the order of one third the electrostatic energy and opposite in sign. The mean-square excursion from equilibrium is given by

$$\langle (r-r_c)^2 \rangle = \frac{1}{6}\left(\frac{12}{\pi}\right)^{1/6} \frac{1}{Z^{\frac{1}{3}}} \left(\frac{\mu_e}{m_p c^2}\,\frac{\hbar c}{e^2}\right)^{\frac{1}{2}} r_c^2, \tag{7.8}$$

which is at most $\sim 0.03\, r_c^2$.

In table 5 we compare calculations of $\mu_p^{(G)}$, (7.7), with the value of the proton chemical potential in the nucleus calculated from

$$\mu_p^{(N)} = \mu_n - \mu_e + (m_n - m_p)c^2. \tag{7.9}$$

We see that up until the point where the nuclei begin to touch, there is no proton drip. (Of course, when the nuclei are near touching the evaluation of the zero-point energy in terms of a harmonic oscillator must be improved; such a refinement would further discourage proton drip.)

TABLE 5

The proton chemical potential inside and outside nuclei

ρ (g/cm^3)	μ_n (MeV)	$\mu_p^{(N)}$ (MeV)	$\mu_p^{(G)}$ (MeV)	$\mu_{p,es}^{(G)}$ (MeV)	$\mu_{p,zp}^{(G)}$ (MeV)
4.66×10^{11}	0.14	−24.89	− 0.30	−0.34	0.12
8.79×10^{11}	0.55	−25.67	− 0.97	−0.37	0.13
1.47×10^{12}	0.91	−26.38	− 1.88	−0.39	0.14
2.67×10^{12}	1.42	−27.44	− 3.49	−0.42	0.15
6.25×10^{12}	2.45	−29.69	− 7.33	−0.49	0.18
1.50×10^{13}	4.07	−33.64	−14.00	−0.61	0.22
3.44×10^{13}	6.47	−40.34	−24.20	−0.83	0.30
8.01×10^{13}	10.36	−52.66	−40.35	−1.24	0.47
1.30×10^{14}	13.77	−63.52	−53.64	−1.57	0.63
2.00×10^{14}	18.11	−75.79	−69.34	−1.91	0.84
2.39×10^{14}	20.37	−81.92	−77.80	−2.08	0.96

ρ is the total mass density, and μ_n the neutron chemical potential; $\mu_p^{(N)}$ is the proton chemical potential inside the nuclei, $\mu_p^{(G)}$ is the proton chemical potential in the neutron gas; $\mu_{p,es}^{(G)}$ is the electrostatic contribution to $\mu_p^{(G)}$, and $\mu_{p,zp}^{(G)}$ is the zero-point energy contribution to $\mu_p^{(G)}$. As long as $\mu_p^{(N)} < \mu_p^{(G)}$ there is no proton drip.

We note that there does not appear from our calculations to be a possibility of having equilibrium between two phases in bulk, each with finite proton concentration; that is, there are no solutions to the equations

$$\begin{aligned} \mu_n(k, x) &= \mu_n(k', x'), \\ \mu_p(k, x) &= \mu_p(k', x'), \\ P(k, x) &= P(k', x'), \end{aligned} \tag{7.10}$$

for $x \neq 0$, $x' \neq 0$ and k', given the density of one phase (k). This can be seen by examining fig. 2.

8. The neutron liquid

At sufficiently high densities the nuclei disappear and the matter becomes a uniform liquid composed primarily of neutrons with a small percentage of protons and electrons, and, as we shall see, an even smaller fraction of muons. We shall refer to this phase as the *neutron liquid*, to distinguish it from the pure *neutron gas* present with the nuclei. In order to determine the density at which the nuclei disappear, and the nature of the transition, we must determine the properties of the neutron liquid phase.

The total energy per unit volume of the neutron liquid is

$$E_{\rm tot}(n, x, n_{\rm e}, n_\mu) = nW(k, x)+n[(1-x)m_{\rm n}+xm_{\rm p}]c^2+E_{\rm e}(n_{\rm e})+E_\mu(n_\mu) \quad (8.1)$$

where $n = k^3/1.5\pi^2$ is now the number density of nucleons, $n_{\rm e}$ is the electron number density and n_μ the μ^- density; E_μ is the energy density of free muons, and W is the energy function determined in sect. 3. The equilibrium conditions are found by minimizing (8.1) at fixed baryon density n, subject to the condition of charge neutrality:

$$xn = n_{\rm e}+n_\mu . \quad (8.2)$$

Keeping n_μ fixed and minimizing $E_{\rm tot}$ with respect to $n_{\rm e}$ we find the β-stability condition:

$$\frac{\partial W(k, x)}{\partial x} = \mu_{\rm p}-\mu_{\rm n} = -\mu_{\rm e}+(m_{\rm n}-m_{\rm p})c^2, \quad (8.3)$$

where

$$\mu_{\rm n} = n\left(\frac{\partial W}{\partial n}\right)_{xn}, \qquad \mu_{\rm p} = n\left(\frac{\partial W}{\partial n}\right)_{(1-x)n}, \quad (8.4)$$

and $\mu_{\rm e} = \partial E_{\rm e}/\partial n_{\rm e}$. If there are no muons present, corresponding to $\mu_{\rm e} \leqq m_\mu c^2 = 105.66$ MeV, where m_μ is the muon rest mass, eqs. (8.3) and $xn = n_{\rm e}$ serve to determine the equilibrium value of x for given n. When muons are present there is one further condition, found by minimizing $E_{\rm tot}$ with respect to n_μ at fixed $n_{\rm e}+n_\mu$; this condition is

$$\mu_\mu = \mu_{\rm e}, \quad (8.5)$$

where

$$\mu_\mu = \frac{\partial E_\mu}{\partial n_\mu} = c[(\hbar k_\mu)^2+(m_\mu c)^2]^{\frac{1}{2}} \quad (8.6)$$

is the muon chemical potential, and k_μ is the muon Fermi wave number. Thus

$$k_\mu = \left[\left(\frac{\mu_{\rm e}}{\hbar c}\right)^2 - \left(\frac{m_\mu c}{\hbar}\right)^2\right]^{\frac{1}{2}}. \quad (8.7)$$

TABLE 6

Properties of the equilibrium uniform neutron-proton liquid

$\rho\times10^{-14}$ (g/cm^3)	x (%)	k (fm^{-1})	μ_n (MeV)	μ_e (MeV)	P (MeV/fm^3)	n_b (fm^{-3})	n_μ/n_e
1.52	2.7	1.10	15.20	82.51	0.49	0.090	0
1.69	3.0	1.14	16.23	87.59	0.59	0.100	0
1.83	3.1	1.17	17.04	91.35	0.67	0.108	0
1.98	3.2	1.20	17.89	95.04	0.77	0.117	0
2.13	3.4	1.23	18.79	98.65	0.88	0.126	0
2.29	3.5	1.26	19.73	102.17	1.00	0.135	0
2.46	3.6	1.29	20.72	105.60	1.14	0.145	0
2.64	3.7	1.32	21.73	108.91	1.29	0.155	0.014
2.82	3.9	1.35	22.79	112.06	1.46	0.166	0.037
2.89	3.9	1.36	23.15	113.08	1.52	0.170	0.045
3.02	4.0	1.38	23.89	115.07	1.65	0.177	0.062
3.15	4.1	1.40	24.67	116.98	1.79	0.185	0.079
3.22	4.1	1.41	25.06	117.91	1.86	0.189	0.087
3.43	4.3	1.44	26.29	120.61	2.10	0.202	0.112
3.65	4.3	1.47	27.59	123.17	2.37	0.215	0.136
3.89	4.4	1.50	28.96	125.61	2.66	0.228	0.158

ρ is the total mass density; the density of nucleons equals $k^3/1.5\pi^2$; x is the fractional concentration of protons, μ_n the neutron chemical potential, μ_e the electron chemical potential, P the total pressure, n_b the total density of baryons, n_e the density of electrons and n_μ the density of muons. Note that the liquid is unstable for $\rho \lesssim 2.85\times10^{14}$ g/cm^3.

Eqs. (8.5), (8.3) and (8.2) are most readily solved by treating n as the independent variable. For a given x, eq. (8.3) specifies $\mu_e(k, x)$. Then the total density of negative charge is, from (8.7),

$$n_e+n_\mu = \frac{(\mu_e/\hbar c)^3}{3\pi^2}\left[1+\left(1-\left(\frac{m_\mu c^2}{\mu_e}\right)^2\right)^{\frac{3}{2}}\right] = nx. \tag{8.8}$$

This latter equation can be solved numerically for x as a function of n. The resulting properties of the neutron liquid are listed in table 6. The pressure of the liquid is given by

$$P = n^2\frac{\partial W}{\partial n}+P_e+P_\mu \tag{8.9}$$

where P_e and P_μ are the free electron and muon pressures.

In doing this calculation we have neglected Coulomb interactions between the muons; this is valid if

$$n_\mu \gg \frac{3}{4\pi}\left(\frac{m_\mu e^2}{\hbar^2}\right)^3 = \frac{9\pi}{4}\left(\frac{m_\mu c^2}{\mu_e}\frac{e^2}{\hbar c}\right)^3 n_e.$$

Since muons are present only if $\mu_e > m_\mu c^2$, this condition is

$$\frac{n_\mu}{n_e} \gg 3 \times 10^{-6}, \tag{8.10}$$

which obtains rapidly above the threshold for having muons present.

TABLE 7

Properties of the pure neutron gas

ρ (g/cm^3)	k (fm^{-1})	μ_n (MeV)	P (MeV/fm^3)	W (MeV)	$\mu_p^{(G)}$ (MeV)	ζ
3.82×10^{11}	0.15	0.55	4.71×10^{-5}	0.35	− 0.73	2.1
1.99×10^{12}	0.26	1.43	6.17×10^{-4}	0.91	− 3.23	3.2
5.29×10^{12}	0.36	2.46	2.78×10^{-3}	1.58	− 7.02	3.9
1.33×10^{13}	0.49	4.08	1.15×10^{-2}	2.63	−13.61	4.2
3.12×10^{13}	0.65	6.49	4.27×10^{-2}	4.19	−23.67	4.1
7.25×10^{13}	0.86	10.44	0.162	6.68	−39.58	3.9
1.18×10^{14}	1.01	13.93	0.357	8.80	−52.70	3.6
1.83×10^{14}	1.17	18.49	0.761	11.46	−68.28	3.2
2.29×10^{14}	1.26	21.53	1.13	13.16	−77.76	3.0
2.46×10^{14}	1.29	22.64	1.29	13.77	−81.04	2.9
3.16×10^{14}	1.40	27.13	2.03	16.19	−93.53	2.6
3.89×10^{14}	1.50	31.93	3.02	18.68	−105.6	2.4

Up to $k = 1.26$ the values of k ($= 2^{-1/3}$ times the actual Fermi wave number of the gas) are taken to be the same as the k_n in tables 1, 2, 3 and 5. ρ is the mass density of the neutron gas, μ_n the neutron chemical potential, P the pressure, W the energy per neutron, and $\mu_p^{(G)}$ the proton chemical potential. The quantity ζ is the number of neutrons that must be added, when one proton is added, to keep μ_n constant.

Comparing the properties of the neutron liquid with those of a pure neutron gas, as given in table 7, we see that for a given mass density, the pressure of the uniform liquid is $\sim 10\,\%$ less than that of the pure gas; this reduction is a consequence of allowing the neutrons to come to β-equilibrium †. For the same μ_n the pressure in the neutron liquid must of course be higher than that in the pure neutron gas; this is again a $10\,\%$ effect here.

9. When and how do the nuclei dissolve?

The transition from the phase with nuclei, described in sect. 6, to the uniform liquid, described in sect. 8, must remove the long-range order of the nuclear phase. This can occur conceivably by having the number of nuclei going to zero, a second-order transition, as proposed by Langer *et al.* [6]), or else by having the density inhomogeneity due to nuclei disappearing at some finite density of nuclei. This latter type of transi-

† Quite generally, if one allows the system to come to equilibrium through a reaction, such as β-decay, the energy of the system will be lowered. One can say with certainty that the pressure is lowered only at densities just above the threshold for the reaction.

tion must, on general arguments [33]), be first order, the density inhomogeneity going to zero discontinuously.

As we have seen in table 1, the number density of nuclei remains quite finite as the mass density increases; the second-order transition in which $n_N \to 0$ certainly does not occur in our calculations. There is a general reason why this type of transition should not occur. Suppose that as we lower the density of the liquid phase it becomes favorable for a nucleus to appear. Then because of the net *attractive* Coulomb interaction between nuclei (the lattice energy) the system would prefer to have a finite number of nuclei present; a state with a vanishingly small number of nuclei cannot be in thermodynamic equilibrium. This argument holds equally well if the nuclear phase is molten.

To establish the criteria for the transition we note that at the boundary in the star between the phase with nuclei (the crust), and the liquid interior, both the neutron chemical potential and the pressure must be continuous; the mass density has a discontinuous increase. The phase present at a given pressure is the one with the lower Gibbs potential

$$\mu = \frac{E_{\rm tot} + P}{n_{\rm b}}, \tag{9.1}$$

where $n_{\rm b}$ is the total density of baryons. In fact, μ equals $\mu_{\rm n}$, the neutron chemical potential; this follows if we write

$$\mu n_{\rm b} = \sum_i \mu_i n_i \tag{9.2}$$

where the sum is over all particle types present. Now if particle type i has charge Q_i and baryon number B_i, then

$$\mu_i = B_i \mu_{\rm n} - Q_i \mu_{\rm e}; \tag{9.3}$$

this guarantees stability of particle i against β-decay. Using (9.3), (9.2) becomes

$$\mu n_{\rm b} = \mu_{\rm n} \sum_i B_i n_i - \mu_{\rm e} \sum_i Q_i n_i; \tag{9.4}$$

from charge neutrality $\sum_i Q_i n_i = 0$, while $\sum_i B_i n_i = n_{\rm b}$, so that $\mu = \mu_{\rm n}$. Thus the phase present at a given pressure is the one with the lower $\mu_{\rm n}$. Alternatively, for a given $\mu_{\rm n}$, the phase present is the one with the larger pressure.

If we compare the P and $\mu_{\rm n}$ calculations in tables 1 and 6 for the nuclear and liquid phases respectively, we see no obvious point at which the $P(\mu_{\rm n})$ curves for the two phases cross; rather, the two curves appear practically to merge. The transition certainly does not occur for $\rho \leqq 1.7 \times 10^{14}$ g/cm^3, and there is no clear transition by $\rho = 2.4 \times 10^{14}$ g/cm^3, when the nuclei begin to touch †.

† As remarked in sect. 1, if one tries to describe the nuclei by the semi-empirical mass formula then one finds that the maximum possible $\mu_{\rm n}$ in the nuclear phase is $\approx$ 8.3 MeV. However at this value of $\mu_{\rm n}$, the pressure in the liquid phase is definitely lower than that in the nuclear phase, so that the nuclear phase is thermodynamically preferable. There is no way, using the semi-empirical mass formula, to have equilibrium between the nuclear and liquid phases; this is a serious inconsistency of using the semi-empirical mass formula in this context.

The key to the nature of the phase transition is the observation that as one lowers the density of the uniform liquid phase, it develops an instability against proton clustering†. The density at which this instability occurs, $\rho_i \approx 2.85 \times 10^{14}$ g/cm^3 is above that at which the nuclei begin to touch. The transition must then be one in which the nuclei merge and the density inhomogeneity in the nuclear phase is smoothed out. As we shall argue, the inhomogeneous phase remains thermodynamically preferable at densities slightly above ρ_i; the inhomogeneity disappears discontinuously in a first-order transition.

We can see the presence of the instability by looking at the variation of the total energy density in the presence of an infinitesimal density inhomogeneity, $\delta n_n(r)$, $\delta n_p(r)$ and $\delta n_e(r)$. (For simplicity we neglect the presence of muons for the moment.) The scale of spatial variation we shall be concerned with is large compared with the range of the nucleon-nucleon interaction, and thus the energy is given, to second order in the δn, by the Thomas-Fermi expressions (4.1) for the local energy, plus (4.14) for the curvature terms, plus the electron and Coulomb energies. In terms of the Fourier transforms of the density variations, the total Coulomb energy is

$$E_{\text{Coul}} = \frac{1}{2}\int \frac{\mathrm{d}^3q}{(2\pi)^3}\,\frac{4\pi e^2}{q^2}\,|\delta n_p(q) - \delta n_e(q)|^2, \tag{9.5}$$

and the curvature energy is

$$E_{\text{curv}} = \frac{1}{n_{\text{NM}}}\int \frac{\mathrm{d}^3q}{(2\pi)^3}\,q^2[B_{nn}|\delta n_n|^2 + B_{pp}|\delta n_p|^2 + B_{np}(\delta n_p^*\delta n_n + \delta n_p\,\delta n_n^*)]. \tag{9.6}$$

The electron curvature energy can be neglected. The local energy, to second order can be written as

$$E_{\text{loc}} = E_0 + \int \mathrm{d}^3r[(\mu_n + m_n c^2)\delta n_n(r) + (\mu_p + m_p c^2)\delta n_p(r) + \mu_e\,\delta n_e(r)]$$
$$+ \int \mathrm{d}^3r\left[\frac{\partial \mu_n}{\partial n_n}(\delta n_n(r))^2 + \frac{\partial \mu_p}{\partial n_p}(\delta n_p(r))^2 + 2\,\frac{\partial \mu_p}{\partial n_n}\,\delta n_p(r)\delta n_n(r) + \frac{\partial \mu_e}{\partial n_e}(\delta n_e(r))^2\right], \tag{9.7}$$

where E_0 is the energy of the uniform liquid, and $(\partial^2 nW/\partial n_n^2) = \partial \mu_n/\partial n_n$, etc. Derivatives with respect to n_n are at fixed n_p, and vice versa, unless otherwise indicated. Using the β-stability condition (8.3), and charge neutrality $[\int \mathrm{d}^3r(n_p(r) - n_e(r)) = 0]$ the first-order term becomes $(\mu_n + m_n c^2)\delta \int \mathrm{d}^3r(n_n(r) + n_p(r))$. If we assume that the variations conserve the total baryon number $\int \mathrm{d}^3r(n_n(r) + n_p(r))$, the first-order term vanishes.

An instability will occur if the energy in the presence of the density inhomogeneity is lower than E_0. Let us assume that $\delta n_p(r)$ is given; then minimizing the total energy

† We are grateful to Dr. J. Arponen for pointing out to us the existence of this instability in the calculated energies for the uniform liquid. Proton clustering in neutron star matter was discussed qualitatively by M. A. Ruderman [34]), and long-wavelength instabilities were investigated quantitatively by R. A. Wolf [35]).

with respect to $\delta n_n(r)$ and $\delta n_e(r)$ we have

$$\left(\frac{\partial \mu_n}{\partial n_n} + \frac{2B_{nn}q^2}{n_{NM}}\right)\delta n_n(q) + \left(\frac{\partial \mu_p}{\partial n_n} + \frac{2B_{np}q^2}{n_{NM}}\right)\delta n_p(q) = 0 \tag{9.8}$$

and

$$\frac{\partial \mu_e}{\partial n_e}\delta n_e(q) = \frac{4\pi e^2}{q^2}(\delta n_p(q) - \delta n_e(q)). \tag{9.9}$$

Solving for δn_n and δn_e in terms of δn_p we find that the variation of the total energy assumes the form

$$E - E_0 = \frac{1}{2}\int \frac{d^3q}{(2\pi)^3} v(q)|\delta n_p(q)|^2, \tag{9.10}$$

where the effective interaction between protons is

$$v(q) = v_0 + \beta q^2 + \frac{4\pi e^2}{q^2 + k_{FT}^2}; \tag{9.11}$$

k_{FT} is given by (5.11), while

$$v_0 = \frac{\partial \mu_p}{\partial n_p} - \frac{(\partial \mu_p/\partial n_n)^2}{(\partial \mu_n/\partial n_n)} \equiv \left(\frac{\partial \mu_p}{\partial n_p}\right)_{\mu_n, n_e}, \tag{9.12}$$

$$\beta = \frac{2}{n_{NM}}(B_{pp} + 2B_{np}\zeta + B_{nn}\zeta^2), \tag{9.13}$$

$$\zeta = -\frac{\partial \mu_p/\partial n_n}{\partial \mu_n/\partial n_n}. \tag{9.14}$$

In (9.11) we have, for consistency, retained only terms of order q^2 in the curvature energy. The parameter ζ equals the number of neutrons that must be added to the system when one proton is added, in order that the neutron chemical potential remain fixed. In the region of the instability, $\zeta \approx 2$; this means that a proton density fluctuation carries with it a neutron density fluctuation of the same sign, and about twice as large in amplitude. We note that as $q \to 0$,

$$v(q) \to \left(\frac{\partial \mu_p}{\partial n_p}\right)_{\mu_n, \mu_e}. \tag{9.15}$$

The second derivative of $v(q)$ at $q = 0$ equals $2(\beta - 4\pi e^2/k_{FT}^4)$ and is always negative in the neutron liquid, since

$$\frac{4\pi e^2}{k_{FT}^4} = \frac{\pi}{12}\left(\frac{\hbar c}{e^2}\right)\frac{(\hbar c)^2}{\mu_e n x} \gg \beta \sim \frac{10^2 \text{ MeV} \cdot \text{fm}^2}{n_{NM}}.$$

(To include muons we must replace μ_e by $\mu_e(1 + k_\mu/k_e)^2$; this does not affect the in-

equality.) Thus $v(q)$ has a minimum at $q = Q$ given by

$$Q^2 = \left(\frac{4\pi e^2}{\beta}\right)^{\frac{1}{2}} - k_{\mathrm{FT}}^2, \tag{9.16}$$

and therefore

$$v(Q) \equiv v_{\min} = v_0 + 2(4\pi e^2\beta)^{\frac{1}{2}} - \beta k_{\mathrm{FT}}^2. \tag{9.17}$$

TABLE 8
Stability of the uniform liquid

$\rho\times10^{-14}$ (g/cm^3)	μ_n (MeV)	v_0 (MeV · fm^3)	$v_{\min}$ (MeV · fm^3)	Q (fm^{-1})	a (fm)	Z_{cell}
2.29	19.73	−1190	−772	0.29	31	68
2.64	21.73	−652	−272	0.30	30	75
2.82	22.79	−397	− 36.4	0.31	29	78
2.89	23.15	−317	38.3	0.31	29	79
3.02	23.89	−162	181	0.31	28	80
3.15	24.67	− 15.4	316	0.32	28	82
3.22	25.06	54.5	381	0.32	28	82
3.43	26.29	252	563	0.33	27	84
3.89	28.96	599	882	0.34	26	86

ρ is the mass density, and μ_n the neutron chemical potential. v_0 is the long-wavelength effective proton-proton interaction, without Coulomb interactions; $v_{\min}$ is the minimum value of $v(q)$, the total effective proton-proton interaction, and Q is the wave number for the minimum. If $v_{\min} < 0$ then the liquid is unstable against proton clustering. $a = 2^3/2\pi/Q$ is the bcc lattice constant of the inhomogeneous phase while Z_{cell} is the number of protons in a primitive unit cell of the bcc lattice.

As may be seen in table 8, v_0 is negative for densities $\rho \lessapprox 3.2\times10^{14}$ g/cm^3. This implies that were Coulomb and curvature effects absent, the liquid could lower its energy, for $\rho \lessapprox 3.2\times10^{14}$ g/cm^3, by generating an infinitesimal long-wavelength density wave. The Coulomb and curvature corrections tend to suppress the instability until $v_{\min}(> v_0)$ turns negative; we denote this density, at which

$$v_0 + 2(4\pi e^2\beta)^{\frac{1}{2}} - \beta k_{\mathrm{FT}}^2 = 0, \tag{9.18}$$

by ρ_1. The k_{FT}^2 term here is generally negligible.

We note that the value of Q at which the instability occurs is determined by a competition between the Coulomb energy and the curvature term βq^2; this is the same situation as in the nuclear phase where the nuclear size is also determined [eq. (6.3)] by the competition between the Coulomb energy and the surface energy (the analogue of the βq^2 term for distinct nuclei).

The scale of values of v_0 in table 8 is essentially set by the derivative

$$\left(\frac{\partial\mu_n}{\partial n_n}\right)_{\mathrm{free}} = \frac{\hbar^2}{m_n}\frac{\pi^2}{2^{\frac{1}{2}}k}, \tag{9.19}$$

for a free neutron gas; at $k = 1.35\,\mathrm{fm}^{-1}$, we have $(\partial\mu_n/\partial n_n)_{\mathrm{free}} = 240$ MeV · fm^3.

The quantity β is uncertain in the neutron liquid, but can be estimated by assuming $B_{nn} = B_{pp} = \frac{1}{2}B_{np} = B$. Then

$$\beta = \frac{2B}{\rho_{NM}}(1+4\zeta+\zeta^2); \tag{9.20}$$

if we take $B \sim 24$ MeV · fm^2, from ref. [27]), then by numerical calculation we find

$$\rho_i \approx 2.85\times 10^{14}\ \text{g/cm}^3; \tag{9.21}$$

at ρ_i, $\zeta = 1.6$ † and $\beta \approx 2.0\times 10^3$. The wave number Q at which the instability first sets in is ≈ 0.3 fm^{-1}. The wavelength corresponding to this Q is ~ 20 fm, which is sufficiently large, compared with the range of the nuclear forces, to justify our keeping only the second-order gradient terms in the curvature energy.

As the density of the uniform liquid is lowered towards the instability, there will in fact generally occur a *first-order* transition to a spatially inhomogeneous state at a density higher than that, ρ_i, at which the liquid becomes unstable. Following Landau [33]) we consider the energy of a phase with an infinitesimal density inhomogeneity having the symmetry of a bcc lattice of lattice constant

$$a = \frac{2\pi\sqrt{2}}{Q}; \tag{9.22}$$

we write

$$n_p(\boldsymbol{r}) = n_p^0 + \delta n_p \sum_{\boldsymbol{Q}} e^{i\boldsymbol{Q}\cdot\boldsymbol{r}} \tag{9.23}$$

$$= n^0 + 4\delta n_p(\cos\sqrt{\tfrac{1}{2}}Qx\cos\sqrt{\tfrac{1}{2}}Qy + \cos\sqrt{\tfrac{1}{2}}Qy\cos\sqrt{\tfrac{1}{2}}Qz + \cos\sqrt{\tfrac{1}{2}}Qz\cos\sqrt{\tfrac{1}{2}}Qx), \tag{9.24}$$

where the sum is over the twelve bcc reciprocal lattice vectors of the form $\sqrt{\frac{1}{2}}Q(i,j,k)$, in which one of i, j, k is zero and the other two can be ± 1 independently. All the Q have the same length. The reason for examining a density inhomogeneity with bcc symmetry will be discussed momentarily.

From (9.10), the energy to second order in δn_p, is given by

$$E = E_0 + \tfrac{1}{2}V\sum_{\boldsymbol{Q}} v(Q)(\delta n_p)^2 = E_0 + 6Vv(Q)(\delta n_p)^2, \tag{9.25}$$

since $v(Q)$ depends only on the magnitude of Q; here V is the volume of the system. Corrections to the total energy of higher order in δn_p are of the general form

$$\frac{1}{6}\int \frac{d^3q}{(2\pi)^3}\frac{d^3q'}{(2\pi)^3}\frac{d^3q''}{(2\pi)^3}(2\pi)^3\delta(\boldsymbol{q}+\boldsymbol{q}'+\boldsymbol{q}'')v_3(\boldsymbol{q},\boldsymbol{q}',\boldsymbol{q}'')\delta n_p(\boldsymbol{q})\delta n_p(\boldsymbol{q}')\delta n_p(\boldsymbol{q}'') + \ldots . \tag{9.26}$$

† ζ in our calculations falls rapidly with x, at fixed k; further work is necessary to determine if this is a physical effect or simply a spurious feature of the interpolation formula for $W(k, x)$.

Substituting from (9.23) for $\delta n_p(r)$ into (9.26), the third-order energy becomes

$$\tfrac{1}{6}V \sum_{\boldsymbol{Q}\boldsymbol{Q}'\boldsymbol{Q}''} v_3(\boldsymbol{Q}, \boldsymbol{Q}', \boldsymbol{Q}'')\delta_{\boldsymbol{Q}+\boldsymbol{Q}'+\boldsymbol{Q}'',0}(\delta n_p)^3. \tag{9.27}$$

The sum will be non-zero for trios of $\boldsymbol{Q}$ of the form

$$\sqrt{\tfrac{1}{2}}Q(1, 1, 0), \qquad \sqrt{\tfrac{1}{2}}Q(-1, 0, 1), \qquad \sqrt{\tfrac{1}{2}}Q(0, -1, -1)$$

(the three vectors describe an equilateral triangle). Given $\boldsymbol{Q}$, there are four possible choices for $\boldsymbol{Q}'$ and one for $\boldsymbol{Q}''$; since by symmetry the $v_3(\boldsymbol{Q}, \boldsymbol{Q}', \boldsymbol{Q}'')$ for these Q trios must all be equal and real (we denote it by $v_3(Q)$), the third-order energy is $8v_3(Q)(\delta n_p)^3V$. The variation in the energy per unit volume to third order in δn_p is thus

$$\delta E = (6v(Q)+8v_3(Q)\delta n_p)(\delta n_p)^2. \tag{9.28}$$

At density ρ_i, $\delta E \sim (\delta n_p)^3$; therefore an infinitesimal but non-zero δn_p with $v_3(Q)\delta n_p < 0$ will lower the energy of the system below that of the uniform liquid. (Except by accident $v_3(Q)$ will be non-zero.) For densities slightly above ρ_i, where $v(Q)$ is infinitesimally small and positive, an infinitesimal δn_p such that $8v_3(Q)\delta n_p < -6v(Q)$ will also lower the energy below that of the uniform liquid. There will certainly exist such a non-uniform state of lower energy as long as the fourth- and higher-order terms in the energy can be neglected. The important point is that the minimum $|\delta n_p|$ required increases with density above ρ_i. Thus as the density of the uniform liquid is lowered towards ρ_i one will reach a point before ρ_i where it is favorable for the system to generate discontinuously a density inhomogeneity of non-zero amplitude.

Crucial in the above argument was our being able to form a density inhomogeneity that was a linear combination of Fourier components, the magnitude of whose wave numbers all were Q, and for which the cubic term (9.26) is non-vanishing. If we try to repeat the argument for a face-centered cubic lattice symmetry (for which the reciprocal lattice vectors are of the form $\sqrt{\tfrac{1}{3}}Q(i, j, k)$ where i, j and k are independently ± 1) the cubic term always vanishes, since it is impossible to satisfy $\boldsymbol{Q}+\boldsymbol{Q}'+\boldsymbol{Q}'' = 0$. The same is true for a simple cubic lattice also. For a lattice with hexagonal close-packed symmetry there are eight fundamental reciprocal lattice vectors:

$$Q\,(\pm\tfrac{1}{2}, \tfrac{1}{2}\sqrt{3}, 0), Q(\pm\tfrac{1}{2}, -\tfrac{1}{2}\sqrt{3}, 0), Q(\pm 1, 0, 0), Q(0, 0, \pm 1);$$

the lattice constant a equals $2\pi/Q$. For a density inhomogeneity of the form (9.23) with the sum over these $\boldsymbol{Q}$, the second-order term is $4v(Q)(\delta n_p)^2$. In the third-order term the equilateral triangles must lie in the $x-y$ plane; there are six choices for $\boldsymbol{Q}$, two choices for $\boldsymbol{Q}'$ and one for $\boldsymbol{Q}''$. The total energy variation to third order is then

$$\delta E = (4v(Q)+2v_3(Q)\delta n_p)(\delta n_p)^2. \tag{9.29}$$

The matrix element $v_3(Q)$ is the same as for the bcc case, since $\boldsymbol{Q}$, $\boldsymbol{Q}'$ and $\boldsymbol{Q}''$ form

equilateral triangles in both cases. Comparing (9.29) with (9.25) we see that the cubic term is relatively smaller (by a factor $\frac{3}{8}$) for the hcp than for the bcc density inhomogeneity. These arguments imply that if the uniform liquid makes a discontinuous transition to a phase with an infinitesimally small δn_p, then the ordered phase will have bcc symmetry. If the transition is to a phase with a density inhomogeneity of finite amplitude, then we cannot predict the lattice structure or lattice constant *a priori*.

The density of lattice sites n_L in the ordered phase just below the phase transition can be estimated by assuming that the basic reciprocal lattice vector of the ordered phase is not altered in magnitude from Q; then from (9.22),

$$n_L = \frac{2}{a^3} = \sqrt{\frac{1}{2}}\left(\frac{Q}{2\pi}\right)^3. \tag{9.30}$$

Taking the estimate $Q = 0.3\ \mathrm{fm}^{-1}$ we find $n_L \approx 8\times 10^{34}/\mathrm{cm}^3$, a number consistent with the number of nuclei present, $\sim 2\times 10^{34}/\mathrm{cm}^3$, at the point where the nuclei begin to touch. One does not expect perfect agreement between these two numbers because the proton (and neutron) distribution when distinct nuclei are present is quite different from the simple form (9.23) which one might expect at the transition. In particular, for nuclei, the non-linear terms (9.26) in the energy are important, and they will certainly be expected to shift the magnitude of the reciprocal lattice vectors in the nuclear phase. The quantity Z_{cell} in table 8 is the number of protons in a primitive unit cell of the bcc lattice, and is the number of protons per "cluster". That these numbers are smaller than the limiting values of Z in the nuclear phase is again a reflection of the fact that n_Z here is about a factor of 4 greater than in the nuclear phase at densities $\sim 2\times 10^{14}\ \mathrm{g/cm}^3$.

The picture we have of the phase transition is thus the following. As the density increases the nuclei grow until they begin to touch. Beyond this point the density inhomogeneity due to the nuclei begins to smooth out, and becomes smaller with increasing density; finally, somewhat beyond the density ρ_1, above which the liquid is stable, the remaining inhomogeneity disappears discontinuously. The details of this picture require further elaboration; this is a situation for which the Thomas-Fermi method is useful †.

10. The equation of state

In table 9, we give the equation of state of neutron star matter at zero temperature, between $\rho = 4.3\times 10^{11}\ \mathrm{g/cm}^3$, where neutron drip begins, and $\rho = 5\times 10^{14}\ \mathrm{g/cm}^3$, the point beyond which one does not have reliable calculations. The mass density ρ

† In this description of the transition we have not taken into account possible pairing between protons leading to a superconducting state. Such a state is greatly encouraged by the attractive neutron induced "polarization" interaction [the $-(\partial\mu_p/\partial n_n)^2/(\partial\mu_n/\partial n_n)$ term in (9.12)]. The effect of proton superconductivity on the details of the transition between the nuclear phase and the liquid phase remains an interesting problem.

TABLE 9
Equation of state

ρ (g/cm^3)	P (dynes/cm^2)	n_b (cm^{-3})	A	Z	Γ
4.46×10^{11}	7.89×10^{29}	2.67×10^{35}	126	40	0.40
5.23×10^{11}	8.35×10^{29}	3.13×10^{35}	128	40	0.36
6.61×10^{11}	9.10×10^{29}	3.95×10^{35}	130	40	0.40
7.96×10^{11}	9.83×10^{29}	4.76×10^{35}	132	41	0.46
9.73×10^{11}	1.08×10^{30}	5.81×10^{35}	135	41	0.54
1.20×10^{12}	1.22×10^{30}	7.14×10^{35}	137	42	0.63
1.47×10^{12}	1.40×10^{30}	8.79×10^{35}	140	42	0.73
1.80×10^{12}	1.64×10^{30}	1.08×10^{36}	142	43	0.83
2.20×10^{12}	1.95×10^{30}	1.31×10^{36}	146	43	0.93
2.93×10^{12}	2.59×10^{30}	1.75×10^{36}	151	44	1.06
3.83×10^{12}	3.51×10^{30}	2.29×10^{36}	156	45	1.17
4.93×10^{12}	4.77×10^{30}	2.94×10^{36}	163	46	1.25
6.25×10^{12}	6.48×10^{30}	3.73×10^{36}	170	48	1.31
7.80×10^{12}	8.75×10^{30}	4.65×10^{36}	178	49	1.36
9.61×10^{12}	1.17×10^{31}	5.73×10^{36}	186	50	1.39
1.25×10^{13}	1.69×10^{31}	7.42×10^{36}	200	52	1.43
1.50×10^{13}	2.21×10^{31}	8.91×10^{36}	211	54	1.44
1.78×10^{13}	2.85×10^{31}	1.06×10^{37}	223	56	1.46
2.21×10^{13}	3.93×10^{31}	1.31×10^{37}	241	58	1.47
2.99×10^{13}	6.18×10^{31}	1.78×10^{37}	275	63	1.49
3.77×10^{13}	8.77×10^{31}	2.24×10^{37}	311	67	1.51
5.08×10^{13}	1.39×10^{32}	3.02×10^{37}	375	74	1.53
6.19×10^{13}	1.88×10^{32}	3.67×10^{37}	435	79	1.54
7.73×10^{13}	2.66×10^{32}	4.58×10^{37}	529	88	1.56
9.83×10^{13}	3.90×10^{32}	5.82×10^{37}	683	100	1.60
1.26×10^{14}	5.86×10^{32}	7.47×10^{37}	947	117	1.65
1.59×10^{14}	8.59×10^{32}	9.37×10^{37}	1390	143	1.70
2.00×10^{14}	1.29×10^{33}	1.18×10^{38}	2500	201	1.74
2.52×10^{14}	1.90×10^{33}	1.48×10^{38}			1.81
2.76×10^{14}	2.24×10^{33}	1.62×10^{38}			1.82
3.08×10^{14}	2.75×10^{33}	1.81×10^{38}			1.87
3.43×10^{14}	3.37×10^{33}	2.02×10^{38}			1.92
3.89×10^{14}	4.29×10^{33}	2.28×10^{38}			1.97
4.64×10^{14}	6.10×10^{33}	2.71×10^{38}			2.03
5.09×10^{14}	7.39×10^{33}	2.98×10^{38}			2.05

ρ is the mass density, P the pressure and n_b the density of baryons. A and Z are the nucleon number and proton number of nuclei, when they are present, and $\Gamma = (n_b/P)\,\partial P/\partial n_b$ is the adiabatic index.

is the total energy density, (2.4) in the nuclear phase, and (8.1) in the liquid phase, divided by c^2; this is the source for the gravitational field. The pressure is given by (2.20) in the nuclear phase, and (8.9) in the liquid. We have taken the phase transition, the dissolving of the crust material, to take place when the nuclei touch, $\rho \sim 2.4\times10^{14}$ g/cm^3; the equation of state is, however, insensitive to the actual transition density, since near the transition there is so little difference between the pressures of the two phases, at given μ_n.

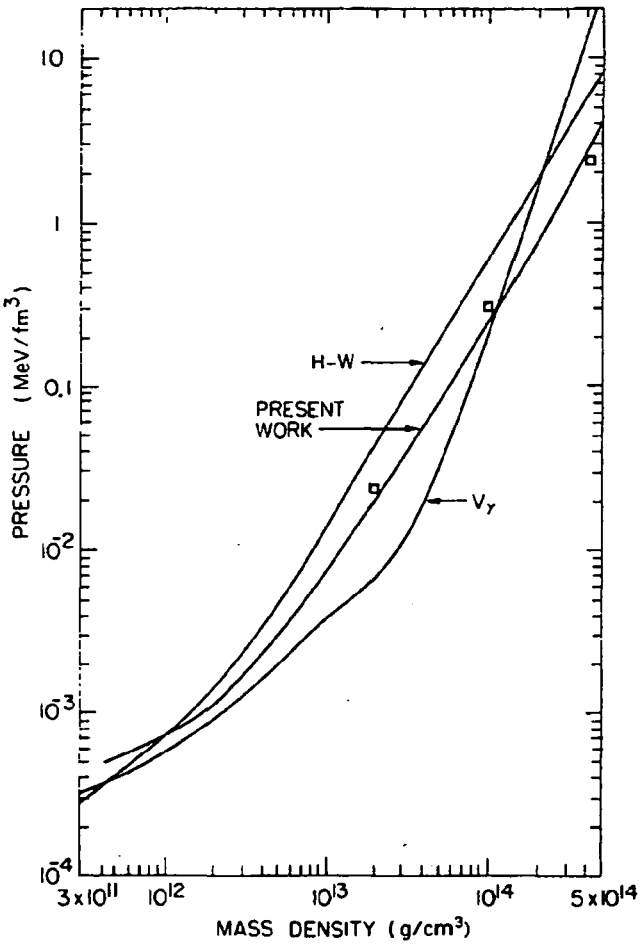

Fig. 3. Equation of state. The pressure versus mass density as calculated here, as compared with the Harrison-Wheeler (H-W) equation of state [36]), the V_γ equation of state [6, 37]) and the Wang *et al.* equation of state (indicated by squares) [21]).

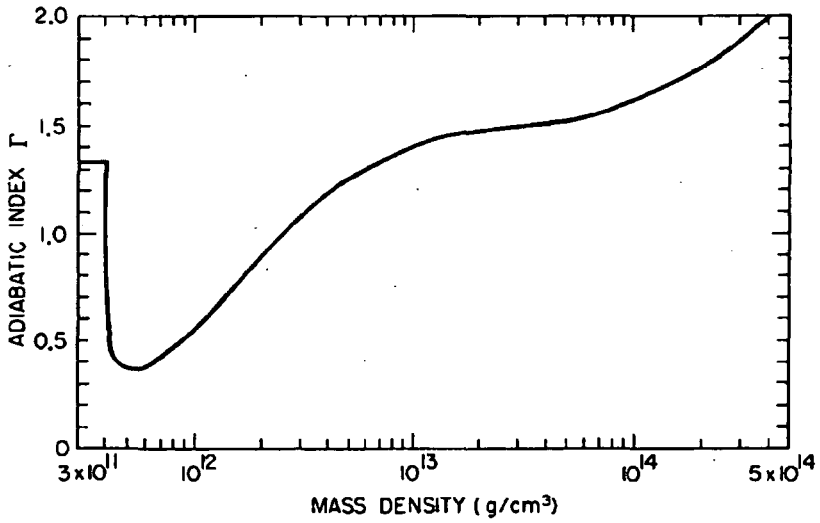

Fig. 4. The adiabatic index $\Gamma = \partial \ln P/\partial \ln n_b$ as a function of mass density.

In fig. 3 we compare our equation of state with that of Harrison and Wheeler, as given by Hartle and Thorne [36]); the V_γ equation of state of Langer *et al.* [6]) (for $\rho \leqq 1\times10^{14}$ g/cm^3) and Langer and Rosen [37]) (for $\rho \geqq 1\times10^{14}$ g/cm^3); and Wang *et al.* [21]), extracted from their fig. 1. The present equation of state is nearly proportional, above $\rho \sim 10^{13}$ g/cm^3, to the Harrison-Wheeler equation of state, which was calculated for non-interacting nucleons, allowing for β-decay; above 10^{13} g/cm^3 it is also within a few percent of the Wang *et al.* equation of state, which was calculated for a pure neutron gas using realistic nucleon-nucleon potentials, but including neither protons nor nuclei. The V_γ equation of state, by comparison, is much softer between 10^{12} and 10^{13} g/cm^3, and is then much harder above 4×10^{13} g/cm^3. This behavior of the V_γ equation of state is due to the strong velocity dependence of the Levinger-Simmons V_γ potential, which leads to a positive term in the pressure varying as $\rho^2 k_f^2 \sim \rho^{\frac{4}{3}}$, dominating at high densities.

The general-relativistic adiabatic index, defined by

$$\Gamma = \frac{n_b}{P}\frac{\partial P}{\partial n_b} = \frac{\rho + P/c^2}{P}\frac{\partial P}{\partial \rho}, \tag{10.1}$$

is shown in fig. 4. The dip in Γ after neutron drip is due to the fact that as free neutrons appear, they contribute significantly to the mass density, but very little to the pressure.

The singularity in Γ at neutron drip is of the form

$$\Gamma(\rho) - \Gamma(\rho_d) \sim -(\rho-\rho_d)^{\frac{1}{2}} \tag{10.2}$$

for ρ just above ρ_d, the threshold density for neutron drip. We may see this by expanding both the density and pressure above ρ_d in terms of μ_n, which vanishes at drip. Writing

$$\rho(\mu_n) = \rho_e(\mu_n) + \rho_n(\mu_n), \tag{10.3}$$

where ρ_e is the nuclear plus electron mass density, $\rho_e(0) = \rho_d$, and ρ_n is the mass density of the free neutrons, we have

$$\rho(\mu_n) = \rho_d + \left(\frac{\partial \rho_e}{\partial \mu_n}\right)_d \mu_n + \frac{(2m_n\mu_n)^{\frac{3}{2}} m_n}{3\pi^2\hbar^3}, \tag{10.4}$$

just above drip; for ρ_n we have taken the free neutron result. Similarly the pressure

$$P(\mu_n) = P_e(\mu_n) + P_n(\mu_n) \tag{10.5}$$

takes the form

$$P(\mu_n) = P_d + \left(\frac{\partial P_e}{\partial \mu_n}\right)_d \mu_n + \frac{(2m_n\mu_n)^{5/2}}{15\pi^2\hbar^3 m_n}, \tag{10.6}$$

where the latter term is the free neutron pressure, and P_d is the pressure at drip. The derivatives $\partial\rho_e/\partial\mu_n$ and $\partial P_e/\partial\mu_n$ are continuous through the neutron drip point, and the presence of the neutron gas may be neglected in calculating their values at ρ_d.

From (10.4) and (10.6) we have

$$\frac{\partial P}{\partial \rho} = \frac{\partial P/\partial \mu_n}{\partial \rho/\partial \mu_n} = \frac{(\partial P_c/\partial \mu_n)_d + (2m_n \mu_n)^{\frac{3}{2}}/3\pi^2\hbar^3}{(\partial \rho_c/\partial \mu_n)_d + m_n^2(2m_n \mu_n)^{\frac{1}{2}}/\pi^2\hbar^3}\ ; \tag{10.7}$$

to lowest order in μ_n, the $\mu_n^{\frac{3}{2}}$ can be neglected and $\mu_n = (\rho - \rho_d)/(\partial \rho_c/\partial \mu_n)$. Thus we find

$$\Gamma = \Gamma_d \left[1 - (\rho - \rho_d)^{\frac{1}{2}} \frac{m_n}{2\pi^2\hbar^3} \left(\frac{2m_n}{\partial \rho_c/\partial \mu}\right)^{\frac{1}{2}}\right]. \tag{10.8}$$

11. Conclusion

The calculations presented here, while containing what we believe to be the essential physics of the free neutron regime, can and should certainly be improved upon. The detail most in need of further work is the theory of the nuclear surface energy, especially in the presence of an external neutron gas.

More extensive calculations of the bulk energy $W(k, x)$ are also desirable. Firstly, one would like to have calculations of W, in the nuclear matter pair approximation, over a wider range of k and x, particularly for $x \lesssim 0.25$, where most of the nuclei are found. Effects on W of three- and four-body correlations, as well as proton and neutron superfluid pairing should be studied. As Yang and Clark have shown, neutron pairing has a substantial influence on the energy of neutron matter at $\rho \sim 10^{13}$ g/cm^3. The proton chemical potential, even at $x \approx 0$, is sensitive to these higher-order correlations. Generally, chemical potentials depend on derivatives of W, so that rapidly varying terms which contribute little to W could conceivably influence proton and neutron chemical potentials considerably; derivatives of chemical potentials are even more sensitive measures of such effects. Lastly, the fitting of bulk matter parameters in the region of ordinary nuclei will need improvement; this problem is closely tied to our understanding of the nuclear surface energy.

Among remaining theoretical problems, we mention the detailed description of the transition between the solid and liquid phases, including possible proton and neutron superfluidity; and also the nature and role of nuclear deformations at high densities – these will reflect the cubic symmetry of the lattice. One theoretical refinement would be the development of a calculation of the high-density nuclear phase starting from the bulk coexistence of nuclear matter with a pure neutron gas, as described in sect. 3, and treating the total surface and Coulomb energies as perturbations; such a calculation is presently in progress.

We wish first to express our gratitude to Professor Chr. Møller and the staff of Nordita for their kind hospitality in Copenhagen which made possible this collaborative work. We are also grateful to Professor Aa. Bohr, Professor G. E. Brown, Professor B. Mottelson and Professor D. Pines for their constant interest in this problem. We thank Dr. J. W. Negele and Dr. P. J. Siemens, who gave us much

useful critical advice and carried out a number of detailed calculations on the properties of bulk nuclear matter; and Dr. J. Arponen for calling our attention to the instability of the uniform liquid state. We have had helpful discussions with other colleagues in Copenhagen, especially Dr. J. Damgaard, Dr. A. Lande, Dr. V. R. Pandharipande and Mr. P. Sutherland. To Dr. J. Gunn and the Niels Bohr Institute computer staff, especially Mr. P. Jepsen and Mr. L. Poulsen, we owe a particular debt of gratitude for their patient advice and assistance in the running of the Gier computer. C.J.P. wishes to thank the President and Fellows of Magdalen College for granting him leave to work in Copenhagen. This research was supported in part by the National Science Foundation Grants GP-16886 and 20006.

References

1) T. Gold, Nature **218** (1968) 731; **221** (1969) 25
2) E. E. Salpeter, Astrophys. J. **134** (1961) 669
3) M. A. Ruderman, J. de Phys. **30**, supplément C3 (1969) 152
4) G. Baym, C. J. Pethick and P. G. Sutherland, Astrophys. J. **170** (1971)
5) H. A. Bethe, G. Börner and K. Sato, Astron. and Astrophys. **7** (1970) 279
6) W. D. Langer, L. C. Rosen, J. M. Cohen and A. G. W. Cameron, Astrophys. Spa. Sci. **5** (1969) 259
7) W. D. Myers and W. J. Swiatecki, Nucl. Phys. **81** (1966) 1
8) J. Németh and D. W. L. Sprung, Phys. Rev. **176** (1968) 1496
9) W. D. Myers and W. J. Swiatecki, Ann. of Phys. **55** (1969) 395
10) R. A. Weiss and A. G. W. Cameron, Can. J. Phys. **47** (1969) 2171, 2211
11) G. Baym and D. Pines, Ann. of Phys. **66** (1971)
12) R. A. Coldwell-Horsfall and A. A. Maradudin, J. Math. Phys. **1** (1960) 395
13) N. W. Ashcroft and D. C. Langreth, Phys. Rev. **155** (1967) 682
14) R. V. Reid, Ann. of Phys. **50** (1968) 411
15) See e.g., F. Coester, S. Cohen, B. Day and C. M. Vincent, Phys. Rev. **C1** (1970) 769
16) P. J. Siemens, Nucl. Phys. **A141** (1970) 225
17) T. K. Dahlblom, Nordita Publ. no. 315; also Acta Acad. Aboensis, **B29**, no. 6 (1969)
18) B. Day, Phys. Rev. **187** (1969) 1269
19) G. E. Brown and A. M. Green, Nucl. Phys. **A137** (1969) 1
20) J. W. Negele, Phys. Rev. **C1** (1970) 1260
21) C. G. Wang, W. K. Rose and S. L. Schlenker, Astrophys. J. **160** (1970) L117
22) E. Østgaard, Nucl. Phys. **A154** (1970) 202
23) P. J. Siemens, to be published
24) C.-H. Yang and J. W. Clark, Nucl. Phys. **174** (1971) 49
25) A. B. Migdal, Nuclear theory: the quasiparticle method (Benjamin, New York, 1968) p. 6
26) G. Baym and C. J. Pethick, to be published
27) H. A. Bethe, Phys. Rev. **167** (1968) 879
28) J. Németh, Nucl. Phys. **A156** (1970) 183
29) K. A. Brueckner, J. R. Buchler, R. C. Clark and R. J. Lombard, Phys. Rev. **181** (1969) 1543
30) J.-R. Buchler and Z. Barkat, Astrophys. Lett. **7** (1971) 167
31) H. A. Bethe and R. F. Bacher, Rev. Mod. Phys. **8** (1936) 82
32) F. J. Dyson, Ann. of Phys. **63** (1971) 1
33) L. D. Landau, Phys. Z. Sowjet **11** (1937) 545; JETP (Sov. Phys.) **7** (1937) 627; Collected papers of L. D. Landau, ed. D. ter Haar (Pergamon, Oxford, 1965) p. 209
34) M. A. Ruderman, Proc. of the fifth annual eastern theoretical physics Conf., ed. D. Feldman (Benjamin, New York, 1967) p. 25
35) R. A. Wolf, Astrophys. J. **145** (1966) 834
36) J. B. Hartle and K. S. Thorne, Astrophys. J. **153** (1968) 807
37) W. D. Langer and L. C. Rosen, Astrophys. Spa. Sci. **6** (1970) 217
38) J. W. Negele, private communication

Molecular Mechanics

Background

The "mechanical" molecular model was developed out of a need to describe molecular structures and properties in as practical a manner as possible. The range of applicability of molecular mechanics includes:

- Molecules containing thousands of atoms.
- Organics, oligonucleotides, peptides, and saccharides (metallo-organics and inorganics in some cases).
- Vacuum, implicit, or explicit solvent environments.
- Ground state only.
- Thermodynamic and kinetic (via molecular dynamics) properties.

The great computational speed of molecular mechanics allows for its use in procedures such as molecular dynamics, conformational energy searching, and docking, that require large numbers of energy evaluations.

Molecular mechanics methods are based on the following principles:

- Nuclei and electrons are lumped into atom-like particles.
- Atom-like particles are spherical (radii obtained from measurements or theory) and have a net charge (obtained from theory).
- Interactions are based on springs and classical potentials.
- Interactions must be preassigned to specific sets of atoms.
- Interactions determine the **spatial distribution** of atom-like particles and their **energies**.

Note how these principles differ from those of quantum mechanics.

The Anatomy of a Molecular Mechanics Force-Field

The mechanical molecular model considers atoms as spheres and bonds as springs. The mathematics of spring deformation can be used to describe the ability of bonds to stretch, bend, and twist:

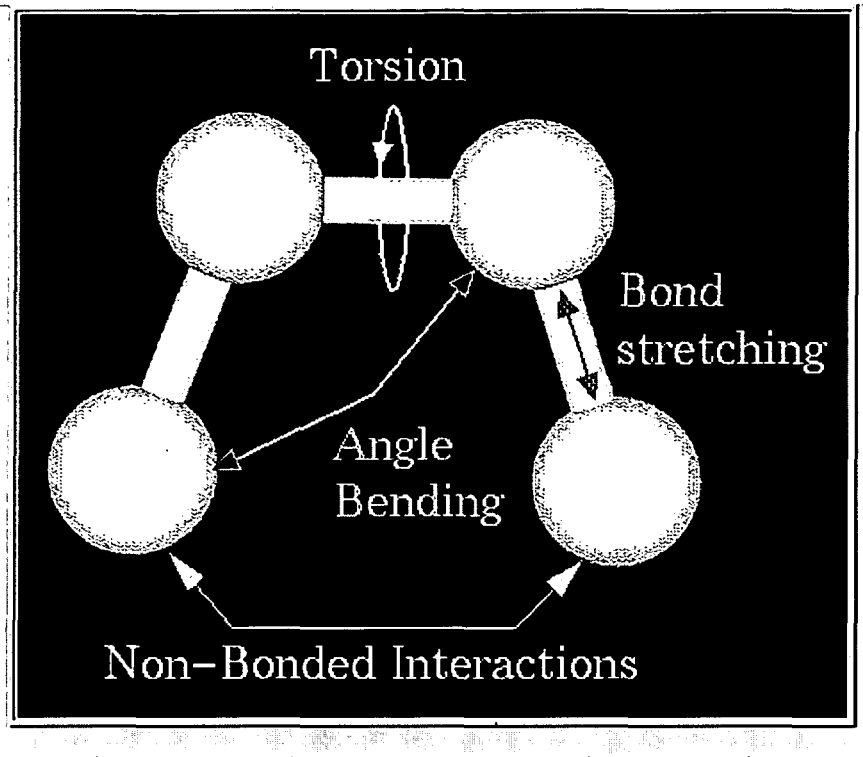

Non-bonded atoms (greater than two bonds apart) interact through van der Waals attraction, steric repulsion, and electrostatic attraction/repulsion. These properties are easiest to describe mathematically when atoms are considered as spheres of characteristic radii.

The object of molecular mechanics is to predict the energy associated with a given conformation of a molecule. However, molecular mechanics energies have no meaning as absolute quantities. Only differences in energy between two or more conformations have meaning. A simple molecular mechanics energy equation is given by:

Energy =
Stretching Energy +
Bending Energy +
Torsion Energy +
Non-Bonded Interaction Energy

These equations together with the data (parameters) required to describe the behavior of different kinds of atoms and bonds, is called a force-field. Many different kinds of force-fields have been developed over the years. Some include additional energy terms that describe other kinds of deformations. Some force-fields account for coupling between bending and stretching in adjacent bonds in order to improve the accuracy of the mechanical model.

The mathematical form of the energy terms varies from force-field to force-field. The more common forms will be described.

- **Stretching Energy**

$$E = \sum_{bonds} k_b (r - r_o)^2$$

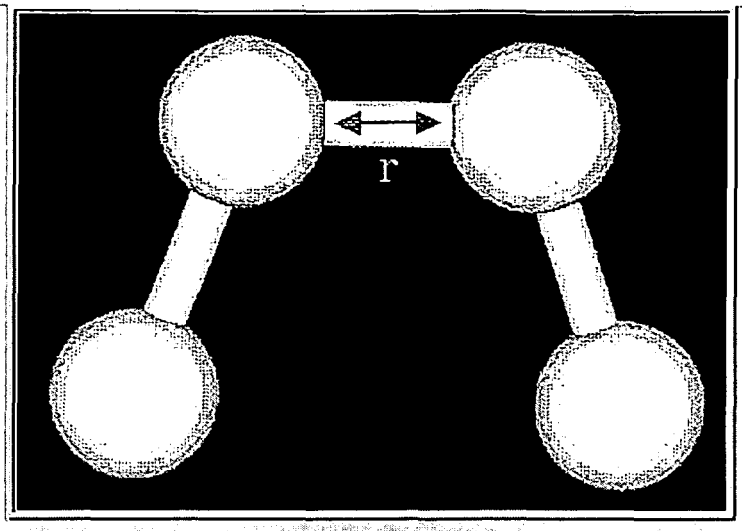

The stretching energy equation is based on Hooke's law. The "k*b*" parameter controls the stiffness of the bond spring, while "r*o*" defines its equilibrium length. Unique "k*b*" and "r*o*" parameters are assigned to each pair of bonded atoms based on their types (e.g. C-C, C-H, O-C, etc.). This equation estimates the energy associated with vibration about the equilibrium bond length. This is the equation of a parabola, as can be seen in the following plot:

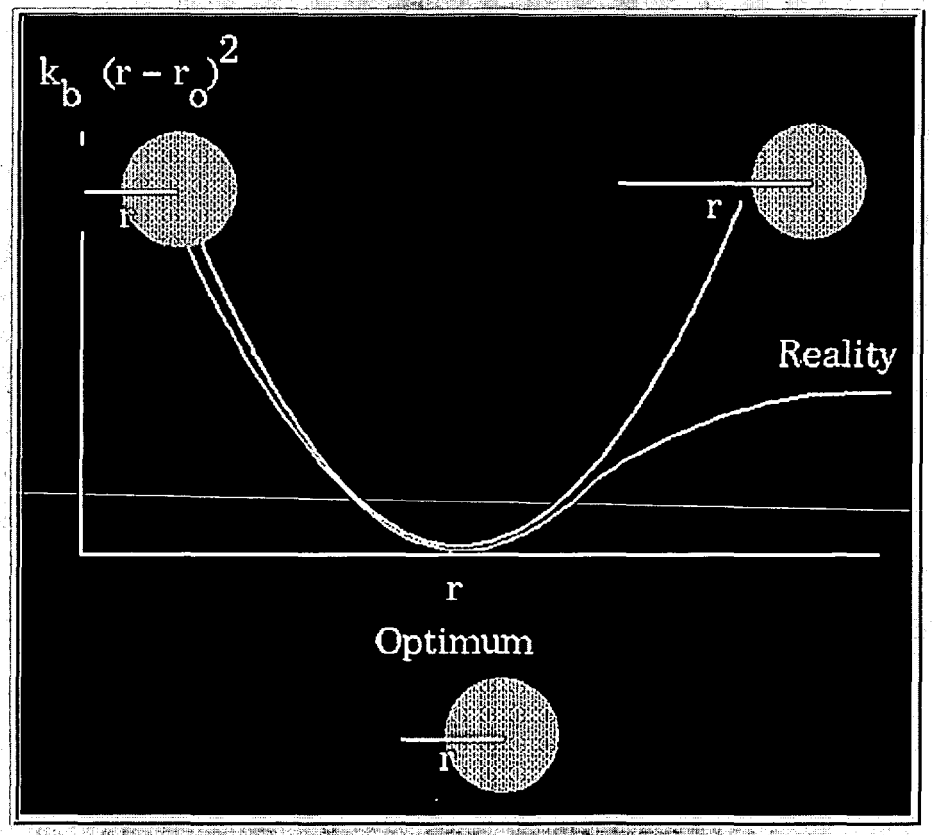

Notice that the model tends to break down as a bond is stretched toward the point of dissociation.

- **Bending Energy**

$$E = \sum_{\text{angles}} k_\theta \, (\theta - \theta_o)^2$$

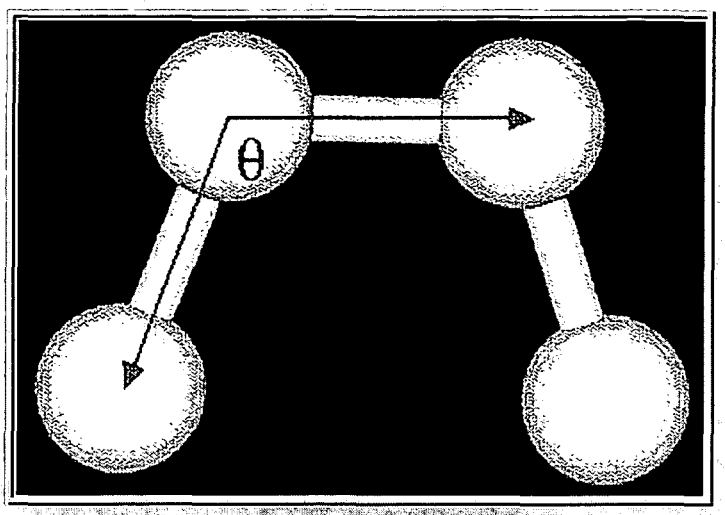

The bending energy equation is also based on Hooke's law. The "k*theta*" parameter controls the stiffness of the angle spring, while "theta*o*" defines its equilibrium angle. This equation estimates the energy associated with vibration about the equilibrium bond angle:

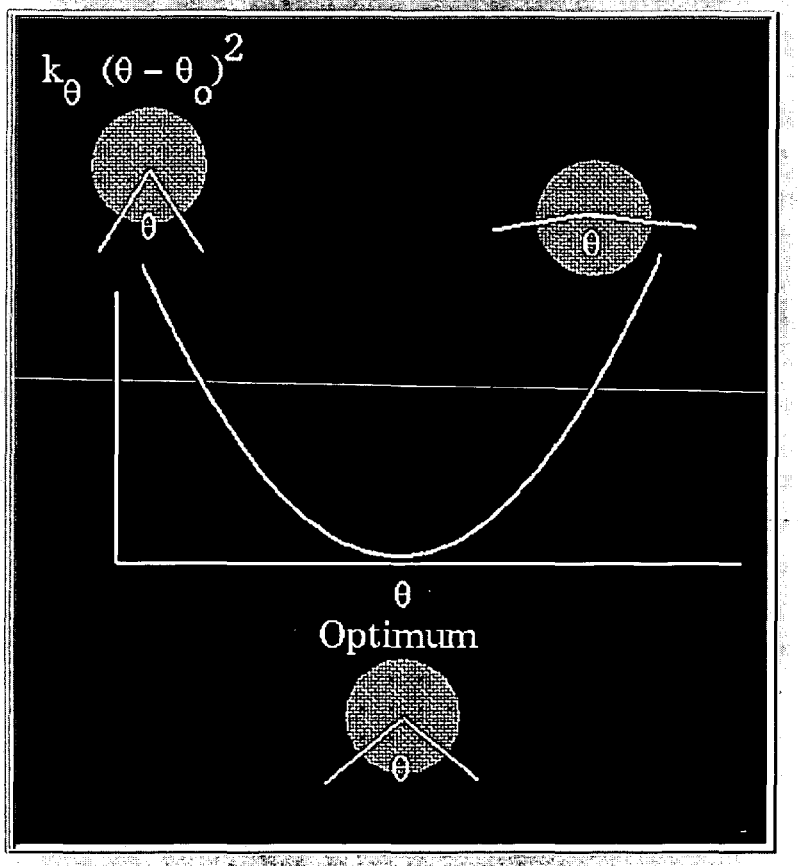

Unique parameters for angle bending are assigned to each bonded triplet of atoms based on their types (e.g. C-C-C, C-O-C, C-C-H, etc.). The effect of the "k*b*" and "k*theta*" parameters is to broaden or steepen the slope of the parabola. The larger the value of "k", the more energy is required to deform an angle (or bond) from its equilibrium value. Shallow potentials are achieved for "k" values between 0.0 and 1.0. The Hookeian potential is shown in the following plot for three values of "k":

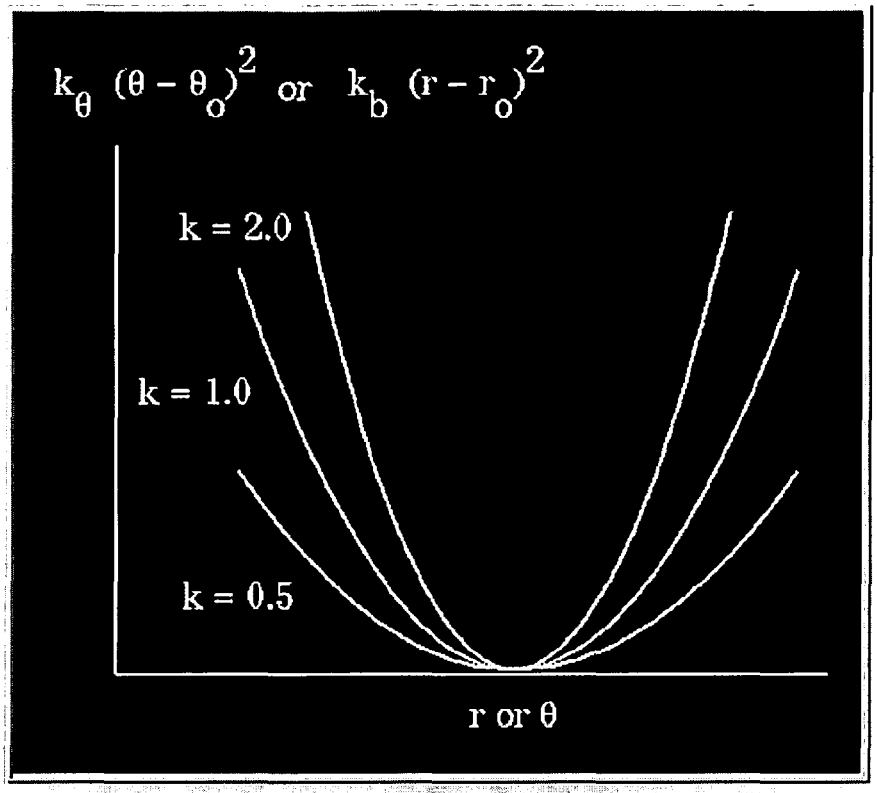

- **Torsion Energy**

$$E = \sum_{\text{torsions}} A\,[1 + \cos(n\tau - \phi)]$$

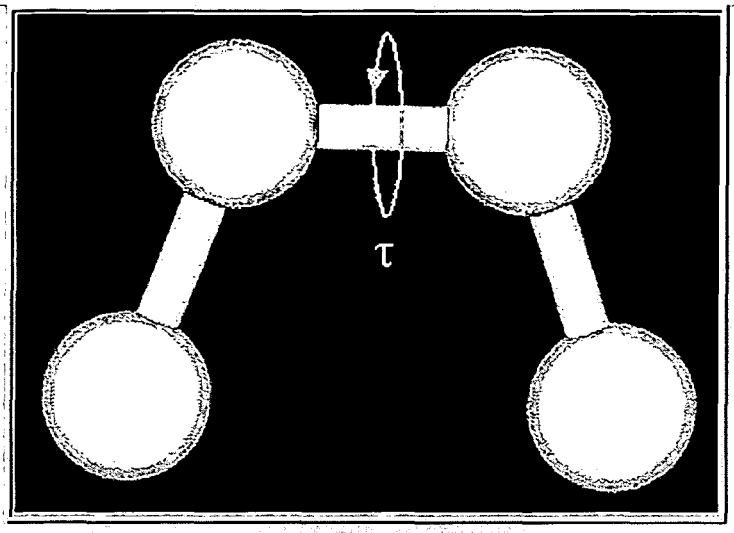

The torsion energy is modeled by a simple periodic function, as can be seen in the following plot:

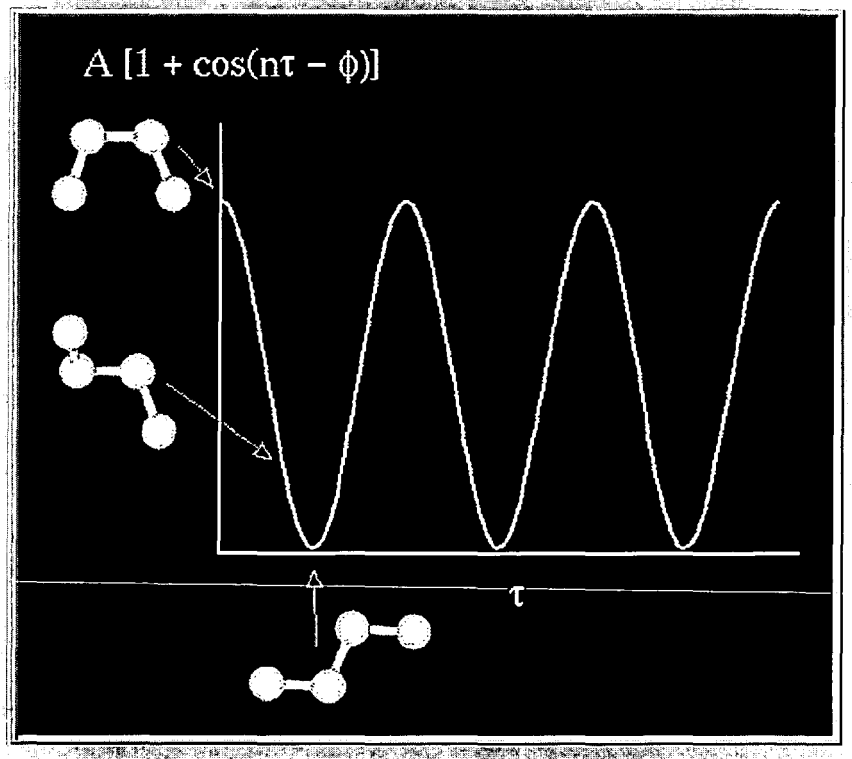

The torsion energy in molecular mechanics is primarily used to correct the remaining energy terms rather than to represent a physical process. The torsional energy represents the amount of energy that must be added to or subtracted from the Stretching Energy + Bending Energy + Non-Bonded Interaction Energy terms to make the total energy agree with experiment or rigorous quantum mechanical calculation for a model dihedral angle (ethane, for example might be used a a model for any H-C-C-H bond).

The "A" parameter controls the amplitude of the curve, the n parameter controls its periodicity, and "phi" shifts the entire curve along the rotation angle axis (tau). The parameters are determined from curve fitting. Unique parameters for torsional rotation are

assigned to each bonded quartet of atoms based on their types (e.g. C-C-C-C, C-O-C-N, H-C-C-H, etc.). Torsion potentials with three combinations of "A", "n", and "phi" are shown in the following plot:

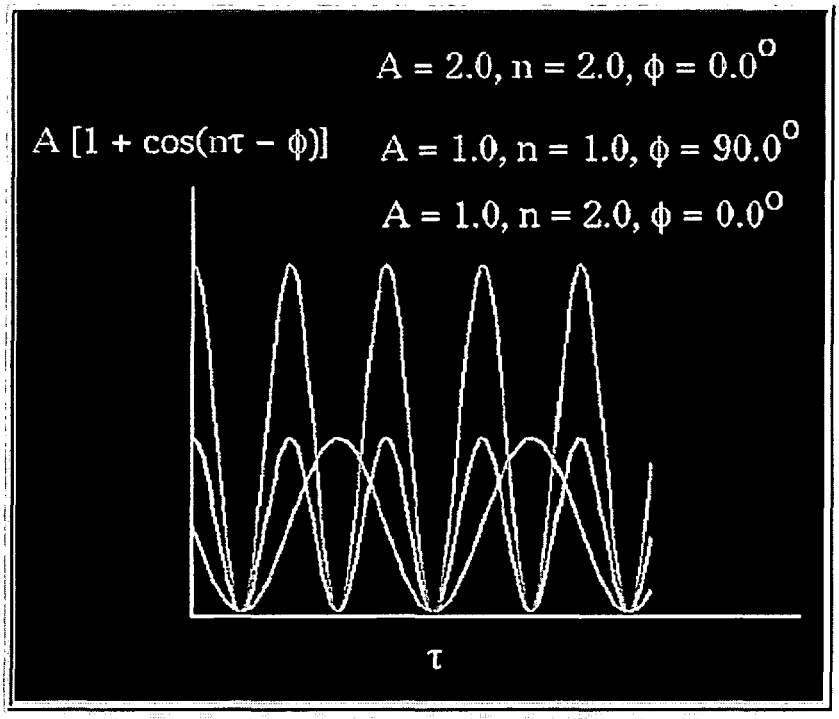

Notice that "n" reflects the type symmetry in the dihedral angle. A CH3-CH3 bond, for example, ought to repeat its energy every 120 degrees. The *cis* conformation of a dihedral angle is assumed to be the zero torsional angle by convention. The parameter phi can be used to synchronize the torsional potential to the initial rotameric state of the molecule whose energy is being computed.

• Non-Bonded Energy

The non-bonded energy represents the pair-wise sum of the energies of all possible interacting non-bonded atoms i and j:

$$E = \underbrace{\sum_i \sum_j \left(\frac{-A_{ij}}{r_{ij}^6} + \frac{B_{ij}}{r_{ij}^{12}} \right)}_{\text{van der Waals term}} + \underbrace{\sum_i \sum_j \frac{q_i q_j}{r_{ij}}}_{\text{Electrostatic term}}$$

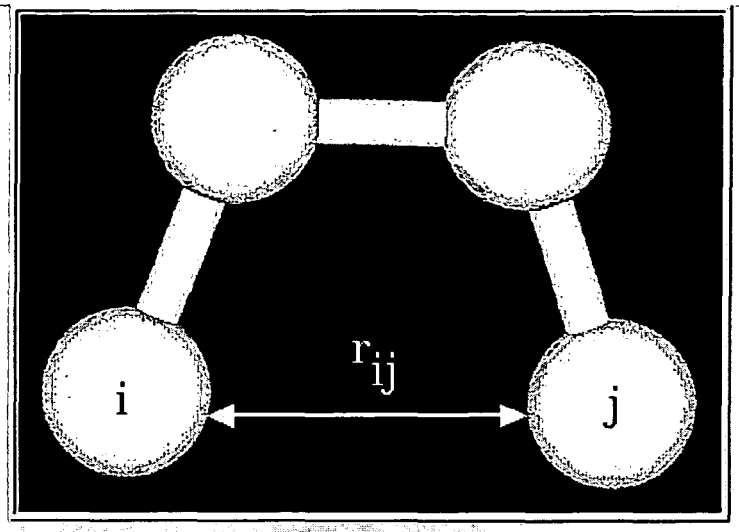

The non-bonded energy accounts for repulsion, van der Waals attraction, and electrostatic interactions. van der Waals attraction occurs at short range, and rapidly dies off as the interacting atoms move apart by a few Angstroms. Repulsion occurs when the distance between interacting atoms becomes even slightly less than the sum of their contact radii. Repulsion is modeled by an equation that is designed to rapidly blow up at close distances (1/r^12 dependency). The energy term that describes attraction/repulsion provides for a smooth transition between these two regimes. These effects are often modeled using a 6-12 equation, as shown in the following plot:

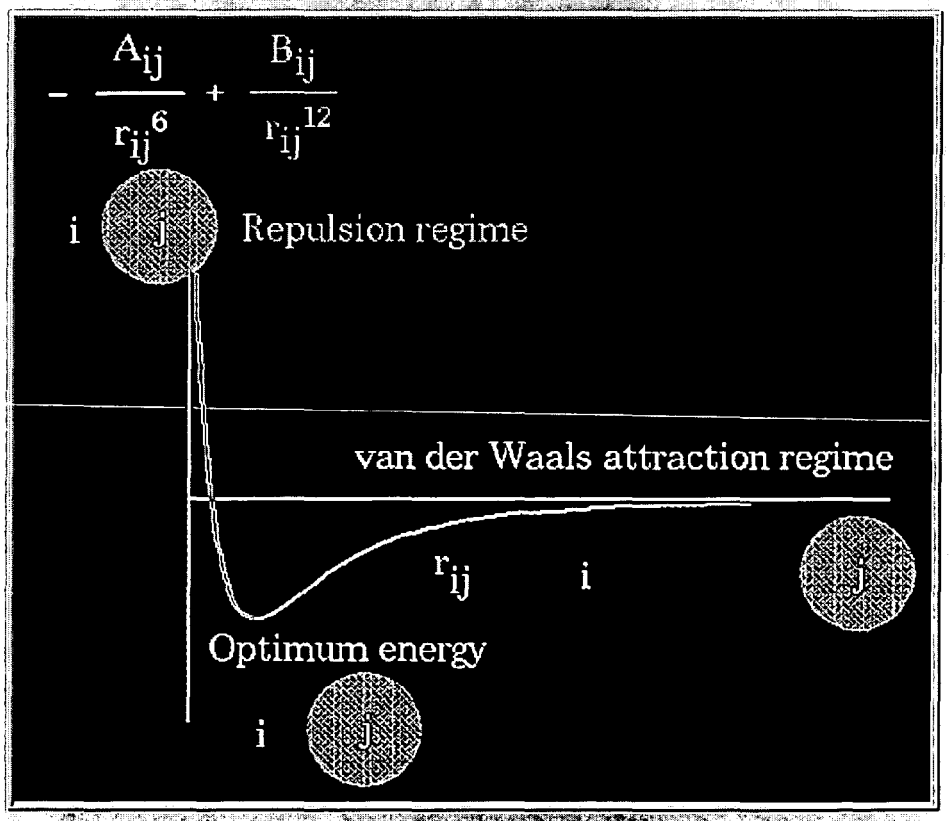

The "A" and "B" parameters control the depth and position (interatomic distance) of the potential energy well for a given pair of non-bonded interacting atoms (e.g. C:C, O:C, O:H,

etc.). In effect, "A" determines the degree of "stickiness" of the van der Waals attraction and "B" determines the degree of "hardness" of the atoms (e.g marshmallow-like, billiard ball-like, etc.).

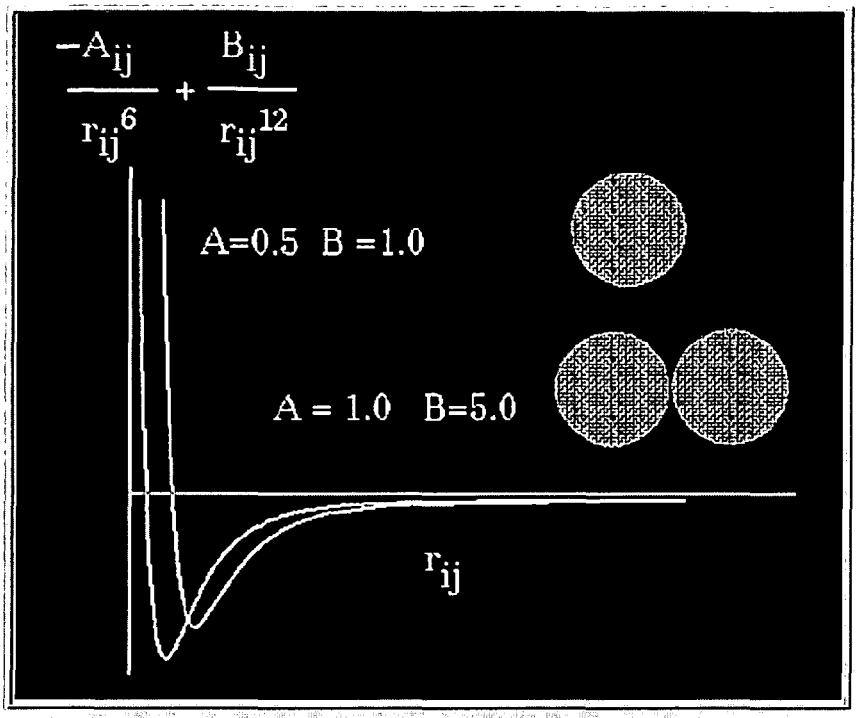

The "A" parameter can be obtained from atomic polarizability measurements, or it can be calculated quantum mechanically. The "B" parameter is typically derived from crystallographic data so as to reproduce observed average contact distances between different kinds of atoms in crystals of various molecules.

The electrostatic contribution is modeled using a Coulombic potential. The electrostatic energy is a function of the charge on the non-bonded atoms, their interatomic distance, and a molecular dielectric expression that accounts for the attenuation of electrostatic interaction by the environment (e.g. solvent or the molecule itself). Often, the molecular dielectric is set to a constant value between 1.0 and 5.0. A linearly varying distance-dependent dielectric (i.e. 1/r) is sometimes used to account for the increase in environmental bulk as the separation distance between interacting atoms increases.

Partial atomic charges can be calculated for small molecules using an *ab initio* or semiempirical quantum technique (usually MOPAC or AMPAC). Some programs assign charges using rules or templates, especially for macromolecules. In some force-fields, the torsional potential is calibrated to a particular charge calculation method (rarely made known to the user). Use of a different method can invalidate the force-field consistency.